Federal University of Rio Grande do Sul
Physics Institute

Marcio de Sousa Mateus Junior

Resonant dark matter production through a new spin-1 massive mediator (Produção de matéria escura em ressonância através de um novo mediador massivo de spin-1)*

Brasil

2024

*The present work was financed by the National Council for Scientific and Technological Development of Brazil (CNPq).

Marcio de Sousa Mateus Junior

Resonant dark matter production through a new spin-1 massive mediator
(Produção de matéria escura em ressonância através de um novo mediador massivo de spin-1)

This thesis was submitted to the Graduate Program in Physics of the Physics Institute at the Federal University of Rio Grande do Sul as partial requirement for obtaining the degree of Doctor in Science.

Federal University of Rio Grande do Sul

Physics Institute

Graduate Program in Physics

Supervisor: Dr. Gustavo Gil da Silveira

Brasil

2024

Marcio de Sousa Mateus Junior
Resonant dark matter production through a new spin-1 massive mediator (Produção de matéria escura em ressonância através de um novo mediador massivo de spin-1)/ Marcio de Sousa Mateus Junior. – Brasil, 2024-
132p. : il. (some colors.) ; 30 cm.

Supervisor: Dr. Gustavo Gil da Silveira

PhD Thesis – Federal University of Rio Grande do Sul
Physics Institute
Graduate Program in Physics, 2024.

1. Physics. 2. Cosmology. 3. Dark Matter. I. Dr. Gustavo Gil da Silveira. II. Federal University of Rio Grande do Sul. III. Physics Institute. IV. Title.

Marcio de Sousa Mateus Junior

Resonant dark matter production through a new spin-1 massive mediator
(Produção de matéria escura em ressonância através de um novo mediador massivo de spin-1)

This thesis was submitted to the Graduate Program in Physics of the Physics Institute at the Federal University of Rio Grande do Sul as partial requirement for obtaining the degree of Doctor in Science.

Public defense held in Porto Alegre, RS, Brazil, on March 28th, 2024:

Prof. Dr. Gustavo Gil da Silveira
Advisor

Prof. Dr. Thiago Rafael Fernandez Perez Tomei
Universidade do Estado de São Paulo

Prof. Dr. Alexandre Alves
Universidade Federal de São Paulo

Prof. Dr. César Augusto Bernardes
Universidade Federal do Rio Grande do Sul

Prof. Dr. Dimiter Hadjimichef
Universidade Federal do Rio Grande do Sul

Brasil

2024

I dedicate this work to my mother, Cleonice Alves de Souza, who persevered with me from the beginning.

Acknowledgements

I firstly thank my mother, Cleonice, for everything. Without her, I would not be here, and for her, I have come further. I also thank my partner, Roberta Shinkai, for motivating me and supporting me during this journey.

I would also like to thank my advisor, Prof. Gustavo Gil da Silveira, who accompanied me on this journey of highs and lows, comings and goings, rejections and acceptances, and knew how to guide and prepare me, establishing the path to become a better scientist.

Also to friends inside and outside academia, I leave my thanks for the companionship as always, especially to all the colleagues and organizers of the Les Houches Dark Matter Summer School of 2021, I record here to not forget my immense gratitude for the unforgettable knowledge and experiences.

I also thank all the teachers and staff who helped me in the twenty-eight years of my education from elementary school to here.

I also record here my gratitude to the funding agencies that financed this research, especially CAPES and CNPq, which directly contributed to my postgraduate studies.

—

Agradeço primeiramente à minha mãe, Cleonice, por tudo. Sem ela não estaria aqui, e por ela eu cheguei mais longe. Agradeço também à minha companheira, Roberta Shinkai, por me motivar e suportar durante essa trajetória.

Também gostaria de agradecer ao meu orientador, Prof. Gustavo Gil da Silveira, que me acompanhou nessa jornada de altos e baixos, idas e vindas, rejeições e aceites, e soube me conduzir e me preparar, estabelecendo o caminho para me tornar um cientista melhor.

Também aos amigos de dentro e fora da academia, deixo aqui meu agradecimento pelo companheirismo de sempre, especialmente à todos os colegas e organizadores da Les Houches Dark Matter Summer School de 2021, registro aqui para não esquecer da minha imensa gratidão pelos conhecimentos e experiências inesquecíveis.

Agradeço ainda à todos os professores e funcionários que me auxiliaram nos vinte e oito anos da minha formação desde a educação elementar até aqui.

Também deixo aqui registrado a gratidão às agências de fomento que financiaram esta pesquisa, especialmente CAPES e CNPq, que contribuíram diretamente para minha pós-graduação.

Le vide absolu existe-t-il
quelque part dans l'espace Universel?
"Non, rien n'est vide;
ce qui est vide pour toi est occupé par
une matière qui échappe à tes sens et à tes instruments."

36^{th} question from *The Spirits Book*, Allan Kardec, 1860

Abstract

Investigations on Dark matter (DM) and new models have been at the forefront of physics over the last decade. A variety of models have been put forward to account for cosmological aspects of DM, such as explaining its abundance in the early Universe and replicating the behavior of galaxies and large-scale structures believed to be influenced by DM. Furthermore, an ideal DM candidate should suggest observables detectable in current and future experiments, including sufficiently high cross sections for detection and processes that result in the emission of Standard Model (SM) particles. Moreover, theoretical models must adhere to known conservation and symmetry constraints and typically need to respect mechanisms of production, scattering, and (co-)annihilation, especially if proposing a new particle within the framework established by quantum field theory. The search for new mediators within the dark sector in accelerators, such as the Large Hadron Collider (LHC), aims to evaluate the data for new interactions, where processes of new physics, if observed, must incorporate cosmological and astrophysical constraints to be identified as originating from DM. Our calculations for the estimated DM thermal relic density from the primordial universe are performed for processes enhanced by resonance scenarios in the s-channel, compatible with the expected parameters for high energy colliders. However, such an assessment is non-trivial and scarcely discussed in the literature. In addition to presenting this proper calculation, we also show how these processes could be observed by the emission of an initial state photon as a radiative correction to the initial radiation of the process. This study investigates a simplified interaction model, which aligns with current SM physics but introduces a new spin-1 mediator to interact with three potential particles that could constitute some or all of the DM in the Universe. We demonstrate that both the accurate calculation of the relic density and the factorization for this initial radiation have implications on the parameter space observed for such processes. This leads to corrections in predictions for particle colliders, particularly the LHC and future electron-positron colliders.

Keywords: dark matter. particle physics. cosmology. simplified models. massive mediators

Resumo

Pesquisas e modelos para matéria escura (ME) estiveram na vanguarda da física ao longo da última década. Diversos modelos foram propostos, onde espera-se que se justifique aspectos cosmológicos conhecidos a respeito da ME, como explicar a sua abundância produzida no Universo primordial, assim como reproduzir o comportamento de galáxias e estruturas de larga escala que se acredita serem afetados pela presença de ME, por exemplo. Também é desejável que um bom candidato à ME proponha observáveis que possam ser vistos em experimentos atuais e futuros, como seções de choque altas o suficiente para serem de fato detectadas e processos cuja emissão de partículas do SM possa ser constatada. Além disso, modelos teóricos não podem fugir de restrições de conservação e simetria já conhecidas, e usualmente precisam respeitar os mecanismos de produção, espalhamento e (co)aniquilação, caso na hipótese de que seja proposto uma nova partícula nos moldes já estabelecidos por uma teoria quântica de campos. A busca por novos mediadores com o setor escuro em aceleradores, como o Grande Colisor de Hádrons (LHC), tentam caracterizar nos dados evidências por novas interações, onde processos de nova física, caso sejam observados, precisam incluir restrições cosmológicas e astrofísicas para que possam ser identificados como provenientes da ME. Realizamos cálculos da densidade de relíquia de ME para processos realçados por cenários de ressonância no canal s. Tal avaliação não é trivial e é raramente abordada na literatura. Além de apresentar o cálculo apropriado da densidade de relíquia em cenários de ressonância, também demonstramos como esses processos poderiam ser evidenciados pela emissão de um fóton do estado inicial, na forma de uma correção radiativa para a radiação inicial do processo. Este trabalho analisa um modelo de interação simplificado, consistente com a física do modelo padrão atual, mas introduz um novo mediador *spin*-1 para interagir com três partículas potenciais que poderiam constituir parte ou toda a ME presente no Universo. Mostramos que tanto o cálculo correto da densidade de relíquia quanto a fatorização para esta radiação inicial têm implicações no espaço de parâmetros observado para tais processos. Isso leva a correções nas previsões feitas para colisores de partículas, especialmente o LHC e futuros colisores elétron-pósitron.

Palavras-chave: matéria escura. física de partículas. cosmologia. modelos simplificados. mediadores massivos.

List of Figures

List of abbreviations and acronyms

ATLAS	A Toroidal LHC ApparatuS
ALP	Axion Like Particle
BBN	Big Bang Nucleosynthsis
BEH	Brout-Englert-Higgs boson
BSM	Beyond Standard Model
CDM	Cold Dark Matter
CERN	European Organization for Nuclear Research
CHAMP	CHarged Massive Particles
CL	Confidence Level
CLIC	The Compact Linear Collider
CMB	Cosmic Microwave Background
CMS	Compact Muon Solenoid
CNPq	*Conselho Nacional de Desenvolvimento Científico e Tecnológico*
CP	Charge-Parity
DM	Dark Matter
FIMP	Feebly Interacting Massive Particle
FRLW	Friedmann-Lemaître-Robinson-Walker
GR	General Relativity
GUT	Grand Unified Theory
HEP	High Energy Physics
LCDM	Lambda Cold Dark Matter
LEP	Large Electron-Positron Collider
LHC	Large Hadron Collider
MoND	Modified Newton Dynamics
MSSM	Minimal Supersymmetric Standard Model
PBH	Primordial Black Holes
PDF	Parton Density Function
QCD	Quantum Chromodynamics
QED	Quantum Electrodynamics
QFT	Quantum Field Theory
QM	Quantum Mechanics
SIMP	Strongly Interacting Massive Particles
SM	Standard Model
SUSY	Supersymmetry
TOE	Theory of Everything
UED	Universal Extra Dimensions
WIMP	Weakly Interacting Massive Particle

Press Release

(in brazilian portuguese)

Pesquisa Brasileira Ajuda a Esclarecer Alguns dos Mistérios da Matéria Escura

Estudo apresenta modelo simplificado para prever a presença de matéria escura em colisores de partículas, abrindo caminho para novas descobertas.

Porto Alegre, Fevereiro de 2024 – A matéria escura, um dos maiores enigmas da física contemporânea, pode em breve ter alguns de seus segredos esclarecidos, graças a uma nova pesquisa conduzida por cientistas brasileiros. O estudo, publicado recentemente, utiliza um modelo simplificado para tentar prever resultados futuros em colisores de partículas, como o Grande Colisor de Hádrons (LHC) do CERN, na fronteira da Suíça com a França.

A pesquisa destaca-se por utilizar processos produzidos em ressonância, um fenômeno no qual a taxa de eventos é significativamente aumentada quando as partículas envolvidas no processo possuem uma energia próxima daquela que media a força entre elas. Esta abordagem não apenas promete melhorar a precisão das previsões de detecção de matéria escura em experimentos futuros, mas também apresenta um cálculo mais correto para a *densidade de relíquia*, que nada mais é que a quantidade de matéria escura que seria produzida no Universo primordial, caso o modelo proposto esteja correto.

Os cientistas assumiram três diferentes tipos de composição para a matéria escura, sugerindo a existência de três tipos de partículas elementares distintas, além de um novo mediador. Se identificado, este mediador poderia representar uma quinta força fundamental da natureza, expandindo nosso entendimento das forças conhecidas: gravidade, eletromagnetismo, força fraca e força forte. A entrada recente do Brasil no CERN, marcando uma colaboração mais ativa com os experimentos atuais e futuros, incluindo o LHC, ressalta a importância desta pesquisa. A descoberta potencial de uma nova partícula ou força da natureza teria implicações profundas não apenas para a física teórica, mas também para nossa compreensão do Universo. A matéria escura, que compõe cerca de 26% do Universo, permanece invisível através de métodos de observação tradicionais, tornando sua detecção direta um dos principais objetivos da física de partículas hoje.

Contatos para entrevistas:

Marcio de Sousa Mateus Junior, Aluno de Pós-Graduação em Física, Instituto de Física da Universidade Federal do Rio Grande do Sul, Porto Alegre, Brasil, msmateusjr@gmail.com

Gustavo Gil da Silveira, Professor Adjunto, Instituto de Física da Universidade Federal do Rio Grande do Sul, Porto Alegre, Brasil, gustavo.silveira@ufrgs.br.

Fontes das Imagens: *Symmetry Magazine, Sandbox Studio, Chicago*

In this work, we used $\hbar = c = k_B = 1$.

Contents

1 Introduction

The exploration of the composition of the Universe has been an essential aspect of astrophysical research, particularly the investigation of dark matter (DM). While the understanding of baryonic matter, constituting approximately $4.93 \pm 0.06\%$ of the Universe, is relatively advanced, the nature of the remaining $\sim$95%, comprised of $26.5 \pm 0.7\%$ of DM and $68.5 \pm 0.7\%$ dark energy [1, 2], remains elusive.

Originally, the concept of DM first emerged from the observations made by Fritz Zwicky in 1933 of the Coma galaxy cluster [3, 4]. Analyzing its redshift, Zwicky applied the Virial Theorem, revealing that the mass of the cluster – primarily non-luminous – far exceeded that of the visible matter. This led him to hypothesize a form of matter that neither emits nor reflects light, then called *dark matter*. Subsequent studies, including those examining the cosmic microwave background (CMB), have further reinforced the DM hypothesis and its role in the structure of the Universe [5].

Part of the observed mass excess may stem from modifications to gravity, or alternatively, there is a growing acceptance within the scientific community of the hypothesis that it comprises compact objects, such as intermediate-mass black holes formed in the early universe [6, 7]. This perspective has gained traction, especially with advancements in gravitational wave observatories, which have detected a greater number of events associated with these objects than previously anticipated [8].

The pursuit of understanding DM within some mechanism of particle physics has increasingly focused on its potential interactions and composition. Numerous theories propose that DM may exhibit similarities to the electromagnetic or electroweak interactions [9]. The quest for new physics, especially in the context of particle colliders, has been recently a research topic of intense investigation [10, 11]. This includes investigating anomalous couplings and deviations from the predictions of the standard model (SM) of elementary particles. One approach is to employ Quantum Field Theory (QFT) to describe potential mediators of DM, such as new massive bosons, differing from those of conventional matter. Despite persistent efforts and substantial data from accelerators, such as CERN Large Hadron Collider (LHC), some models have remained viable due to statistical and systematic uncertainties from experimental data [10, 12, 13].

However, any DM model must account for its estimated yield produced in the early universe. The production mechanism of DM must suggest a mechanism that gives less than or equal DM density fraction observed in the universe today, otherwise, it would not be consistent with astrophysical observations [2]. One approach to address this is by calculating its *relic density*, which, depending on the production mechanism, may yield

an abundance that is higher or lower than expected. Furthermore, certain processes may present exceptions or complexities that can significantly alter DM predictions, such as the formation of bound states, coannihilation processes, and, as detailed in this work, production via resonance channels, which can significantly modify the DM abundance even in simplified models.

Experimental data, particularly deviations from SM predictions, provide a basis for testing these theories. Significant deviations, like those recently reported by the CDF Collaboration at Fermilab regarding the W boson mass [14], offer intriguing insights about how new physics models can complement previous SM achievements. Comprehensive theories, grounded in well-established scenarios like extensions of the SM, aim to integrate known physical aspects into the search for evidence of new physics. Known examples include the minimal supersymmetric model [15], extra dimensions [16], and the little Higgs model [17], among others [18].

Among the myriad of models extending the SM, many of them feature a Lagrangian focusing solely on new effective couplings, sometimes including conventional matter. These *effective* models, however, encounter limitations and technical issues, such as violating renormalization properties [19]. Overcoming these challenges often involves constraining the model to a specific mass range or using particular approaches like particle singlets [20]. Nevertheless, an answer for these issues could be a closer alignment with SM approaches, employing propagators as interaction mediators, leading to the development of *simplified* models. Those usually anticipate a DM candidate or an entire DM sector, which has its own interaction mediator with the SM [9].

This work focuses on a specific simplified model that introduces a massive spin-1 boson mediator, analogous to the Z boson from SM, here called Z'. This mediator is neutral under electromagnetic and color charges and is postulated to interact with both SM and DM particles, acting as a portal between the two sectors. The Lagrangian for this model comprises kinetic components and source terms for SM fermions, alongside various couplings for different types of DM, including fermion, scalar, and vector DM states. This approach not only offers a very consolidated perspective on the coupling of the Z' boson to DM particles, but also explores novel production mechanisms in high-energy experiments by introducing possible signals to these productions in the initial state of collision processes, especially when these can be enhanced by a resonance channel [21]. The significance of studying resonance channels in the pursuit of new physics becomes evident, considering that the expected event rate for processes beyond the SM is typically quite low. This is due to the observational parameters of current experiments, which have already ruled out many models predicting more abundant events. Therefore, the resonance phenomenon, characterized by an increase in the expected number of events at a specific energy, facilitates the investigation of models that remain observable within the current

generation of experiments searching for evidences of DM interactions.

Moreover, the detection of a particle indicating potential new physics within an experiment does not, by itself, allow for its immediate identification as the source of DM, which is deduced from astronomical observations and further investigation would be imperative to elucidate the characteristics of this novel particle. Among these characteristics, the determination whether the production cross section, mass, and couplings are consistent with the expectations derived from the observed DM abundance is crucial, presumed to have emerged from the primordial Universe. This implies that, given the estimated $\sim$26% of the matter in the Universe and energy density attributed to DM, an accurate verification whether a proposed model – either partially or fully – accounts for this specific fraction is essential. This step is crucial since models or DM candidates often fails on predicting the overabundance density. Furthermore, when considering resonance-driven production processes, such calculations must be approached with caution, as most literature tends to avoid this production mechanism due to its particular complexities.

In this study we not only review the current state of observational evidence and experimental searches for DM but also explore how DM production via resonant states influences the calculation of the phase-space parameters and observables in comparison to the results present in the literature. This includes a particular focus on estimating the amount of DM generated in the early Universe by thermal processes within simplified interaction models through a new massive mediator boson in the dark sector.

In summary, we perceive that the quest to understand DM is not just about identifying an elusive component of the Universe but also about integrating this understanding into a broader landscape of particle physics and cosmology. Theoretical models continue to evolve day by day, reflecting our growing, yet still incomplete, comprehension of the Universe fundamental nature.

1.1 Objectives of this Work

This work aims to delve into the production of DM near the resonance of Z' in monophoton events at high-energy colliders, with a particular focus on their potential observation in the CERN experiments, such as the LHC and the future Compact Linear Collider (CLIC). The purpose of this study is to explore the characteristics of a simplified DM model that could facilitate the detection of such events within the colliders operational parameters considering the higher production cross section near a resonance.

Further, the study will explore the resonant production of DM through a new spin-1 mediator in the early Universe, incorporating the calculation of the appropriate relic density for this regime.

As a result, this investigation provides a scan of the possible parameter space for DM production under the conditions studied, aiming to identify the most viable regions for such processes.

Based on these analyses, this study describes phenomenological models and outcomes for simplified DM candidates, aiming at future experimental data, particularly anticipating the results from the Run-3 phase of the LHC, as well as future electron-positron colliders.. These models will be designed with an eye towards not only capturing the nuances of DM interactions but also enhancing the prospects for empirical validation.

Lastly, the outcomes of this investigation will trace an parallel with existing results in the literature that cover analogous processes. This comparison aims to contextualize our findings within a broader scientific context on DM research, highlighting new contributions and potential paths for future investigations. Through this approach, this work make an effort to contribute significantly to the understanding of DM production mechanisms and their pursuit on collider experiments, especially calculating the DM relic density for processes where its production is given by resonance channels.

2 Observational Evidence for Dark Matter

2.1 Galaxy clusters

Throughout the centuries, experimental observations have consistently affirmed the reliability of gravitational theory as an accurate descriptor of the natural world. By examining celestial bodies, scientists have been able to infer the mass of relatively isolated systems through the motion of these systems relative to other objects in their vicinity. Moreover, the mass of a star (and by extension, an entire galaxy) can be estimated based on the amount of light it emits. It was through such comparative measures that Fritz Zwicky [3] first observed a significant discrepancy in the Coma Cluster, a collection of over 1000 galaxies. He noted that the gravitationally predicted mass of the cluster was nearly 400 times greater [22] than the luminous mass measured from observations. In reaching this conclusion, Zwicky employed the Virial Theorem, which in short states that for a gravitationally stable system that is neither contracting nor expanding, there exists a relationship between the average velocity of the system particles and its gravitational potential energy [5].

Later, redshift measurements revealed that the average dispersion velocity of galaxies in the Coma Cluster was around 700 km/s. The redshift, denoted as z, is an electromagnetic phenomenon observed when the wavelength of light emitted by an object increases relative to an observer, across any spectrum range. This increase in wavelength can occur due to the Doppler effect, the expansion/contraction of space-time through which the light travels, or gravitational effects. The redshift of a galaxy can be calculated by measuring the shift in the spectral line of a known atom, such as hydrogen. This shift towards longer (or shorter) wavelengths in the spectrum is known as redshift (or blueshift, respectively). Redshift is a dimensionless parameter and can be deduced by knowing the emitted wavelength at the source (λ_{emit}) and the observed wavelength (λ_{obs}), with the emitter stationary relative to the observer. The relationship for calculating redshift is given by:

$$z = \frac{\lambda_{\text{obs}} - \lambda_{\text{emit}}}{\lambda_{\text{emit}}} \Rightarrow 1 + z = \frac{\lambda_{\text{obs}}}{\lambda_{\text{emit}}}. \tag{2.1}$$

In cosmology, the Hubble–Lemaître Law plays a major role, establishing a linear relationship between the redshift z and the current distance $d(t_0)$ from an observer to a celestial object. This law is mathematically represented as:

$$z = H_0 \, d(t_0), \tag{2.2}$$

where H_0 denotes the Hubble parameter.

The observations of the Coma Cluster made by Zwicky demonstrated an intriguing problem. While redshift measurements indicated an average dispersion velocity of galaxies around 700 km/s, this velocity suggested a need for a far greater mass to maintain the cluster cohesion. Specifically, to prevent the galaxies from dispersing away from the gravitational center of the cluster, a mass of about $10^{13} M_{\odot}$ was required, number that starkly contrasted with the estimated luminous mass of the cluster. The disparity led to the realization that the gravitational mass responsible for holding the cluster together exceeded the luminous mass. Zwicky original analysis, while groundbreaking, did not account for the mass of interstellar gas [23], a component later recognized as significantly contributing to the total mass of such clusters. However, even with the inclusion of interstellar gas mass in contemporary assessments, the total mass of the Coma Cluster remains significantly lower (approximately six times less) than the mass needed to bind the galaxies within a single gravitational potential.

In confronting those discrepancies between theoretical models and observational data in astrophysics, two primary hypotheses emerged. The first was a radical rethinking of gravitational theory and the methods used to determine the luminous mass of galaxies. This line of research led to the development of Modified Newtonian Dynamics (MoND) [24]. This framework proposed a modification to the Second Law of Motion of Newton for scenarios involving large accelerations, reformulating the force equation as:

$$\vec{F} = m\vec{a} \;\rightarrow\; \vec{F} = m\vec{a}\mu(a), \tag{2.3}$$

where $\mu(a)$ is approximately 1 for low accelerations and changes to $\mu(a) = a/a_0$ for high accelerations, with $a_0 \approx 10^{-10}$ m/s^2 as a constant [22]. Although MoND provided a compelling explanation for the velocity dispersion observed in galaxies and clusters, it struggled to account for other phenomena indicating the presence of additional mass, such as cluster collisions and insights from the CMB.

The second hypothesis, pioneered by Zwicky and gaining more widespread acceptance over time, suggested the existence of an unseen form of matter. Zwicky, noting the vast discrepancy between the gravitational mass and the luminous mass in the Coma Cluster, posited a type of matter that neither emitted nor reflected light, and hence was undetectable by telescopes.This hypothesis has been supported by a range of large-scale astronomical observations since the 1930s. Interestingly, all indications of DM existence, from the initial studies of the Coma Cluster to more recent investigations, point to its presence in structures significantly larger than globular star clusters. This discrepancy underscores the existence of unseen matter, now known today as *dark matter*, which continues to be a central topic in astrophysical research and theoretical modeling.

2.2 Galactic Halo

The initial reception to concept of DM by Zwicky was held with skepticism, with a scientific community reluctant to embrace this idea [25]. It persisted until late 1960s, when new lines of evidence began to surface, notably from the studies by Vera Rubin [26]. The investigation performed by Rubin focused on the behavior of stars in spiral galaxies, particularly those distant from the galactic center. Her observations revealed a curious anomaly: contrary to expectations, the radial velocity of these stars did not decrease in line with the $1/\sqrt{R}$ relation, where R represents the radial distance from the galactic center. Rather, these velocities remained constant, suggesting that stars at the periphery of galaxies should theoretically be thrown out into space unless some unseen force was acting upon them.

This phenomenon can be illuminated through the principles of Newtonian dynamics. The theory dictates that the centripetal acceleration needed to sustain an object in uniform circular motion is given by:

$$|\vec{a}_c| = \frac{v_{rad}^2}{R}, \tag{2.4}$$

with v_{rad} being the radial velocity. In a galactic context, if this acceleration arises from a spherically symmetric mass distribution $M(R)$ within the galaxy, Newtonian gravitation provides the equation:

$$|\vec{a}_c| = \frac{v_{rad}^2}{R} = \frac{GM(R)}{R^2}, \tag{2.5a}$$

$$v_{rad} = \sqrt{\frac{GM(R)}{R}}, \tag{2.5b}$$

where $M(R)$ is the mass enclosed within a sphere of radius R, given a density distribution $\rho(r)$, calculated as:

$$M(R) = 4\pi \int_0^R \rho(r) r^2 \mathrm{d}r. \tag{2.6}$$

The distribution of luminous mass in spiral galaxies, predominantly concentrated in the central core and disk, follows a specific mass distribution profile $M(R)$, enabling the estimation of the galaxy total mass. However, as shown in Figure 1, the radial velocities of stars within these galactic disks defy expected patterns. Rather than decreasing as $1/\sqrt{R}$ for distances beyond 10 kpc (1 pc $\simeq 10^{13}$ km), these velocities remain relatively constant. This observation strongly suggests the presence of an additional, unseen mass component in the galactic halo.

The presence of DM is not exclusive to spiral galaxies; it also manifests in elliptical and irregular galaxies, as evidenced by the mismatch between their observed total mass and the mass inferred from luminous sources. Unlike spiral galaxies, where DM presence is inferred from rotational curves, elliptical and irregular galaxies require different

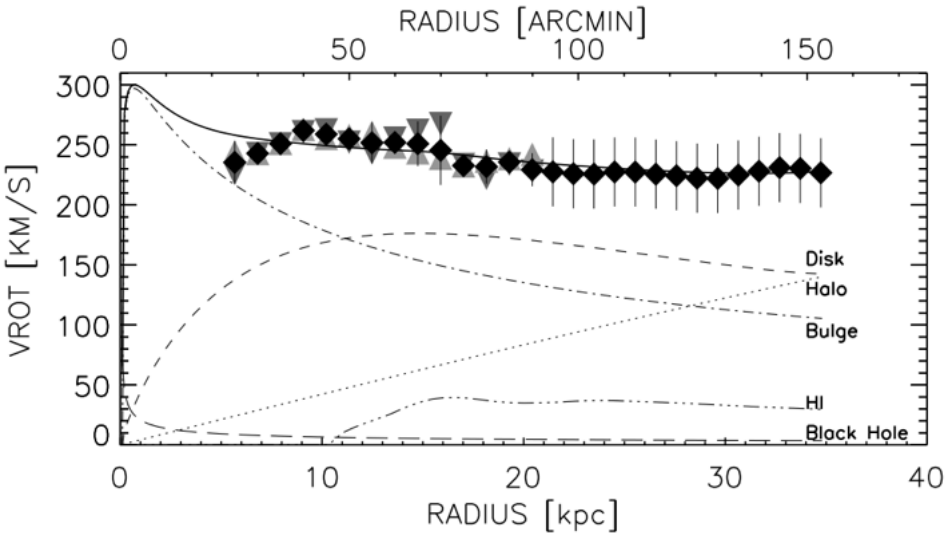

Figure 1 – The rotation curves of the Andromeda Galaxy (M31) offer a compelling visualization as the radial velocity of the most distant stars does not decay with $1/\sqrt{R}$ in the expected way, remaining almost constant as the radius of the galaxy halo increases. The data shown are measurements obtained with advanced telescopes and enhanced data and image processing techniques as documented in [27]. This flatness of the rotation curves contrasts with the expected decrease in rotational velocity based on the distribution of luminous mass alone and supports the hypothesis of an additional, unseen mass – suggesting the presence of Dark Matter in the outer regions of the galaxy.

observational techniques to detect DM. A prominent method employed for these galaxy types is the study of gravitational lensing effects. Gravitational lensing, a concept that will be elaborated in the subsequent section, offers an excellent tool for detecting and understanding DM in these less structurally defined galaxies. The effectiveness of this method substantiates the widespread existence of DM across various galactic forms.

2.3 Lensing Effects

The DM gravitational influence extends far beyond the motion of stars and galaxies, as it also affects light, a phenomenon consistent with General Relativity (GR) predictions. This effect was first empirically demonstrated in a landmark 1919 expedition to Sobral, in Brazil [1]. During a solar eclipse, scientists observed a deviation in the apparent position of a star near the solar corona, consistent with predictions made by Albert Einstein [28]. The observed deviation, approximately 1.7" arc, matched earlier theoretical predictions proposed by Einstein that light rays passing near a massive object (like the Sun) would

[1] An expedition was also sent to the island of Principe, off the west coast of Africa, but due to bad weather, confirmation only came from the expedition headed to Brazil. Besides, during the years before this confirmation, expeditions tried to measure deviations in other parts of the world, including another one to Brazil, at Passa Quatro, in the state of Minas Gerais, which also did not result in confirmation of the theory at the time.

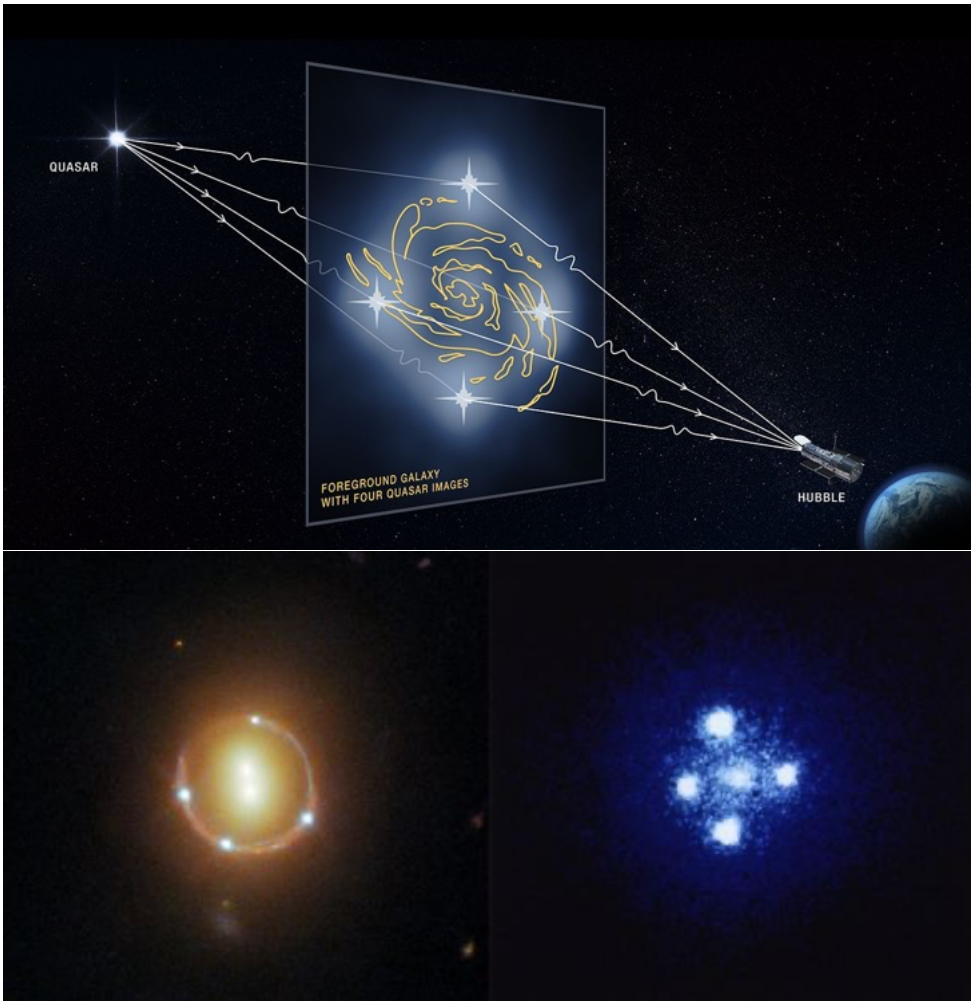

Figure 2 – (Top panel) Schematic representation of the distortion of light due to gravitational lensing effects [29]. (Bottom panel) Observational image of a distant quasar, distorted and multiplied by lensing effects. [29].

bend [5]. This bending, or deflection angle, is given by $\alpha = 4GM/b$, where M represents the mass source of the gravitational field and b the impact parameter between the light ray and the mass, illustrated in Figure 3.

Given DM greater total mass compared to baryonic matter, it is reasonable to hypothesize that DM in galaxies forms a spherical halo around them, distributed in a relatively homogeneous and isotropic manner (see Figure 2). This technique can test whether DM is comprised of Massive Compact Halo Objects (MACHOs), potentially familiar astrophysical objects like brown dwarfs, white dwarfs, neutron stars, or black holes [5]. If MACHOs were a significant component of DM, it could negate the necessity for new physics to explain the observed mass discrepancies.

However, recent studies using gravitational lensing [30, 31] suggest that MACHOs contribute only to a small fraction to the total mass of galaxies. The lack of substantial lensing effects from MACHOs is what implies their limited presence. Besides, the search for MACHOs continues, as recent gravitational wave detections indicate a larger-than-expected

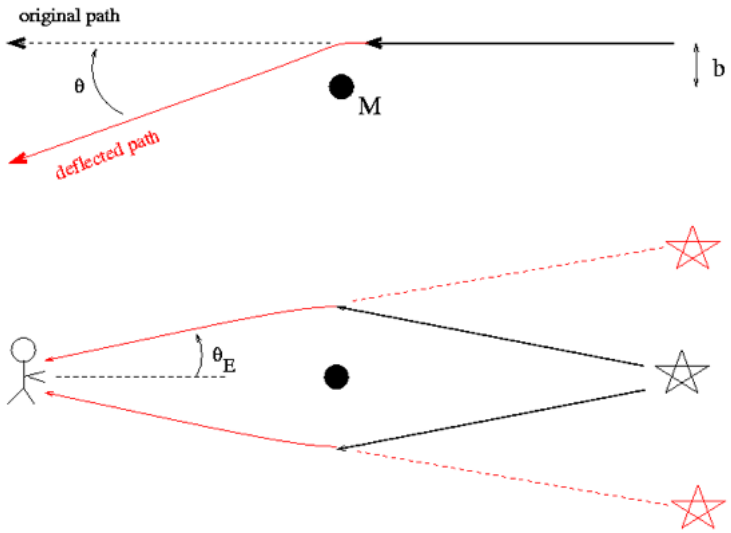

Figure 3 – The deflection of light by a massive object is a critical concept, visually represented here as how a light ray is bent by a massive object [5]. A distant observer, in addition to being able to observe the same object in a different location than expected, depending on the angle in relation to the observed object, can see two or more images of the same object.

population of massive objects, such as black holes and neutron stars [32], which could revise our understanding of DM composition.

The Bullet Cluster

The Bullet Cluster, comprising colliding galaxy clusters, stands as an important piece of observational evidence supporting the existence of DM. This cluster helps to illustrate the separation between gravitational and baryonic masses in colliding galaxy clusters. This separation is inferred from gravitational lensing, tracing the total mass distribution, X-ray emissions, and the hot gas, which is the majority of the baryonic matter. In these observations, the observed hot intra-cluster gas seems to lag from DM, staying behind the galaxies during the collision, as shown in the Figure 4. This phenomenon, depicted through gravitational lensing, indicates that the majority of the mass aligns with the galaxy locations rather than with the gas clouds, suggesting a significant presence of invisible matter.

This event has been important in confirming the concept of a collisionless DM, as the electromagnetic interactions slow down the hot gas during collisions, causing a discrepancy between the distribution of baryonic matter and the gravitational mass. Such observations have prompted revisions in some DM models, especially regarding self-interacting DM (SIDM), by imposing stringent constraints based on the dynamics witnessed within the Bullet Cluster [35, 36].

Studies have make use of large-volume N-body simulations to show that conditions

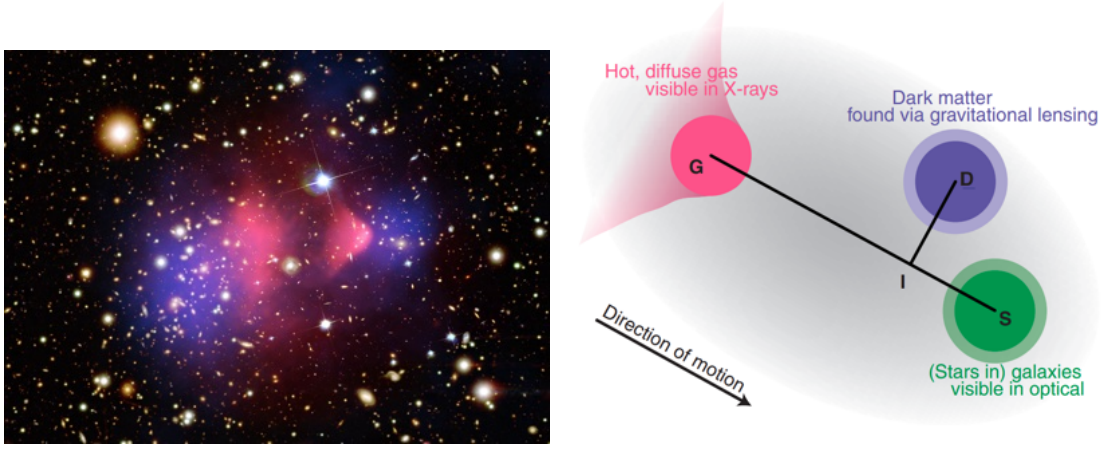

Figure 4 – The image on the left shows an artificially colored photograph of the collision of clusters known as a the Bullet Cluster. The bluish region shows the concentration of DM, while the part colored in red reflects the intracluster gas heated during the collision of the clusters. On the right, we see a diagram showing the direction of motion and where the gravitational centers of gas,DM and stars are visible in the image. [33, 34].

similar to the Bullet Cluster, such as high pairwise velocity and significant separation between dark and baryonic matter, are not only possible but probable within the CDM model, thereby supporting the notion of collisionless DM without challenging the current cosmological framework [37]. Additional research has used observations of 72 galaxy collisions, including both major and minor mergers, to statistically infer the existence of DM with significant confidence, further corroborating the DM hypothesis through observations similar to those made in the Bullet Cluster [34].

Furthermore, the Bullet Cluster has been used to establish upper bounds on the cross section for DM scattering. The negligible observable separation between DM and stellar components in these cosmic events implies that DM particles exhibit minimal interaction with each other and with baryonic matter. Also, the way the positions of gas, stellar and DM gravitational masses are measured can significantly impact derived constraints on DM self-interaction cross section [38]. Several simulations, including both self-interacting DM and gas, showed that, as gas is stripped, it introduces radially dependent asymmetries into the stellar and DM distributions, affecting measurements of separation and, therefore, constraints on interaction cross sections [38]. The lack of deceleration observed in the collision of the Bullet Cluster has constrained the self-interaction cross section to $\sigma_{DM}/m < 1.25$ cm^2/g for long-range forces [1].

Collectively, these insights not only highlight the presence of an additional mass component in clusters via gravitational lensing techniques but also significantly constrain certain DM models. These are convincing arguments that DM is predominantly collisionless, engaging in minimal interaction with both baryonic matter and itself.

2.4 Cosmic Microwave Background

In 1965, a discovery at Bell Laboratories marked an important moment in astrophysics. Radio astronomers Arno Penzias and Robert Wilson, while grappling with persistent noise in their microwave antenna, inadvertently stumbled upon a groundbreaking finding [5, 21]. Despite exhaustive efforts to eliminate this noise (including removing a pair of pigeons nesting in the antenna), the signal persisted. This isotropic microwave noise was not linked to any known celestial source. Only later the significance of this persistent noise became clear: it turned out to be a critical piece of evidence validating the Big Bang theory. Now known as the Cosmic Microwave Background (CMB), this radiation matched the characteristics of a black body spectrum peaking at a temperature of $T = 2.7255 \pm 0.0006$ K [1]. This discovery supported theories that suggested the Universe, once in a hot and dense state, emitted electromagnetic radiation that, due to its expansion, is now observable at very low frequencies.

After the Big Bang, the Universe experienced several cooling phases, including a recombination phase where protons and electrons formed the first hydrogen and helium atoms. Following this phase, with the ongoing expansion of the Universe, there came a time when its matter density allowed previously opaque photons to scatter in all directions. This radiation, emitted during the so-called *last scattering* period, had a black body temperature of around 3000 K. However, due to redshift effects, this radiation now reaches Earth, approximately 13.5 billion years later, with an average temperature of 2.72 K. This discovery of the CMB has been a cornerstone in our understanding of cosmology [21].

The path to our current understanding of the CMB has been challenging. The initial obstacle in studying the CMB was the high noise level in the data, attributed to a infinity of celestial sources. Overcoming this required intricate noise reduction techniques. An illustrative example involved adjusting for the detection satellites velocity relative to the Universe, considering the motion of the Earth around the Sun, the motion of the Sun within the Milky Way, and the movement of the galaxy within our local group and beyond [5, 21]. This complex calculation resulted in an effective velocity of about 630 km/s against the cosmic backdrop from which the CMB originates.

The resolution and clarity of the CMB map have progressively improved with each successive experiment. Beginning with the Cosmic Background Explorer (COBE) and advancing through the Wilkinson Microwave Anisotropy Probe (WMAP), the most detailed insights have been provided by the Planck satellite [2]. Planck comprehensive data sets and improved statistical methodologies have greatly refined our understanding of the CMB.

One of the primary goals in studying the CMB is to estimate the current composition of the Universe in terms of matter, radiation, and accelerated expansion. These

investigations provided approximations of the total amount of DM based on standard cosmological models. These models also predict how matter inhomogeneities are distributed throughout the Universe [21]. At the moment of the last scattering, the observable Universe had a radius of merely 0.2 Mpc. In this early stage, DM played a dominant role in shaping the Universe energy density, leading to the formation of the earliest gravitational potential wells. The energy density of DM, $\varepsilon(\vec{r})$, is defined as the sum of the Universe average energy density, $\bar{\varepsilon}$, and small fluctuations, $\delta\varepsilon(\vec{r})$. The gravitational potential, $\delta\Phi$, arising from these fluctuations, can be expressed in Newtonian terms as:

$$\nabla^2 (\delta\Phi) = \frac{4\pi G}{c^2}\delta\varepsilon. \tag{2.7}$$

When CMB photons traverse these gravitational potential wells, they experience energy shifts, a redshift in regions of higher DM density and a blueshift in lower density areas. These shifts manifest as temperature variations in the CMB, as vividly captured in the data of Planck satellite (see Ref. [39]). This phenomenon was mathematically detailed by Sachs and Wolfe in 1967 [40], who established the relationship between these temperature fluctuations and the gravitational potential variations:

$$\frac{\delta T}{T} = \frac{1}{3}\frac{\delta\Phi}{c^2}, \tag{2.8}$$

where T represents the CMB average temperature, δT its variation, and $\delta\Phi$ the gravitational potential fluctuation. This relationship underscores the intricate interplay between the matter of the Universe distribution and the properties of the CMB. The Sachs-Wolfe effect, described by Equation 2.8, reveals a fundamental aspect of cosmology: the temperature variations in the CMB provide insights into the gravitational potential wells of the early Universe, predominantly shaped by DM. This effect traces the relationship between the CMB temperature differences and the gravitational fields of the Universe, which are significantly influenced by the uneven distribution of DM. Sophisticated analyses of these variations enable scientists to derive estimates of various cosmological quantities, including the total amounts of DM, baryonic matter, and radiation [5].

Advancements in this field of study have led to a more comprehensive understanding of the matter-energy composition of the Universe. Current data and interpretations, as illustrated in Figure 5, suggest a Universe composed of about $(68.5 \pm 0.7)\%$ dark energy, which drives the accelerated expansion of the Universe, $(26.5 \pm 0.7)\%$ DM, and merely $(4.93 \pm 0.06)\%$ conventional baryonic matter [1,2]. This distribution characterizes a cosmos where dark energy and DM dominate, far surpassing the baryonic matter that constitutes the visible part of the Universe. These findings are central to understand the structure of the Universe and evolution.

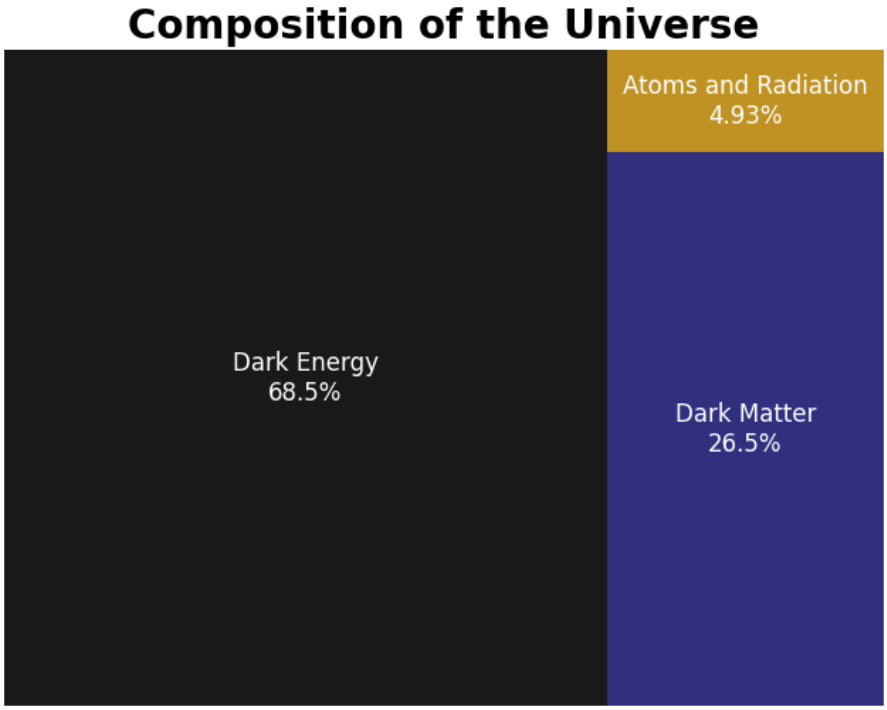

Figure 5 – This graph is a visual representation of the current distribution of matter and energy in the known Universe. This distribution has not been static; it has evolved as the Universe has aged. Recent measurements and studies, however, suggest that the current proportions, as depicted in this graph (errors omitted for clarity), accurately reflect the Universe present state [1, 2].

2.5 Evidence from large scale structures

The most common cosmological model indicates that DM in the Universe must be of a *cold* nature during the matter-radiation dominated era [5]. This classification implies that any detectable DM particle should have an average velocity significantly lower than a third of the speed of light, ensuring that these particles are nonrelativistic. Understanding why this condition is essential requires examining the large-scale structures within the Universe and their formation.

The story of DM began with its influence on the movement of galaxies and stars, but its implications extend much further, affecting the distribution and positioning of massive cosmic structures much bigger than galaxies itself. These large-scale structures provide crucial observational evidence for the existence of DM [5]. To study these structures, astronomers often employ the redshift of galaxies, using the Hubble relation $d = (1/H_0)\, z$, where H_0 is the Hubble constant, estimated to be around 67.4 km s^{-1} Mpc^{-1} [1, 2]. Analysis of galaxy distributions shows that galaxies are not randomly scattered but form specific structures, like clusters and superclusters, and vast voids. Superclusters, still collapsing under their gravity, contrast with smaller, more stable clusters. Voids are characterized by their low density and approximate spherical shape. Cosmologists often describe the

arrangement of these large-scale structures using terms like *spongy* or *foamy* [5].

The formation of these structures, far from being straightforward, can be understood as the result of the growth of gravitational instabilities [5]. These instabilities originate from initial inhomogeneities in the matter distribution of the early Universe. This process is crucial for understanding the role of cold DM, as it is the gravitational effect of this unseen matter that drives the formation and evolution of these cosmic structures. The study of these structures, hence, not only supports the existence of DM but also provides insights into its nature and distribution in the cosmos.

The analysis of gravitational instabilities reveals a significant insight: solely relying on baryonic matter, not enough time would have passed since the Big Bang for such matter to collapse into large structures like galaxy clusters. This timing issue arises because the decoupling of baryonic matter from radiation occurred relatively late, about 300,000 years after the Big Bang (at a redshift of approximately 1100). Consequently, the Universe must have had some initial assistance in forming these gravitational instabilities, a role fittingly played by DM [21]. The DM, in contrast to the baryonic matter, interacted minimally with conventional matter and decoupled much earlier in the history of the Universe (see chapter 4). This early decoupling allowed DM to form the initial gravitational potential wells, which later attracted baryonic matter and radiation.

To replicate the cosmic structures we observe today, DM particles had to be predominantly nonrelativistic when matter and radiation densities were equivalent [5]. If DM were relativistic, its high-velocity particles would smooth out small-scale gravitational instabilities, leading to the formation of only massive structures like super-clusters. However, observational data [41], particularly from high redshifts, show a different sequence. Stars and galaxies formed first, followed by the ongoing formation of clusters and superclusters from these smaller entities. This pattern is indicative of the presence of cold DM [21]. While there is a possibility for *hot* or *warm* DM, such as neutrinos, to exist, their contribution to the total density of the Universe is limited (between 0.12% and 3% [1]). Exceeding this range would challenge the accuracy of our current observational data. Therefore, the majority of the relic DM in the Universe today is believed to be cold DM. This conclusion is drawn from both observational evidence and theoretical models related to the formation of the large-scale structures of the Universe.

The Lambda Cold Dark Matter (LCDM) model, that incorporates the cosmological constant Λ, is a great piece for our current understanding of cosmology. It has been remarkably successful in describing the large-scale structure of the Universe, the CMB radiation, and the accelerating expansion of the Universe due to the dark energy related to Λ. Despite its triumphs at large scales, the LCDM model faces significant challenges at smaller scales, particularly in galaxy formation and dynamics within approximately 1 Mpc [1, 42]. These discrepancies between observations and the simulations predictions

have led to what are commonly referred to as the *small-scale challenges* [42].

Among the most prominent of these challenges are the *missing satellites problem*, the *cusp-core problem*, and the *too-big-to-fail problem*. The missing satellites problem arises from the observation that the number of satellite galaxies detected orbiting the Milky Way and other similar galaxies is significantly fewer than the number predicted by LCDM simulations. The cusp-core problem refers to the density profiles of DM in the central regions of galaxies. While LCDM predicts sharp, cuspy density profiles, observations of low-surface-brightness galaxies and dwarf galaxies suggest that the density profiles are much flatter, or *cored*. Lastly, the too-big-to-fail problem highlights the issue that the most massive sub-halos in LCDM simulations of Milky Way-like galaxies appear to be too dense to host the brightest observed satellite galaxies, contradicting expectations based on the model. Solutions proposed range from invoking baryonic physics processes, such as feedback from supernovae and active galactic nuclei, which could alter the distribution of DM in galaxies, to considering alternative DM properties, such as self-interacting DM, which could lead to less dense central regions in galaxies. Furthermore, advances in astronomical observations, including deeper surveys of satellite galaxies and more precise measurements of galaxy rotation curves, along with improvements in numerical simulations that incorporate complex baryonic physics, hold the promise of resolving these challenges [1, 42].

The analysis of the role of DM in the formation and evolution of large scale cosmic structures shows its importance in cosmology. This evidence, drawn from the distribution of galaxies and observed gravitational instabilities, strongly supports the predominance of cold DM component in the universe. Despite the success of LCDM in explaining these structures and the accelerating expansion of the Universe, challenges at smaller scales highlight the need for further refinement of our understanding of the DM nature and interactions. These efforts not only aim to solve small-scale challenges, but also deepen our understanding of the fundamental components and forces that shape the Universe.

3 Approaches for dark matter searches

The SM of particle physics is an extraordinary theory for successfully elucidating a wide array of physical phenomena. However, it falls short in addressing several unresolved issues in physics, particularly at extremely high-energy scales, like those near the Planck scale (around $M_P \approx 1.2 \times 10^{19}$ GeV) [43]. Theories extending beyond the SM, especially those aiming for a grand unified theory (GUT) [44], face the challenge of explaining the stark disparity between the various fundamental interactions (strong, electromagnetic, weak, and gravitational) observed at the energy scales accessible by current experiments. The absence of a description of gravity at quantum level within the SM framework is also a significant limitation, highlighting the hierarchy problem [45] and the need for a quantum theory of gravity [46].

Besides that, one notable gap in the SM is of course its complications to include a particle that matches the known characteristics of DM, which has been evidenced through gravitational effects in the Universe (see chapter 2). Some SM particles, due to their low masses, have relativistic velocities at the time of decoupling from baryonic matter, which would classify them as *hot* DM, inconsistent with astrophysical observations [1], as outlined in chapter 4. Thus, neutrinos for example, contribute only marginally to the unidentified matter in the Universe. Given these inadequacies, exploring SM extensions that might encompass new particles and interactions seems not only plausible but necessary for a more comprehensive understanding of the Universe. So far, no significant deviations from the SM have been observed, and the quest for new physics largely revolves around theoretical speculations and indirect evidence, such as the gravitational detection of DM and fine-tuning in symmetry violation parameters [47].

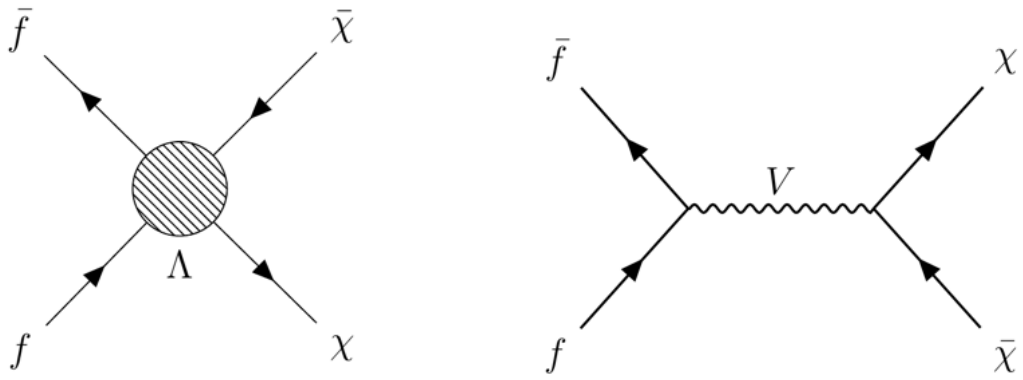

Figure 6 – (Left) Simplified diagram of an effective model for $f\bar{f} \to \chi\bar{\chi}$, where Λ represents a scale factor, in mass units, determining the viability energy scale of this process. Models like this, which do not take into account many details of the physics involved, are called *effective*. (Right) Simplified diagram of an interaction model for DM, where the dark sector interacts with the SM through a spin-1 mediator.

Extensions of the SM are often explored through various models, including effective, simplified, or more comprehensive ones, each with its set of advantages and limitations in both theoretical and experimental contexts. However, even the simplest effective models can offer substantial insights into the nature of potential new physics [48]. These models typically focus on the initial and final states of a process without delving into the specifics of the mediator particle where the emphasis is on a scale factor Λ (see Figure 6). Simplified models, such as the one this work will present, are valuable for their focused approach to studying new interactions. They describe particles and interactions using a limited set of parameters that have direct correlations with experimental observations, including particle masses, decay widths, and production cross sections [49]. Despite some limitations in generalization, simplified models avoid the complexities and constraints of more complete models [21]. In the upcoming chapters, we will explore how these models can be fine-tuned to reflect experimental data more accurately, enhancing our understanding of potential new physics.

In crafting an extension to the SM through simplified models, particularly for incorporating DM, developing a new Lagrangian that integrates novel degrees of freedom is crucial. The model proposed in section 3.5 adheres to several critical criteria essential for a viable DM extension: (i) The stability of the DM particle, that is the foremost requirement of the DM particle being introduced, as a stable DM particle is fundamental for it to persist across the cosmic timeline and to exert the gravitational influences observed in galactic and large-scale structures; (ii) the renormalizability and symmetry consistency, as operators within the new model Lagrangian must be renormalizable, ensuring that the its predictions remain finite under various conditions, and the model must maintain consistency with established symmetries, notably Lorentz and gauge invariance, which are foundational principles in modern physics; (iii) Also, the extended model should respect core SM symmetries, such as the conservation of baryon and lepton numbers, for while there may be potential for flavor symmetry violations through new physics associated with DM, any such deviations must be minimal to align with existing experimental evidence [21].

The proposed model which we will address in this work, consisting of the proposal of a new spin-1 mediator boson that mediates interactions with the dark sector, is widely applied and well known in the literature [49–55], meets these requirements and offers a framework for exploring DM properties and interactions. By focusing on the critical components and parameters, the simplified models facilitates a clearer understanding of how DM might interact within the broader context of the SM. This simplified model serves as a theoretical tool for understanding DM within the context of particle physics and provides a basis for experimental investigations in particle colliders.

3.1 Theoretical Models Plethora

In recent decades, various approaches have been explored to integrate DM into the SM [51, 55–58], each distinct in its methodology. These approaches aim to address the intricacies of DM by proposing models that not only align with the known physics but also venture into new theoretical territories. While discussing these models, it is essential to adhere to certain fundamental criteria for a viable DM candidate, as previously outlined. These criteria include gravitational interaction with conventional matter, an explanation for the observed DM abundance in the CMB, and the existence of stable or long-lived particles that do not exhibit electromagnetic interactions. Additionally, the candidate should be *cold*, i.e. nonrelativistic, during the matter-radiation equality era to facilitate the formation of the first gravitational potential wells of the Universe [21].

Several DM candidates have been proposed in the literature. Before diving into our specific model of interest, we will briefly overview some of the more prominent categories of DM candidates:

WIMPs (Weakly Interacting Massive Particles): These are among the most extensively studied DM candidates. Such particles are attractive because they can naturally produce the correct DM abundance observed in the CMB through thermal equilibrium processes in the early Universe. The expected annihilation cross section of WIMPs falls within the range necessary to account for the DM abundance, making them a focal point of both theoretical studies and experimental searches. Various models fall under the WIMP category, including Higgs Portals, dark photons, Z' bosons, and a range of effective models [55, 59–64].

Axions: Initially proposed to address the CP violation in strong interactions in the Peccei-Quinn theory [65], axions have also been considered potential DM candidates. They are theorized to be pseudo-scalar particles with very small mass and weak interactions with ordinary matter. Axions have been implicated in various astrophysical phenomena and are a subject of ongoing studies [66, 67].

Supersymmetry (SUSY): Models that extend the SM by introducing superpartners for each particle, differing in spin by half a unit. These models offer potential DM candidates, like the neutralino, and address other significant theoretical issues, such as the hierarchy problem. Despite the lack of direct evidence for SUSY, its theoretical appeal keeps it at the forefront of DM research [68].

Extra Dimensions: Theories involving extra dimensions propose that our known Universe might just be a part of a larger multidimensional structure. These models suggest that DM could be composed of particles associated with these extra dimensions, presenting a novel way to conceptualize the nature and behavior of DM [68–71].

MAssive Compact Halo Objects (MACHOs): Due to the absence of direct

experimental evidence for a specific particle candidate, the hypothesis that DM problem might be explained by MACHOs has gained traction. This category includes low-mass black holes or compact stars that remain elusive to astronomical observations. The MACHO framework presents a fascinating alternative that could account for all or a significant portion of the observed DM abundance. This hypothesis confronts theoretical challenges, particularly in reconciling with CMB observations and elucidating the mechanisms by which such massive compact objects could form in the early Universe. The advent of gravitational wave astronomy has opened new avenues for exploring these challenges. The detection of gravitational waves from black hole mergers by facilities like LIGO and Virgo has not only confirmed the existence of black holes in mass ranges that were previously speculative [72, 73] but also provided a tool for probing the early dynamics of the Universe. These observations could offer indirect evidence of MACHO-type DM by revealing a population of black holes or compact objects that contribute to the gravitational framework of the cosmos.

Other than that, there is a diverse range of theoretical possibilities, such as sterile neutrinos, WIMPzillas, FIMPs (Feebly Interacting Massive Particles), SIMPs (Strongly Interacting Massive Particles), CHAMPs (CHarged Massive Particles), and more. Each of these offers unique insights and theoretical implications for the nature of DM [74–77]. In this work, our focus will be on simplified WIMP model that introduces a new massive spin-1 mediator, Z', and explores three types of stable DM candidates. These candidates are primarily differentiated by their interaction with the Z' boson. This model, which we will detail in the forthcoming sections, aims to provide a comprehensive and scientifically plausible framework for DM.

In an effort to characterize DM as a particle, studies have proposed a variety of experimental strategies. While gravitational evidence for DM is compelling, as detailed in chapter 2, it ends up not sufficient for unraveling the full spectrum of DM properties. To bridge this gap, scientists have turned to experimental approaches on Earth and in space, based on the premise that DM might engage in nongravitational interactions with ordinary matter [78]. Despite the challenges and lack of conclusive results thus far, these experiments have progressively refined our understanding of DM by excluding a great range of parameter space [1, 57, 79].

The quest to detect DM particles is grouped into three primary categories: indirect, direct, and collider detection. The *indirect detection* hinges on capturing potential byproducts of DM annihilation, such as photons, neutrinos, and antimatter, originating from cosmic sources. The focus is on the detection of these secondary particles as indirect evidence of DM. As *direct detection* we understand the approaches that involves observing scattering events between DM and SM particles using fixed targets. The hypothesis is that the DM permeating our galaxy would interact with Earth-based detectors, revealing

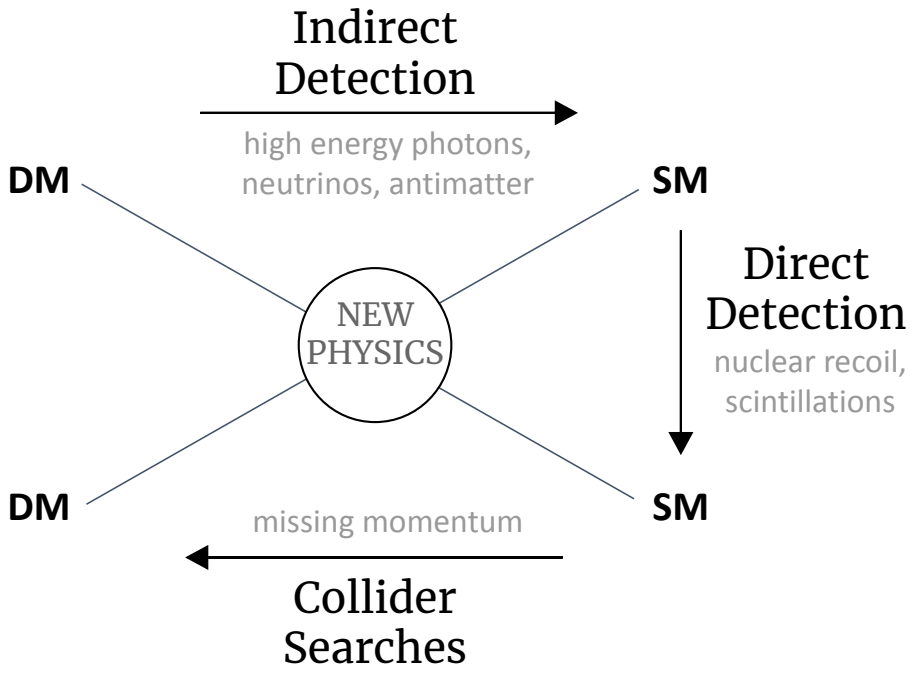

Figure 7 – Illustrative diagram of potential interaction channels between SM particles and DM. The diagram illustrates three primary research methods: Indirect Detection (via high energy photons, neutrinos, antimatter), Direct Detection (through nuclear recoil, scintillations), and Collider Searches (characterized by missing momentum and signals from initial state radiation).

their presence through atomic nucleus recoils. The efficiency of these experiments relies on accurately determining the velocity, density, and interaction cross section of DM with nucleons [68]. Also, the *collider detection* (or collider searches) aims its efforts to generate DM particles through high-energy collisions of SM, focusing on identifying missing momentum (p_T^{miss}) indicative of DM production. These methods are visually summarized in Figure 7, and further explored in subsequent sections, focusing on key experiments and their contributions to our understanding of DM.

3.2 Direct Detection

If the galaxy is teemed with DM particles, like WIMPs, these should be detectable as they interact with terrestrial targets.Direct detection experiments are grounded in a concept that resonates with it. The motion of the Earth relative to the galactic plane could result in a discernible DM *wind*, with the recoil of atomic nuclei in detectors providing measurable signals. The key to these experiments lies in the DM particles speed, their density distribution, and the scattering cross section with nucleons [68]. These experiments have evolved over the years, employing various materials and detection techniques. These range from scintillators, which emit photons upon excitation, to direct photon detection in strong magnetic fields, and ionization-based methods where DM interactions ionize atoms

within the detector. Each technique has its unique advantages and challenges, contributing to the diverse experimental landscape of DM research [1, 68, 80–83].

When a DM particle collides with an atomic nucleus within a detector, it imparts energy, resulting in nuclear recoil. This recoil manifests as a detectable signal, providing direct evidence of DM. The frequency of such events hinges on the velocity distribution of WIMPs, their density within the galaxy, and their scattering cross section with standard nucleons [68]. We can express the event rate R in a detector as:

$$R \approx \sum_i \left(\frac{\text{Total Mass of Detector}}{\text{Atomic Mass of species } i} \right) \times \left(\frac{\rho_\chi}{m_\chi} \right) \times \langle \sigma_{i\chi} \rangle, \tag{3.1}$$

where ρ_χ and m_χ denote the energy density and mass of the DM particle χ, respectively, and $\langle \sigma_{i\chi} \rangle$ represents the scattering cross section between the DM particle and a nucleon species i in the detector.

Innovative methods such as combining ionization and scintillation, or ionization with photo-detection, are being employed to enhance the detection capabilities for potential DM events. The XENONnT [84], a leading experiment of its kind situated in Italy, operates using a vessel filled with liquid and gaseous Xenon, all within an electric field. This setup ensures that any interaction by a DM particle within the tank leads to scintillation, which is then captured by photo-multiplier tubes positioned at both ends of the cylindrical tank. The XENONnT Collaboration has recently published findings that cast doubt on low-mass DM models, challenging previous assumptions of an observed excess indicative of Axion Like Particles (ALPs) or other bosonic forms of DM [85].

Furthermore, experiments like DAMA/LIBRA [86] and SABRE [87], the latter having facilities in both Italy and Australia, are pioneering in isolating DM signals from experimental noise by monitoring the annual modulation of such events. Due to the minimal nature of this modulation, extensive exposure times and high experimental sensitivity are crucial for detecting these subtle variations [68]. This challenge is compounded by the need to mitigate systematic errors related to seasonal effects, such as changes in weather and solar activity. Remarkably, after several years of observation, DAMA/LIBRA has reported a confidence level of 12.9σ in the annual modulation of detected signals, attributed to DM scatterings in the 10 keV range [86]. These groundbreaking results, however, await independent verification by similar experimental setups, including SABRE. The dual-location of the SABRE operation, near DAMA in Italy and in Australia, aims to eliminate background noise associated with seasonal variations, thus providing a rigorous test of findings of the DAMA/LIBRA experiments [87].

Figure 8 presents the exclusion limits and future projections from various direct detection experiments. These experiments, which primarily focus on atomic nucleus scattering with DM, employ diverse materials and detection technologies. The results from

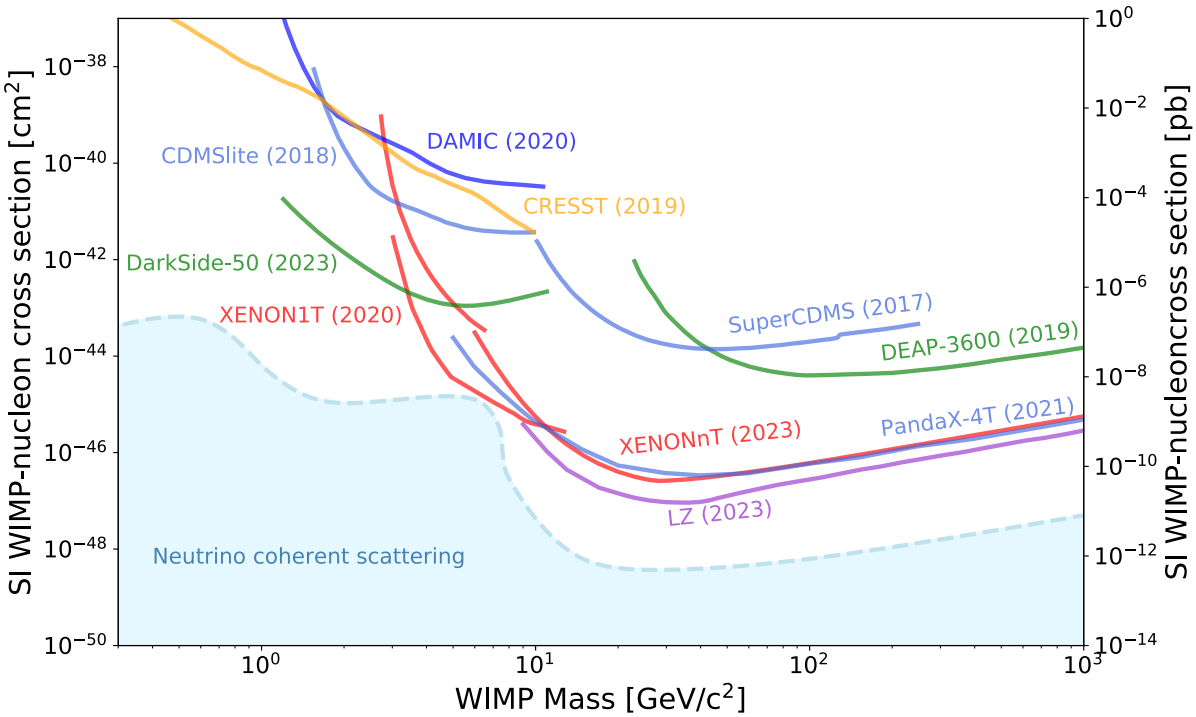

Figure 8 – Compilation of exclusion limits for WIMP-nucleon spin-independent interactions from various direct detection experiments, along with future projections. The region in pale blue is known as *neutrino fog* and marks the threshold where neutrino interactions from coherent scatterings may start to dominate the background noise, complicating the detection of DM signals [1, 79].

these experiments are important for parameterizing DM models and identifying areas that require further theoretical and experimental exploration [1, 79, 88].

Furthermore, recent advancements propose novel methods for detecting light DM particles, applying new techniques by employing materials with low-band gaps, such as superconductors, super-fluids, and Dirac materials, to improve sensitivity to DM-electron scattering at lower energy thresholds. For DM particles in the keV-MeV range, detection strategies include monitoring nuclear recoils in super-fluid helium and observing the breaking of chemical bonds [89]. In the case of ultralight DM – meV-eV range –, methods such as absorption by conduction electrons of superconductors or scattering in polar materials sensitive to dark photons are explored. These developments face the challenge of accurately detecting and differentiating subtle energy depositions from background noise [1].

3.3 Indirect Detection

The quest to detect DM is not only confined to direct methods but also extends to indirect detection strategies. These efforts hinge on the gravitational inferences about existence of DM and aim to detect the after-effects of DM interactions, specifically

annihilation events that produce observable particles [21]. Current calculations estimates the local density of DM at about 0.3 GeV cm^{-3} [1], a value significantly lower than the density of the galactic disk, yet believed to be higher in regions with stronger gravitational fields, like near the center of galaxies or within stars. The expectation is that in these regions, DM densities are high enough to sustain annihilation processes that produce detectable SM particles, despite the cessation of such annihilations post-*freeze-out* as per the standard cosmological model [78, 90].

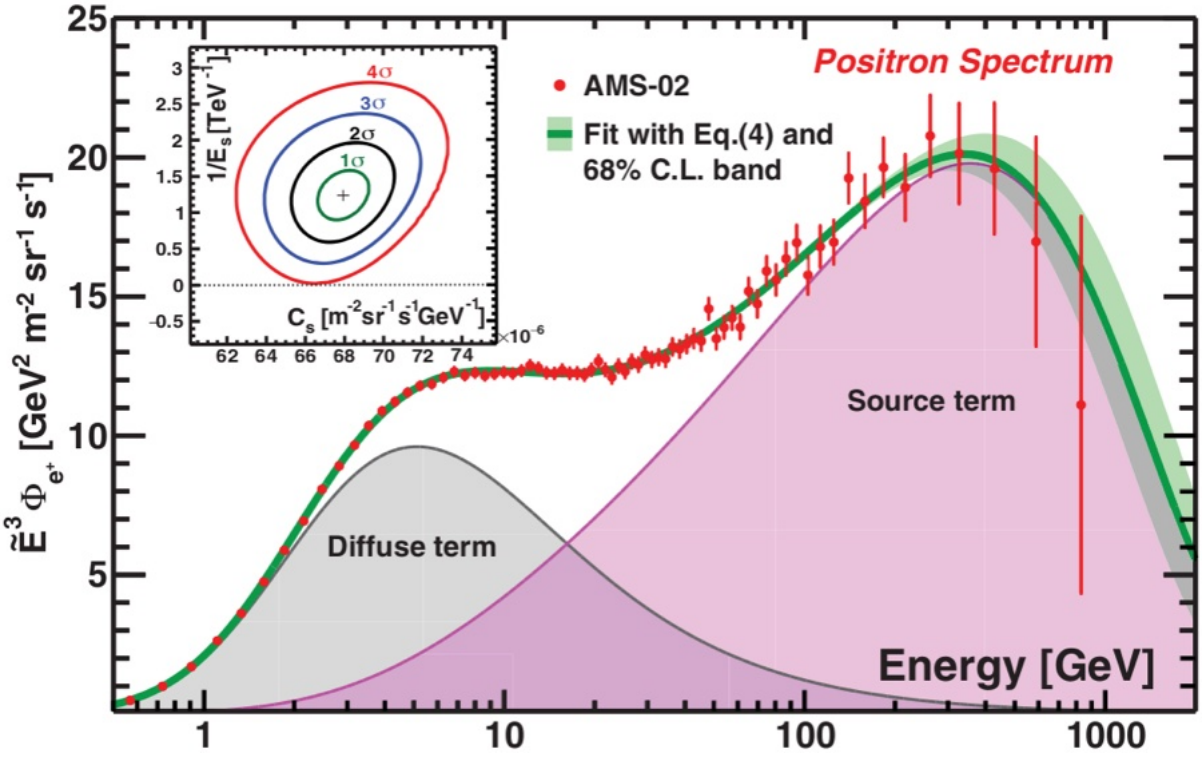

Figure 9 – Precision measurements of cosmic rays by the Alpha Magnetic Spectrometer (AMS-02), with an observed excess in positron flux (pink area) above the expected background (grey area), suggesting potential DM annihilation events [91]. The insert are projections of regions of significance related to cutoff energy (E_s) and a normalization factor (C_s), with 1σ (green), 2σ (black), 3σ (blue), and 4σ red [91].

This annihilation hypothesis claims that DM particles, upon annihilating, produce pairs of particles and antiparticles, or photons, belonging to the SM. These byproducts, especially in the form of electrons, positrons, and photons, are detectable as anomalous surges in flux compared to predictions from known astrophysical sources [78]. Given the slow-motion of DM particles relative to the galactic plane, the energy spectrum of these annihilation products can be analyzed as though the annihilation occurred at rest. This assumption simplifies the analysis and improves the accuracy of detecting these events [78]. Indirect detection experiments thus search for signs of leptons, antiprotons, or photons that might have originated from such annihilations. A typical $2 \rightarrow 2$ annihilation process involving DM might yield positrons or antiprotons, especially if the DM has a way to

couple with quarks. Moreover, secondary particles such as neutrinos could result from the decay of primary annihilation products.

The Fermi Gamma-ray Space Telescope (Fermi-LAT) plays a crucial role in this field by detecting high-energy photons, particularly from gamma-ray sources. Despite the ongoing debate over the data it collects [92, 93], the excess gamma rays observed by Fermi-LAT, especially those emanating from the galactic center, align with predictions for DM annihilation in terms of energy spectrum and intensity. Experiments such as PAMELA and AMS-02 have reported excesses in positron flux, as shown in Figure 9, potentially indicative of DM annihilations [78, 91, 94]. However, these observations alone are not conclusive evidence for DM, as the excesses could also be explained by astrophysical sources like pulsars. Furthermore, these findings are somewhat at odds with data from the CMB [78].

Thus, the observed excess in cosmic rays has been attributed to DM annihilation, yet the absence of similar anomalies in other observational channels, such as antiprotons and gamma rays, coupled with the unique spectral shape, necessitates complex DM models for explanation. An alternative hypothesis postulates that the excess primary positrons could originate from the magneto-spheres of nearby pulsars. However, this pulsar-based theory faced skepticism [1]. Besides, those fluxes of electrons and positrons emanating from DM efficiently lose energy through radiation across various wavelengths, making secondary radiative emission a potential indirect detection channel with distinct spectral and morphological signatures [96, 97]. The primary mechanisms for energy dissipation in high-energy electrons and positrons include inverse Compton (IC) up-scattering of background photons and synchrotron radiation within magnetic fields.

Furthermore, the emergence of gravitational wave detection has sparked a renewed interest in the hypothesis that a portion of DM density, as inferred through observational data, could be accounted for by MACHOs. Such entities, potentially including Primordial Black Holes (PBH) that could have formed in the nascent Universe amid significant density fluctuations, offer a good opportunity for DM research. Figure 11 delineates the exclusion limits for the proportion of DM density these objects might constitute [6, 7].

In summary, while direct detection experiments focus on capturing DM particles themselves, indirect detection methods like those employed by PAMELA, AMS-02, and Fermi-LAT and the future LSST [98] aim to capture the secondary particles produced by DM annihilation. These methods, though still inconclusive, have narrowed the search for DM by providing critical data on its possible interactions and effects.

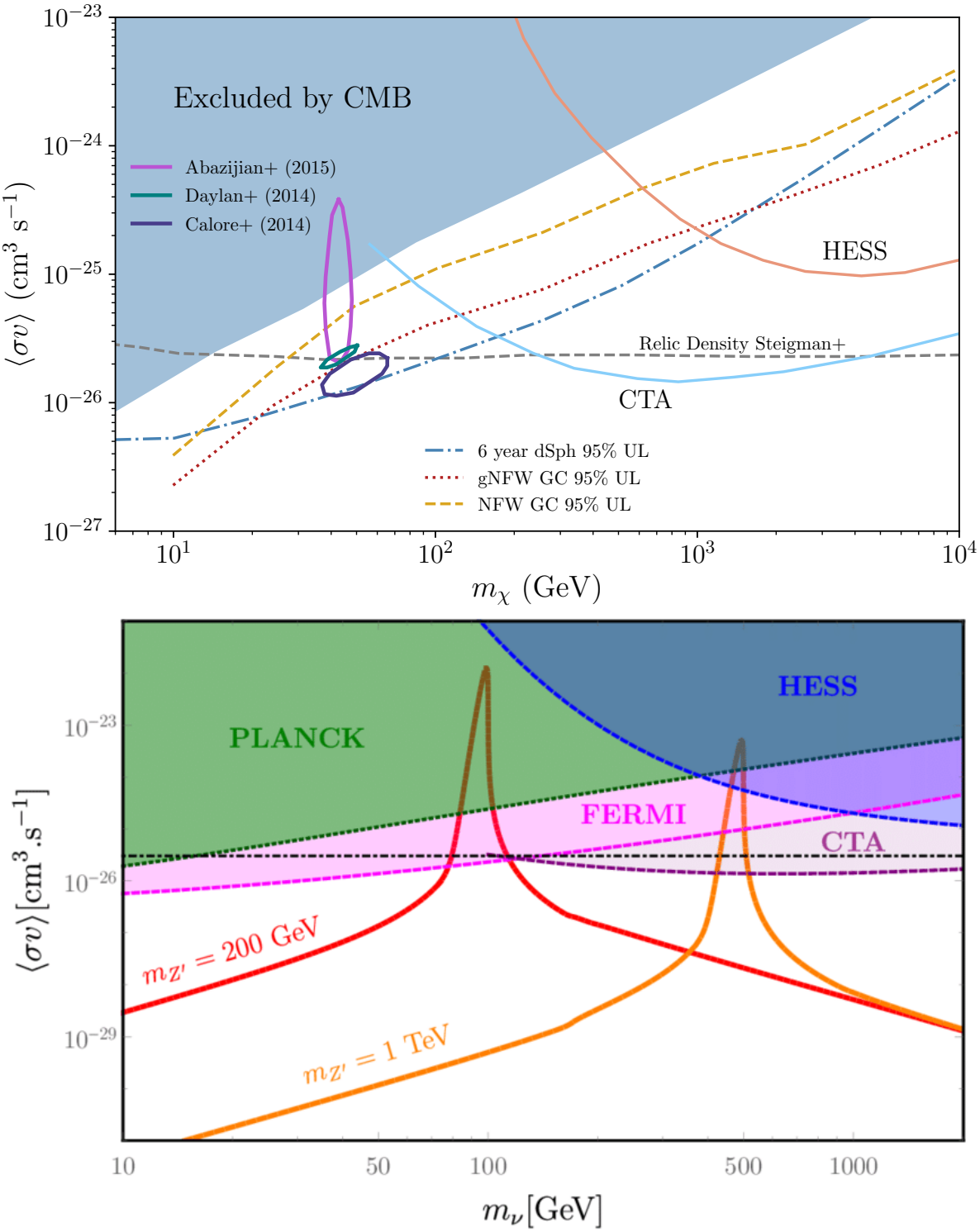

Figure 10 – (Top panel) Upper bounds and foreseen sensitivity by the Cherenkov Telescope Array (CTA) on the pair-annihilation rate as a function of DM mass derived from gamma-ray and CMB observations [1]. (Bottom panel) Several constraints on the average thermal cross section for DM annihilation via vector mediators (Z') with 200(1000) GeV are presented, where couplings with the dark sector are assumed to be of the order of $\mathcal{O}(10^{-1})$ [95].

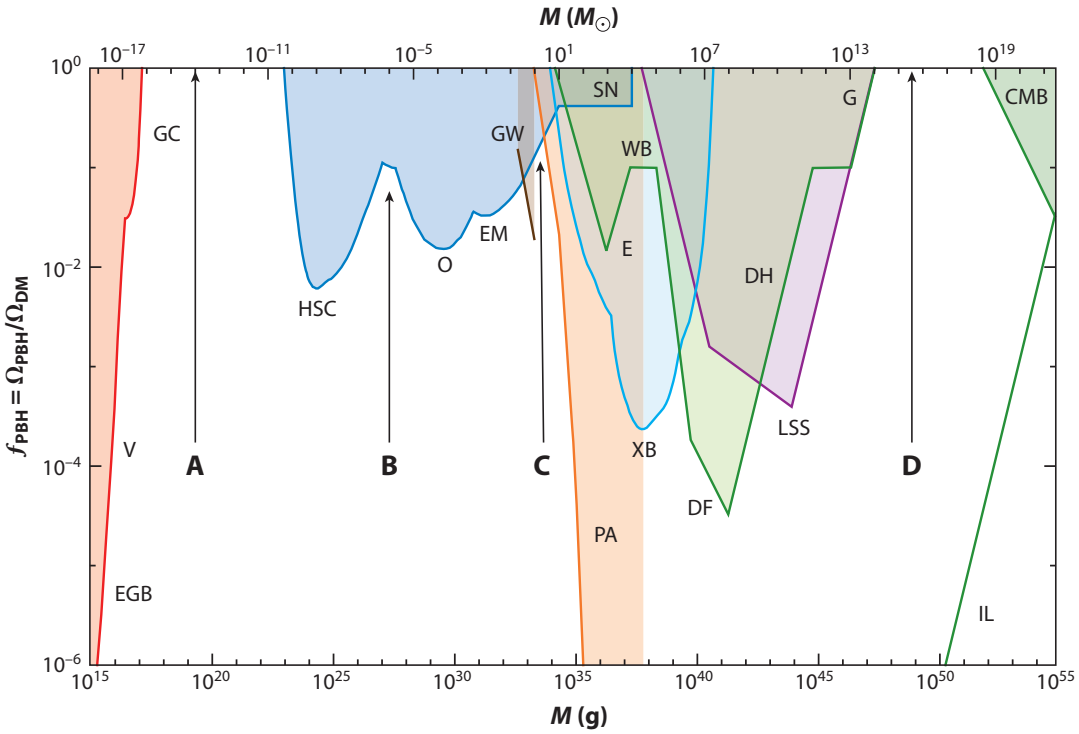

Figure 11 – Constraints on the monochromatic mass function for PBH due to evaporation (red), gravitational lensing (blue), gravitational waves (grey), dynamic effects (green), accretion (light blue), distortions in the CMB (orange), and large-scale structures (purple). Further details can be found in Ref. [6].

3.4 Collider Searches

In the landscape of modern physics, particle colliders represent a frontier for probing the fundamental constituents of nature. Theoretical frameworks usually claim that DM can interact with SM particles, either directly or through intermediary forces, requiring new interaction Lagrangians for exploration of such processes [78]. The pursuit of DM in collider environments is loaded with challenges, notably due to the anticipated feebleness of DM interactions.

Colliders, by design, are versatile instruments capable of investigating a plethora of physical phenomena across a vast number of events, with their potential limited mainly by their energy and luminosity. For example, the next phase of LHC experiments, called High Luminosity LHC (HL-LHC) aims to accumulate 3000 fb^{-1} in pp collisions from 2029 to 2041, which is ten times more than the nominal LHC performance expected for the period from 2010 to 2021 [99–101]. This capability, however, introduces the complexity of managing and interpreting the background noise inherent to such high-energy processes. A significant aspect of collider experiments is their ability of providing new data to refine theoretical models through precise measurements and observations. Thus, the detection of DM-like particles within collider setups would not directly confirm their cosmological role due to the vast differences in observational scales and conditions [1, 102]. The relationship

between the cross section of potential DM-producing processes and the colliders luminosity underscores the precision and scope of these investigations. Such experiments offer a unique vantage point for exploring resonant phenomena, which could illuminate the properties of possible mediators more than the DM particles themselves.

Reflecting on past achievements, such as the discovery and characterization of the Z boson at the LEP collider, or the remarkable observation of the BEH boson [103, 104], illustrates the synergy between theoretical predictions and experimental validations. These historical milestones underscore the stringent constraints that collider data can impose on new particle interactions. Still, the investigation of resonance processes within high energy physics (HEP) is a fundamental strategy employed in the search for new physics, specially for DM candidates. Resonances, defined as peaks in the cross section, proportional to the interaction probability, often indicate the presence of previously undiscovered particles or states.

For example, a landmark in the significance of resonance processes for particle discovery was the identification of the J/ψ meson in 1974. This discovery was quite significant, providing unequivocal evidence for the existence of the charm quark. It led to a comprehensive revision of the SM at time and ultimately to the awarding of the Nobel Prize in Physics to Burton Richter and Samuel Ting [105]. The events to characterize this new particle was detected in the energy distribution of electron-positron collisions, by two different groups at the time, led by the later Nobel laureates. Another significant breakthrough was the discovery of the W and Z bosons in the early 1980s by Carlo Rubbia and Simon van der Meer [105]. These particles, which mediate the weak force, were detected in resonance peaks observed in proton-antiproton collisions. This discovery served as a confirmation of the electroweak theory and also resulted in a Nobel Prize.

Resonant processes, in a general sense, occur when a system absorbs energy more efficiently at a specific frequency, resulting in a substantial increase in amplitude at that frequency. In the context of HEP, resonance typically involves the generation of an unstable, intermediate particle state during a particle collision. This state forms when the energy of the colliding particles aligns with the energy required to produce a new particle, leading to a resonance condition. The state is highly unstable and decays rapidly into other particles. The resonance condition is satisfied when the total energy of the system matches the mass of the resonant particle, with the cross section of such events usually described by the Breit-Wigner profile [90]:

$$\sigma_{\text{res}} \approx \frac{4\pi}{p^2} \frac{M_{\text{R}}^2 \Gamma_{\text{i}} \Gamma_{\text{f}}}{\left(s - M_{\text{R}}^2\right)^2 + M_{\text{R}}^2 \Gamma_{\text{R}}^2}, \tag{3.2}$$

where Γ is the decay width of the resonance particle into its initial (i) and final (f) states, and Γ_R is the total decay width of the produced particle. Also, p is the four-momentum of the initial particles, s is the Mandelstam variable related to the total energy of the process

squared, and finally M_R is the mass of the particle.

At energies near the resonance, the cross section experiences a significant enhancement, manifesting as a spike in the event rate. This spike serves as a definitive signal of the emergence of a new particle or state. Through the analysis of events across various experiments, physicists can deduce the event rate and, thereby, the cross section of the studied process. This enables the determination of the properties of the involved particles, including their masses and decay rates. This increase in the event rate, when taking into account the inherent difficulties in the background and analysis of signals in particle colliders, is what most favors the search for events of this kind. Hence the importance of understanding well the implications of such processes, especially in scenarios containing new physics. Furthermore, such analyses allow for the validation of theoretical predictions and models within particle physics and the investigation of the forces that govern particle interactions.

Looking ahead, the proposed next-generation lepton colliders, including the FCC-ee, CEPC, ILC, and CLIC, promise to extend the energy frontier, potentially uncovering new aspects of electroweak interactions and DM phenomena at energies surpassing those previously achievable [106–109].

In collider experiments such as those in operation at the LHC, one method to manage the analysis of the vast number of events generated is through the implementation of triggers. These triggers are essential due to the impracticality of examining each event individually. Specifically, the selection of triggers plays a relevant role in the search for DM in hadron collider environments. This usually involves identifying events that exhibit missing momentum, which may indicate the presence of an invisible entity, although reconstructing such events can be challenging [110]. The primary strategy for detecting DM involves accounting for the missing transverse momentum ($\vec{p}_T$) from particles that can be observed by the trackers and calorimeters of the detector following event reconstruction . Given the conservation of momentum in the plane perpendicular to the beam direction (transverse plane), and the large momentum carried by the colliding particles in the beam direction, we can consider that the initial transverse momentum is negligible, leading to an expected net transverse momentum of zero when considering all the detectable final state particles. When one or more particles escape detection, either because they are weakly interacting (like neutrinos or DM particles), an imbalance in the transverse momentum is observed. This imbalance is quantified as the missing transverse momentum, $\vec{p}_T$.

Mathematically, $\vec{p}_T^{\,\text{miss}}$ is defined as the negative vector sum of the transverse momenta ($\vec{p}_T$) of all detected particles in an event [111]:

$$\vec{p}_T^{\,\text{miss}} + \sum_{\text{detected particles}} \vec{p}_T = 0. \tag{3.3}$$

In searches for DM particles produced in collider experiments, events with a significant

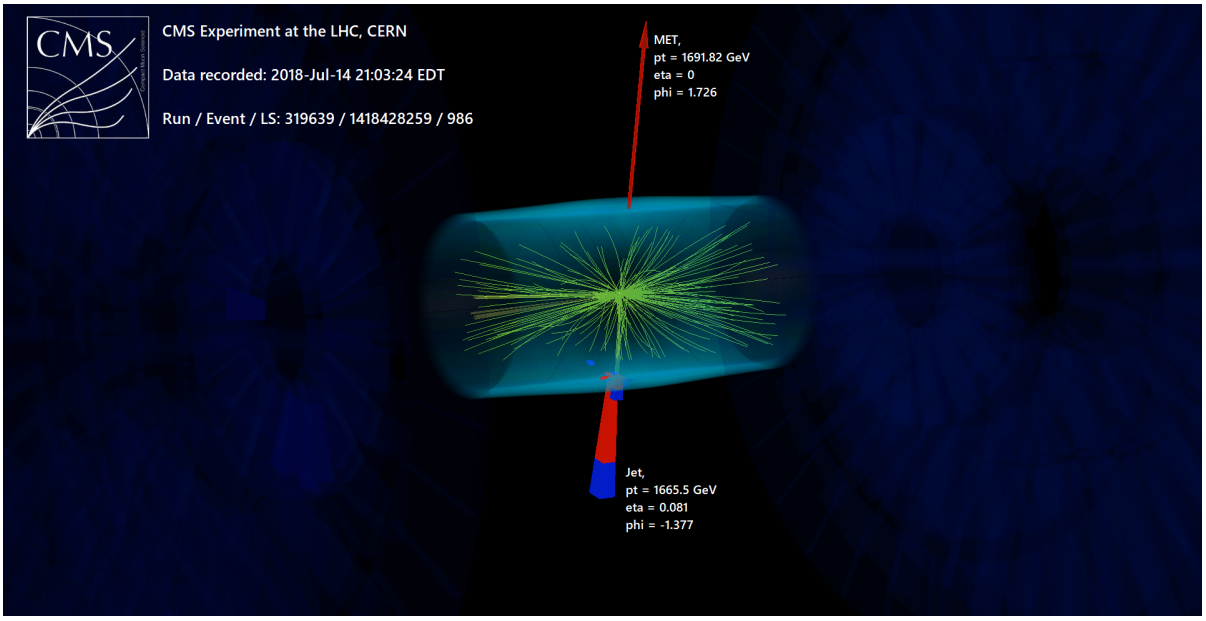

Figure 12 – Portrayal of a event in CMS with high-$\vec{p}_T^{\,\text{miss}}$ (red arrow) for a monojet, which has its calorimeter deposits indicated by the red and blue towers [114].

$\vec{p}_T^{\,\text{miss}}$ are of particular interest. These events could indicate the production of DM particles that escape the detector unseen, their existence inferred from a momentum imbalance, as shown in Figure 12.

Essentially, the focus is on events that involve DM and somehow correlate with the production of detectable SM particles by collider experiments, such as muons, electrons, photons, jets, etc. Searches that are predicated on the emission of a single particle from an initial-state quark, leading to the production of monojets, mono-Z, monophotons, and similar phenomena, are collectively referred to as *mono-X* searches. Additionally, DM searches in colliders include triggers for dileptons (the production of two lepton pairs in the final state) [112] and dijets (the production of two particle jets in the final state, possibly originating from a DM-related vertex) [110,113]. While these analyses have not yet provided definitive evidence of DM, they contribute to narrowing the parameter space and extending the exclusion limits for various DM models, especially those involving massive mediators [110].

The search for new physics in accelerator experiments is increasingly focused on detecting particle production signals that align with conventional gauge theories, based on the interaction Lagrangian form from QFT. This involves exploring signals of DM arising from particle collisions with kinematic distributions similar to those observed in $2 \to 2$ or $2 \to 4$ processes, as previously studied in the `CDF` and `D0` experiments at the Tevatron in Fermilab and now at the ATLAS and CMS experiments at the CERN LHC.

The pursuit of DM at colliders essentially focuses on two main production channels: DM production associated with conventional matter or radiation emitted in the initial state

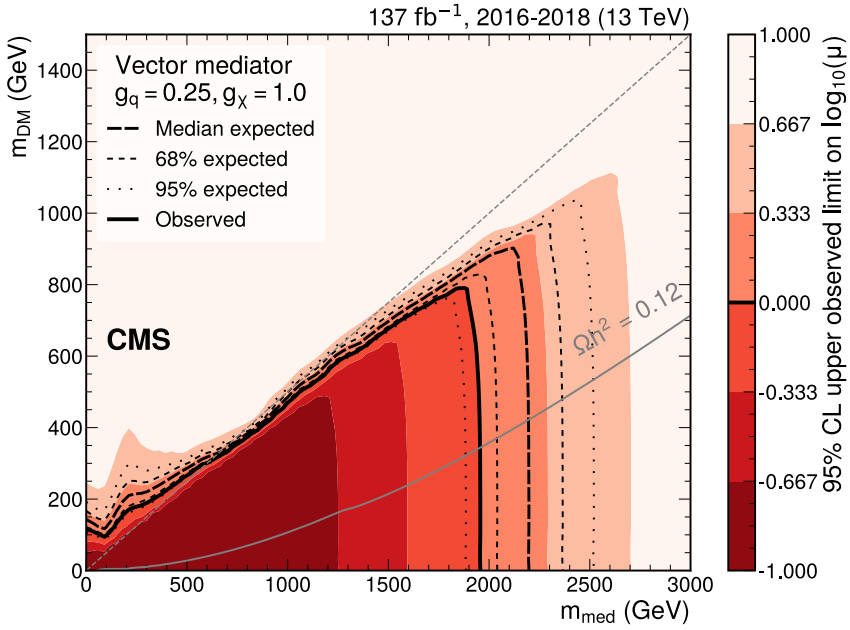

Figure 13 – Exclusion limits at 95% confidence level (CL) for a vector mediator. These results indicates an exclusion up to $M_{\text{med}} = 1.95$ TeV for $m_\chi \simeq 1$ GeV. This kind of plot on the mass-mass plane for DM particle and its mediator is widely used for benchmark studies on beyond Standard Model (BSM) physics [114].

and direct production. In both scenarios, the experimental signal measured is the missing momentum, derived after reconstructing the involved particles and determining their momenta and energy. This imbalance in energy, relative to the initial collision energy of the proton, indicates the amount of energy carried away by undetected, invisible particles. The CMS Collaboration has been eagerly exploring potential DM production signals at the LHC, especially under conditions of high luminosity. For example, Figure 14 presents exclusion limits at 95% confidence level (CL) for searches in proton-proton collisions at 13 TeV for a vector mediator, in the mediator mass plane (M_{med}) versus the DM and SM couplings, g_χ and g_q respectively, for a integrated luminosity of 137 fb$^-$1 [110, 114].

The investigations at the LHC predominantly compare experimental results to these models predictions for proton-proton collision production via quark annihilation, where direct DM production would remain undetectable by the sensors, yielding no hadronic activity signals. In contrast, the proposals consider the parallel production of DM with conventional matter and radiation, yielding detectable signals in LHC experiments. Since DM cannot be directly measured, the signal of conventional matter is assessed, and the reconstruction process reveals an energy loss compared to the initial protons energy. This type of signal can be assessed in the production of DM from one of the initial quarks in the interaction, where an imbalance in energy could be indicated. Such analyses are underway for processes known as monojets [115–118], monophotons [119, 120], mono-Higgs [121–124], mono-Z [125–128], monotop [129, 130], among others [126].

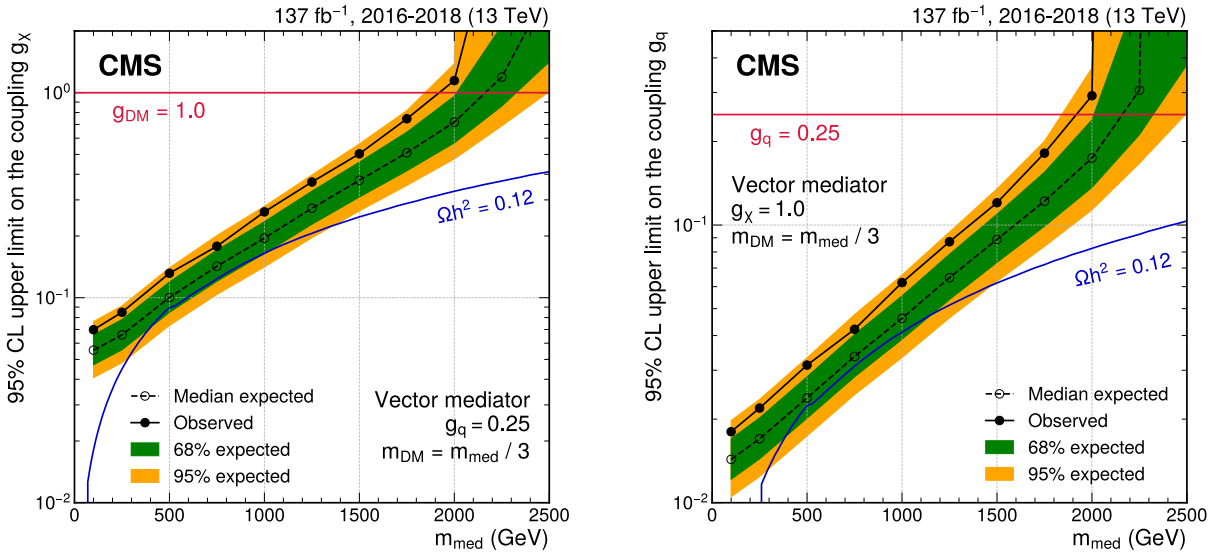

Figure 14 – Exclusion limits at 95% CL for a vector mediator, relative to its couplings with the dark sector (left) and SM quarks (right). Here, m_χ is fixed in $M_{\text{med}}/3$ for comparison, and the blue solid lines represents where this model produce the DM relic density [114].

By complementing direct and indirect detection methods, collider searches for DM continue to refine the understanding of its properties and interactions, aiming to characterize (or refute) dark sector particles. In chapter 5, we will explore processes that characterize DM interactions through an initial state, that is, reactions where decays into invisible final states are anticipated. Consequently, it requires the characterization through signals distinct from those of the conventional reconstruction of final states emanating from a collider event. In this work, we will consider resonance processes to determine the cross sections involved in our theoretical predictions, as well as estimate the impact of this regime on the calculation of DM relic abundance in the primordial universe. This must be done carefully, as usual calculations of this nature present significant discrepancies when resonance processes are not taken into account [90].

3.5 Simplified Spin-dependent Models for DM

In exploring the intricate dynamics between DM and SM particles, our aim is to establish a theoretical framework in which a new spin-1 mediator, designated as Z', operates as a mediator for interactions. Drawing insights from seminal works [49–54, 78], this Z' boson is envisioned not just as a mediator facilitating DM production up to the freeze-out epoch but also as a potential piece to extend the SM reach into the TeV scales.

This paradigm forecast Z' as a portal that facilitates interactions within the dark sector, modulated by a coupling constant g_χ. The feasibility of Z' being the primary DM contradicts the requirement for stability, pushing the narrative towards its mediator role.

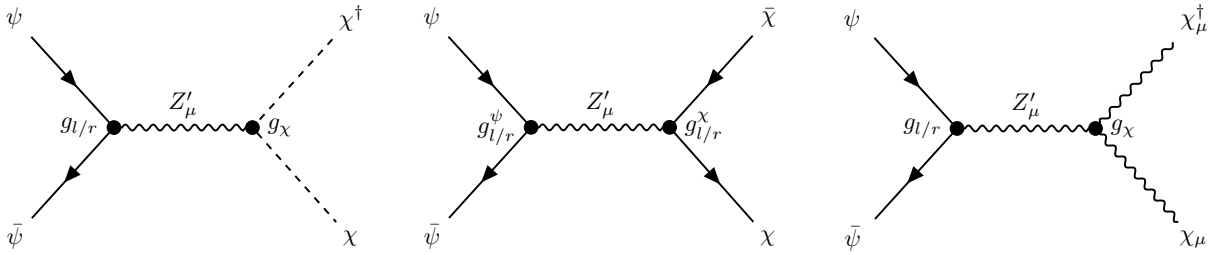

Figure 15 – Feynman diagrams for the s-channel interaction via the spin-1 mediator for the three DM candidates, scalar (left), fermion (middle), and vector (right).

This approach leads to a richer DM sector, potentially comprising scalar, fermion, or complex vector constituents, each engaging with Z' through distinct interaction pathways (see Figure 15). Unlike the scenarios discussed in Ref. [50], we will not initially assume any effective model and will proceed to calculate the total cross section (σ_{tot}) using Feynman rules independently. Furthermore, in all the processes we will describe, the scattering is elastic, but inelastic scatterings or those described by form factors can also be considered [131, 132].

Therefore, an interaction Lagrangian describing an extension of the SM with a new renormalizable symmetry group $U_\chi(1)$, acting as a vector portal to dark matter, and comprising a complex scalar, fermion, or vector field, can be described as we will see. The interaction Lagrangian for a scalar DM candidate χ, that interacts with SM fermions, represented here by the spinor ψ, which interaction is mediated by Z', can be written as:

$$\mathcal{L}_{int}^{scalar} \supset \bar{\psi}\gamma^\mu \left(g_l P_L + g_r P_R\right) \psi Z'_\mu + g_\chi \left(\chi^\dagger \partial_\mu \chi - \chi \partial_\mu \chi^\dagger\right) Z'^\mu, \tag{3.4}$$

where $g_{l/r}$ and g_χ represent the couplings of the mediator boson with the SM particles and with the DM, respectively. The last term contains the usual and adjoint Dirac spinors ψ and $\bar{\psi}$, respectively, relative to the interaction term of the boson Z' with SM particles. The operators P_L and P_R denote the left-handed and right-handed operators, defined by

$$\begin{cases} P_L \equiv \frac{1}{2}(1-\gamma^5), \\ P_R \equiv \frac{1}{2}(1+\gamma^5), \end{cases} \tag{3.5}$$

with g_l and g_r representing the magnitudes of left-handed and right-handed couplings with SM particles, respectively. Finally, the last term containing the scalar fields χ and $\chi^\dagger$ represents the interaction term of the scalar DM with the boson Z'. This formulation hides the kinetic and mass terms of the Z' boson, considering that, similarly to what is seen in the literature, we do not focus here on how the Z' boson acquires its mass, nor do we delve deeper in detail about the gauge regularization of the Lagrangians presented, which does not prevent the derivation of our results or similar studies that follow this same methodology [56]. More comprehensive models on spin-1 mediators and the related final states that prescribe their gauge invariance are described in Refs. [1, 51, 55, 59, 68, 70, 114, 133–136].

For a DM particle described as a fermion, where χ is a Majorana fermion being its own antiparticle, the interaction Lagrangian can be formulated as follows:

$$\mathcal{L}_{int}^{fermion} \supset \left[\bar{\psi}\gamma^{\mu}\left(g_l P_L + g_r P_R\right)\psi + \bar{\chi}\gamma^{\mu}\left(g_\chi P_L + g_\chi P_R\right)\chi\right] Z'_{\mu}, \tag{3.6}$$

where we assume the generalization $g_{l/r}^{\psi} = g_{l/r}^{\chi}$ for the purposes of this discussion. Besides, in this case, the interaction term of the fermion DM with the Z' boson is provided by the last term of the equation, involving the spinor χ and its adjoint $\bar{\chi}$, along with the corresponding left and right-handed operators and couplings.

Finally, in the case of a DM candidate represented by a complex vector field, distinct from the mediator vector boson considered earlier, it is possible to combine two real degrees of freedom from a complex DM field with the singlet defined by the mediator ${Z'}_{\mu}$ to generate a field tensor and a gauge kinetic term akin to what is performed in gauge theories with $SU(2)$ representations. Following the procedure as demonstrated in Ref. [50], we obtain an interaction Lagrangian, ignoring quadratic terms, expressed as:

$$\begin{aligned}\mathcal{L}_{int}^{vector} \supset\ & \bar{\psi}\gamma^{\mu}\left(g_l P_L + g_r P_R\right)\psi Z'_{\mu} - i g_\chi\left(\partial^{\mu} Z'^{\nu} - \partial^{\nu} Z'^{\mu}\right)\chi_{\mu}^{\dagger}\chi_{\nu}, \\ -\ & i g_\chi Z'_{\mu}\chi_{\nu}^{\dagger}\left(\partial^{\mu}\chi^{\nu} - \partial^{\nu}\chi^{\mu}\right) + i g_\chi Z'^{\mu}\chi^{\nu}\left(\partial_{\mu}\chi_{\nu}^{\dagger} - \partial_{\nu}\chi_{\mu}^{\dagger}\right)\end{aligned} \tag{3.7}$$

where the last three terms are the coupling between the vector fields of DM and the field associated with the Z' boson.

These interaction Lagrangians shows that the WIMP χ candidates we propose are neutral regarding both color and electromagnetic charge, and thus, do not undergo scattering with gluons at tree level [137]. Consequently, we have three χ candidates for relic DM: scalar (spin-0), fermion (spin-$\frac{1}{2}$), and vector (spin-1). Each of them interacts with the SM particles through the mediation of a novel massive spin-1 mediator Z' with mass $M_{Z'}$. For further insights and a comprehensive discussion on the simplified DM models presented in this document, interested readers are directed to the appendices sections 2 and 3 from Appendix A [138], sections 2 and 4 from Appendix B [139] and sections 1 and 2 from Appendix C [140], located at the end of this work. There we delve into the theoretical frameworks, calculations of cross sections, decay widths, other mathematical formulations, assumptions and potential implications of the models discussed. We also included a comprehensive discussion on the limitations and strengths of the models and potential pathways for future research.

4 Dark Matter Relic Density Estimation

In DM research, understanding how and when its production occurred during the initial phases of the Universe is essential, especially when we want to describe a new model that explains this abundance. This phase is important because it determines the characteristics of the relic DM observable today through its gravitational effects on structures such as galaxies and clusters.

There are in the literature various mechanisms for DM production in the early Universe, depending on which model is under consideration, each with its unique characteristics. Some low mass scalar DM models can be deduced from the inflaton condensate during inflation and reheating [141]. This production is categorized into gravitational, weak direct coupling (perturbative), and strong direct coupling (non-perturbative) regimes. Scalar DM candidates like Q-balls and axions can significantly impact the matter power spectrum, with constraints derived from Lyman-α measurements suggesting bounds on the DM mass for various production regimes [141]. From MACHOs perspective (see section 3.1), PBHs are believed to form through the gravitational collapse of significant density fluctuations in the early Universe, which can arise through various phenomena such as topological defects (e.g., cosmic strings, necklaces, domain walls), fluctuations during ultra-slow-roll inflation, sound speed resonance, early matter domination periods, or other sub-horizon events like phase transitions and preheating [1, 142].

There is also a so-called freeze-in production, where DM interacts very weakly and is gradually produced by decay or scattering processes. This usually requires larger coupling values for successful DM production, expanding the parameter space for sterile neutrinos and gravitinos as DM candidates. The freeze-in mechanism generates particles out of equilibrium, which then accumulate over the history of the Universe. The quantity of these particles generated at a specific redshift is determined by multiplying the rate of production by the Hubble time at that redshift. This mechanism often leads to scenarios where the lightest particles in the observable sector decay into DM with relatively extended lifetimes, resulting in distinct signatures observable at particle detectors [1, 143].

As for asymmetric DM scenarios, where a particle-antiparticle asymmetry in the dark sector mirrors the baryon asymmetry in the visible sector, the enhanced expansion rate can lead to earlier particle freeze-out and an enhanced relic density [144, 145]. Still, another dark-sector dynamics, including processes like cannibalization and number-changing interactions, can significantly influence the abundance of DM beyond the conventional 2-to-2 interactions. On the other hand, DM can also be produced through non-thermal mechanisms. This involves the decay of a precursor particle (sometimes referred to as a

mother particle) into DM, or the conversion of energy from topological defects, moduli, and other non-standard sources into DM, often mediated by gravitational interactions [1].

Finally, the widely discussed freeze-out scenario, that can be also called the *symmetric freeze-out*, proposes that during the expansion of the Universe and consequent cooling, DM was expected to be in chemical and kinetic equilibrium with other cosmic components. This equilibrium phase is key to understanding why there is now about five times more DM than baryonic matter. As the Universe expanded, DM eventually decoupled from the rest of the matter-energy content, a process known as *freeze-out*. This decoupling effectively *froze* certain properties of DM, such as its numerical density and temperature, when we assume a standard LCDM cosmology [78, 90].

4.1 Thermal Relic Abundance

The Boltzmann equation offers a method to estimate when this freeze-out occurred [90]. It involves the assumption that, at the freeze-out, the SM particles, resulting from DM annihilation, were in total equilibrium with the primordial plasma. Hence, in this equation, the number density of DM particles n_χ varies according to its density $n_{\mathrm{eq},\chi}$ in thermal equilibrium with SM species. The Boltzmann equation is thus expressed as:

$$\frac{\mathrm{d}n_\chi}{\mathrm{d}t} + 3Hn_\chi = -\left[n_\chi^2 - n_{\mathrm{eq},\chi}^2\right]\langle\sigma v\rangle, \tag{4.1}$$

where $\langle\sigma v\rangle$ is the mean thermal cross section times velocity that governs the interaction between the dark and SM sectors, H is the Hubble constant and t is time.

Another assumption in this analysis is the constancy of entropy per unit comoving volume, expressed as $s = S/a^3(t)$, where $a(t)$ is the comoving distance [5]. With $s \propto T^3$, we define a new variable Y, the *yield*, as:

$$Y \equiv \frac{n}{T^3}, \tag{4.2}$$

leading to a re-expressed Boltzmann equation [78, 90]

$$\frac{\mathrm{d}Y(t)}{\mathrm{d}t} = -s\left[(Y(t)^2 - Y_{\mathrm{eq}}(t)^2\right]\langle\sigma v\rangle. \tag{4.3}$$

To better understand the freeze-out process, we introduce a new variable, x, defined as the ratio of the DM particle mass to the photon temperature of the Universe at a certain epoch ($x \equiv \frac{m}{T}$). This variable helps to eliminate the direct dependency on time in our calculations. The Hubble parameter, for an standard cosmology, can be written as

$$H = \sqrt{\frac{8}{3}\pi G\rho_c}, \tag{4.4}$$

with G being the gravitational constant and ρ_c the Universe total energy density. Then, ρ and s can be written in terms of the degrees of freedom of all species involved in the

process and we get the evolution of Y in terms of x as:

$$\frac{dY}{dx} = -\sqrt{\frac{45}{\pi}G}\frac{\sqrt{g_*}m_\chi}{x^2}\langle\sigma v\rangle\left[Y^2 - {Y_{\rm eq}}^2\right]. \tag{4.5}$$

The factor g_* precisely represents the content of the Universe at a certain temperature T and depends on the degrees of freedom of the particles under consideration [78, 90].

The thermal average of the annihilation cross section times velocity, $\langle\sigma v\rangle$, is commonly approximated by expanding the cross section at low relative velocities.

$$\langle\sigma v\rangle = \sigma \cdot v + \mathcal{O}(v^2). \tag{4.6}$$

However, this method may not always provide an accurate approximation, especially in situations where the cross section expansion poorly represents its behavior or is divergent. Under such circumstances, employing an integral formula becomes beneficial, or even mandatory. This approach allows for a more precise computation of the thermal average by directly integrating over the relevant distribution of velocities, thereby capturing the effects that might be missed or misrepresented by a simple low-velocity expansion [90]. This is particularly important where resonant processes need to be taken into account for greater accuracy in parameter space determination, as is the case with the studies presented in the papers resulted from this work in Appendix A [138] and Appendix B [139].

Following the recommendations by Ref. [90], one can get analytical expression for $\langle\sigma v\rangle$ as

$$\langle\sigma v\rangle = \frac{1}{8m_\chi^4 T K_2\left(\frac{m_\chi}{T}\right)^2}\int_{4m_\chi^2}^{\infty} ds\,\sigma(s)\sqrt{s}\left(s - 4m_\chi^2\right)K_1\left(\frac{\sqrt{s}}{T}\right), \tag{4.7}$$

where $K_i(x)$ are modified Bessel functions of second kind. This is initially derived assuming particles follow Maxwell-Boltzmann statistics. Nonetheless, this equation can also be extended to encompass systems characterized by alternative statistical distributions [90]. This broader applicability is contingent upon the condition that the temperature of the system, T, does not exceed three times the mass of the particles ($T \leq 3m_\chi$). This temperature threshold ensures the assumptions of Maxwell-Boltzmann statistics, such as particles moving at non-relativistic speeds, remain valid even when other statistical frameworks are considered.

Moreover, it is important to address the frame of reference for the relative velocity between particles when applying Equation 4.7. Typically, the equation is described in a laboratory frame, which is convenient for most theoretical and practical analyses. However, in situations where the center of mass frame provides a more accurate depiction of the process, adjustments to the equation are necessary [90], which fall outside the scope of this work. To determine the abundance of DM in the current phase of the Universe, it is necessary to find a solution for Equation 4.5, and solving it generally demands a numerical approach due to its nature as a differential equation lacking closed-form solutions for

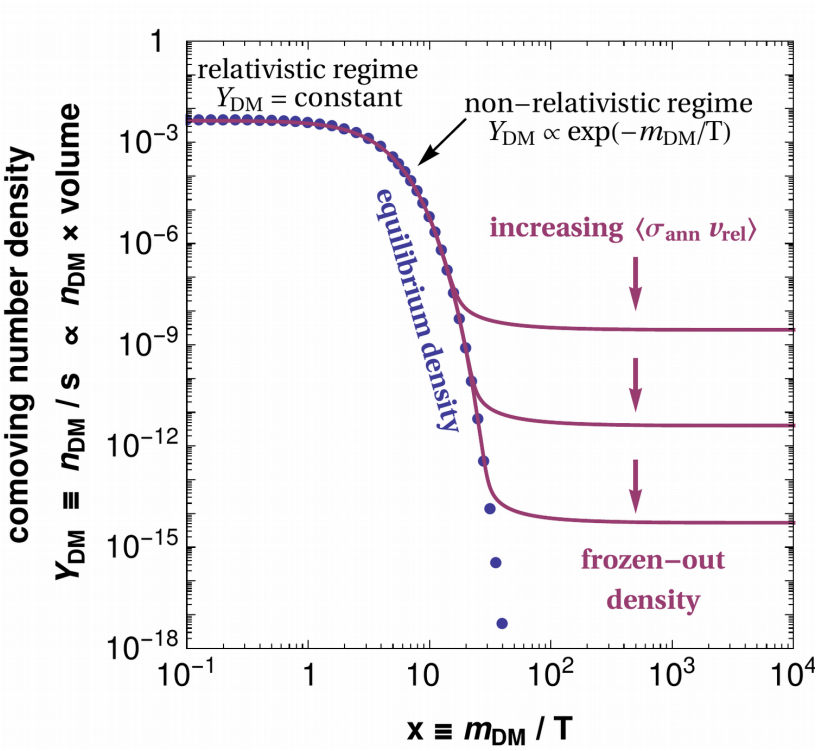

Figure 16 – The typical evolution of the abundance $Y(x)$ during the decoupling (freeze-out) period of DM is depicted in the referenced figure. This graph illustrates the critical phase where DM particles transition from being in thermal equilibrium with the cosmic plasma to becoming the non-interacting, relic density observed today [146].

generic cases. To obtain the current abundance, Y_0, one has to integrate x from the early Universe to present times, where T_0 will be the current photon temperature of the Universe. The equilibrium density is crucial in this context and is given by:

$$Y_{\rm eq} = \frac{45g}{4\pi^4} \frac{x^2 K_2(x)}{h_{\rm eff}(m/x)}, \tag{4.8}$$

where $h_{\rm eff}$ represents the effective degrees of freedom and g the internal degrees of freedom of the species in question. This formulation will allow for an good approximation of the relic density for massive particles, bypassing the need to solve Equation 4.5 numerically [90].

To further refine this approach, one must determine the freeze-out temperature, T_f, which is the temperature of the Universe when the freeze-out specifically occurs. By defining the deviation between in-equilibrium and out-of-equilibrium abundances as $\Delta = Y - Y_{\rm eq}$, we can reformulate Equation 4.5 as:

$$\frac{{\rm d}\Delta}{{\rm d}x} = -\sqrt{\frac{45}{\pi}} G \frac{\sqrt{g_\star} m_\chi}{x^2} \langle \sigma v \rangle \Delta(\Delta + 2Y_{\rm eq}) - \frac{{\rm d}Y_{\rm eq}}{{\rm d}x}. \tag{4.9}$$

Still according to Ref. [90], the variation of ${\rm d}\Delta/{\rm d}x$ is not significantly different before decoupling. As can be seen in Figure 16, the equilibrium density follows Y until the

decoupling occurs, and after that, Y remains almost constant for $x \gg 1$. This indicates that freeze-out effectively occurs only when Δ reaches a specific value such that:

$$\Delta = \delta Y_{\rm eq}. \tag{4.10}$$

This leads to the definition of a freeze-out condition as:

$$\sqrt{\frac{45}{\pi}G}\frac{\sqrt{g_\star}m_\chi}{x^2}\langle\sigma v\rangle Y_{\rm eq}\delta(\delta+2) = -\frac{{\rm d}\ln Y_{\rm eq}}{{\rm d}x}. \tag{4.11}$$

Applying this condition to the defined expression for $Y_{\rm eq}$ in Equation 4.8 yields a transcendental differential equation:

$$\sqrt{\frac{45}{\pi}G}\frac{45g}{4\pi^4}\frac{K_2(x)}{h_{\rm eff}(T)}\sqrt{g_\star}m_\chi\langle\sigma v\rangle\delta(\delta+2) = \frac{K_1(x)}{K_2(x)} - \frac{1}{x}\frac{{\rm d}\ln h_{\rm c}(T)}{{\rm d}\ln T}. \tag{4.12}$$

A comparison with approximations for various cross sections shows that $\delta = 1.5$ is a suitable approximation [90]. Following freeze-out, $Y_{\rm eq}$ can be disregarded as the equilibrium abundance decays exponentially as x increases, as shown in Figure 16. The current abundance, Y_0, is thus derived as:

$$\frac{1}{Y_0} = \frac{1}{Y_f} + \sqrt{\frac{45}{\pi}G}\int_{T_0}^{T_f}\sqrt{g_\star}\langle\sigma v\rangle\ {\rm d}T. \tag{4.13}$$

Typically in the literature, the term $Y_{\rm f}^{-1}$ is omitted, not significantly affecting the approximation for Y_0^{-1}. However, it is noteworthy in Equation 4.13 that different annihilation modes linearly contribute to Y_0^{-1}. This property is particularly useful when considering the production of DM states in resonance in some annihilation channels [90].

Finally, knowing Y_0 allows for the calculation of DM density in the current Universe as:

$$\Omega_\chi = \frac{\rho_{\chi,0}}{\rho_{\rm c}} = \frac{m_\chi s_0 Y_0}{\rho_{\rm c}}. \tag{4.14}$$

Assuming a non-relativistic form for the freeze-out condition as defined in Equation 4.12, it simplifies to:

$$\sqrt{\frac{45}{\pi}G}\frac{45g}{8\pi^4}\frac{\sqrt{\pi}\sqrt{x}\,{\rm e}^{-x}}{h_{\rm eff}(T)}\sqrt{g_{\rm eff}}m_\chi\langle\sigma v\rangle\delta(\delta+2) = 1. \tag{4.15}$$

By disregarding the correction of Y_f in Equation 4.13, we obtain an excellent approximation for the relic density as:

$$\Omega_\chi h^2 \approx 8.7661\times10^{-11}{\rm GeV}^{-11}\left[\int_{T_0}^{T_{\rm f}}\sqrt{g_\star}\langle\sigma v\rangle\ \frac{{\rm d}T}{m_\chi}\right]^{-1}. \tag{4.16}$$

This equation can be used as a powerful equation that connects a large-scale cosmological quantity (DM relic density, $\Omega_\chi h^2$) with a particle physics variable (average thermal annihilation cross section, $\langle\sigma v\rangle$). This relation is quite important to deduce current

properties of DM, highlighting the interplay between cosmology and particle physics. Note that this equation indicates an inverse proportionality: a higher annihilation cross section implies a lower abundance of the DM type under investigation. Such a correlation is vividly depicted in Figure 16, where the abundance Y inversely varies with the thermal average of the annihilation cross section ($\langle\sigma v\rangle$). Interestingly, in a hypothetical scenario where DM particles did not undergo freeze-out, not considering freeze-in scenarios [147], their abundance would effectively be zero at higher x values.

4.2 Relic Abundance for Processes in Resonance

In the literature, the calculation of DM abundance, and thus the cross sections involved in its primordial production, typically assumes processes in equilibrium and distant from the poles or resonances of a given species. However, when considering resonant production processes, one cannot straightforwardly apply the usual solution to the Boltzmann equation in terms of the thermally averaged cross section $\langle\sigma v\rangle$. As likewise detailed in the work by Ref. [90], for a resonance with a Breit-Wigner profile of the form

$$\sigma_{\text{res}} = \frac{4\pi\omega}{p^2} B_{\text{i}} B_{\text{f}} \frac{m_{\text{R}}^2 \Gamma_{\text{R}}^2}{\left(s - m_{\text{R}}^2\right)^2 + m_{\text{R}}^2 \Gamma_{\text{R}}^2}. \tag{4.17}$$

In the context where the statistical factor ω is defined as $(2J+1)/(2S+1)^2$, with p representing the momentum in the center-of-mass frame, and S denoting the spin of the colliding particles respectively, we inspect the dynamics of particle interactions. Furthermore, m_R, Γ_R, and J are the mass, total decay width, and spin of the resonant state, while B_i and B_f represent the branching fractions for the resonance decaying into the initial and final channels, correspondingly [90]. For now on and throughout this work, we will identify the resonance with our spin-1 mediator discussed in section 3.5, then $m_R \to M_{Z'}$ and $\Gamma_R \to \Gamma_{Z' \to \text{all}}$.

We can still reformulate Equation 4.17 to make it expressible in terms of the kinetic energy per unit mass ϵ in the laboratory frame,

$$\epsilon = \frac{s - m_\chi^2}{m_\chi^2}. \tag{4.18}$$

Introducing the parameter ϵ_R, which represents the relative energy scale normalized by the mass of the DM particle (m_χ) and the mass of the mediator Z' ($M_{Z'}$), we have:

$$\epsilon_R = \frac{(M_{Z'}^2 - 4m_\chi^2)}{4m_\chi^2}. \tag{4.19}$$

This leads us to express the resonant cross section σ_{res} as:

$$\sigma_{\text{res}} = \frac{4\pi\omega}{m_\chi^2 \epsilon} B_{\text{i}} B_{\text{f}} \frac{M_{Z'}^2 \Gamma_{Z'}^2}{(\epsilon - \epsilon_{\text{R}})^2 + M_{Z'}^2 \Gamma_{Z'}^2}. \tag{4.20}$$

In the laboratory frame, the relative velocity between two particles can be expressed as:

$$v_{\rm lab} = 2\sqrt{\epsilon(1+\epsilon)}/(1+2\epsilon), \tag{4.21}$$

which allows us to reformulate the resonant cross section as:

$$\sigma_{\rm res} = \frac{8\pi\omega}{m_\chi^2}\frac{M_{Z'}^2\Gamma_{Z'}^2}{(\epsilon-\epsilon_{\rm R})^2 + M_{Z'}^2\Gamma_{Z'}^2} b_R(\epsilon), \tag{4.22}$$

where the function $b_{\rm R}(\epsilon)$ is defined as:

$$b_{\rm R}(\epsilon) \equiv \frac{B_{\rm i}(1-B_{\rm i})(1+\epsilon)^{1/2}}{\epsilon^{1/2}(1+2\epsilon)}. \tag{4.23}$$

This function does not vary significantly near a resonance and hence can be approximated through an expansion or calculated numerically. In this work, aiming for a model-independent expression of the resonance width for non-relativistic DM, we adopt the strategy of following the steps described in Ref. [90]. Thus, we describe $\langle\sigma v\rangle$ for a non-relativistic Breit-Wigner resonance, as would be a cold DM candidate in the LCDM model, in the ensuing form:

$$\langle\sigma v\rangle_{\rm res} = \frac{16\pi}{m_\chi^2}\frac{(2J+1)}{(2S+1)^2} x^{3/2}\pi^{1/2}\,\frac{M_{Z'}\Gamma_{Z'}}{m_\chi^2} B_i(1-B_i)\sum_{l=0}^{\infty}\frac{b_R^{(l)}}{l!}\,F_l(z_R;x). \tag{4.24}$$

The terms $b_R^{(l)}$ are the coefficients of the expansion of a function involving the branching fraction B_i of the form

$$b_R(\epsilon) \equiv \frac{B_i(1-B_i)(1+\epsilon)^{1/2}}{\epsilon^{1/2}(1+2\epsilon)} = \sum_{l=0}^{\infty}\frac{b_R^{(l)}}{l!}\epsilon^l. \tag{4.25}$$

Lastly, the $F_l(z_R;x)$ term results from the thermal average of σv with integration over the energy per unit mass ϵ

$$F_l(z_R;x) = {\rm Re}\frac{i}{\pi}\int_0^\infty \frac{\epsilon^{(l+1/2)}e^{-x\epsilon}}{(z_R-\epsilon)}{\rm d}\epsilon, \tag{4.26}$$

with an ϵ^l factor from Equation 4.25 and an auxiliary variable in terms of the masses and decay widths of the particles involved

$$z_R = \frac{M_{Z'}^2 - m_\chi^2}{m_\chi^2} + i\frac{M_{Z'}\Gamma_{Z'}}{m_\chi^2}. \tag{4.27}$$

In Appendix A [138] and Appendix B [139], we delve into how these outcomes modify the expected cross sections for processes involving resonances of mediators and massive final states across various experimental settings, including electron-positron accelerators and the LHC. The appendices also feature detailed charts and comparisons among each scenario, which we refrain from repeating here for the sake of brevity.

Therefore, by combining equations Equation 4.25 and Equation 4.26, we derive the final expression that underpins all resonant process calculations showcased in this work. This formula is presented as follows:

$$F(z_R; x) = \mathrm{Re}\frac{i}{\pi}\int_0^\infty \frac{(1+\epsilon)^{1/2}e^{-x\epsilon}}{(1+2\epsilon)(z_R-\epsilon)}\mathrm{d}\epsilon. \tag{4.28}$$

This approach enabled the simplification of Equation 4.24 into a more straightforward formulation, avoiding the dependency on the expansion in terms of ϵ^l as previously delineated in Ref. [90]. Consequently, this led to the evaluation through the subsequent expression:

$$\langle\sigma v\rangle_{\mathrm{res}} = \frac{16\pi}{m_\chi^2}\frac{(2J+1)}{(2S+1)^2}x^{3/2}\pi^{1/2}\,\frac{M_{Z'}\Gamma_{Z'}}{m_\chi^2}B_i(1-B_i)\,F(z_R;x). \tag{4.29}$$

Next, this equation was employed to compute the final DM densities, utilizing the framework provided by Equation 4.16 that was delineated earlier in the discussion. This approach allowed for a comprehensive analysis of how resonant production mechanisms influence the relic densities of DM.

In brief, the comprehensive understanding of DM abundance in the Universe extends beyond stellar and galactic velocity dispersion analyses. It also encompasses the study of fluctuations in the CMB. By employing the Boltzmann Equation (Equation 4.1), a link is established between the amount of DM produced primordially and the annihilation cross section of a process that replicates this abundance. In our work we delve into how some models can influence the annihilation cross section of specific processes, thereby affecting DM production estimates during the freeze-out phase. While the general framework for calculating relic densities provides crucial insights, there are significant non-trivial exceptions that warrant attention [90, 148]. These often arise when considering thermal production processes near a pole or resonance. Specifically, the latter can lead to an overestimation of the calculated relic DM density [90]. This situation necessitates corrective measures to accurately define the viable parameter space, especially in experiments probing these regions. When DM production occurs near a resonance, the interaction dynamics can be markedly different from the typical scenarios predicted by SM. This difference often results in a higher effective cross section, thereby influencing the relic density calculations. Consequently, researchers must carefully adjust their models to account for these resonant effects, ensuring that the predictions remain consistent with the observational data. In Appendix A [138] and Appendix B [139], we delve into these specific cases, exploring how close-to-resonance thermal production processes affect DM relic density estimations. This exploration is not only crucial for refining theoretical models but also for guiding experimental efforts. By delineating the correct and still accessible parameter space, we can better target experiments to search for DM in these scenarios, potentially unlocking new aspects of DM behavior.

5 Investigations in Particle Colliders

Experimentally detecting DM is a challenging endeavor. Particularly in collider experiments, to achieve this one has to look for signals, from initial or final particles, that can characterize events with missing transverse momentum (p_T^{miss}). In the HEP physics, the LHC experiments frequently explore phenomena that could hint at the existence of DM, more specifically through proton-proton collisions that might generate DM alongside Quantum Chromodynamics (QCD) jets, leptons, weak and/or Higgs bosons, photons, etc. Given that DM particles are believed to be electrically neutral and stable at cosmological scales, their presence in collider experiments is inferred from the absence of expected energy, manifesting as missing momentum in the readings of the detector [56]. One approach to identifying such events involves considering the emission of some form of radiation from the initial state of the particles involved in the process, like charged leptons, hadronic jets, or photons, often encapsulated in the approach known as mono-X searches. For example, to estimate events that include a monophoton as ISR, radiative corrections become necessary as these processes have different probabilities of occurring compared to other without such emissions. While most of these corrections in the literature are approximated for a *soft photon* emission or are numerically calculated for a $2 \to 3$ process, in this work we opted to adapt the radiative correction for the emission of a *hard photon*, as discussed in Ref. [149], where is proposed a factorization with low-order processes where e^+e^- reactions generate any final state f different than the initial one, plus the emission of a hard photon from the event.

In recent analyses, the LHC experiments have started to include events with up to four jets, demanding that the primary jet exhibit a transverse momentum ($\vec{p}_T$) exceeding 250 GeV while other studies opt for a less restrictive criterion, requiring at least one jet with $\vec{p}_T$ over 100 GeV [56, 114, 150–152]. Despite the promise of these techniques, several challenges dampen the LHC sensitivity to DM. The presence of intricate QCD backgrounds and other detector particularities introduce significant systematic uncertainties in monojet searches. To address these, there is been a push towards leveraging advanced computational techniques, including machine learning algorithms and computer vision, to refine jet identification and enhance signal purity [153, 154].

In the Figure 17, Figure 18 and Figure 19, we collect a comprehensive compilation of mono-X searches, alongside analyses of final states involving jets with ISR or solely missing momentum. These studies highlight the stringent limits imposed for a set of benchmark parameters and models, where the DM candidate is considered to be a Dirac fermion in the final state, and the mediator is a new spin-1 boson, with axial or vector couplings to SM and DM, which may or may not couple exclusively with quarks, in accordance with

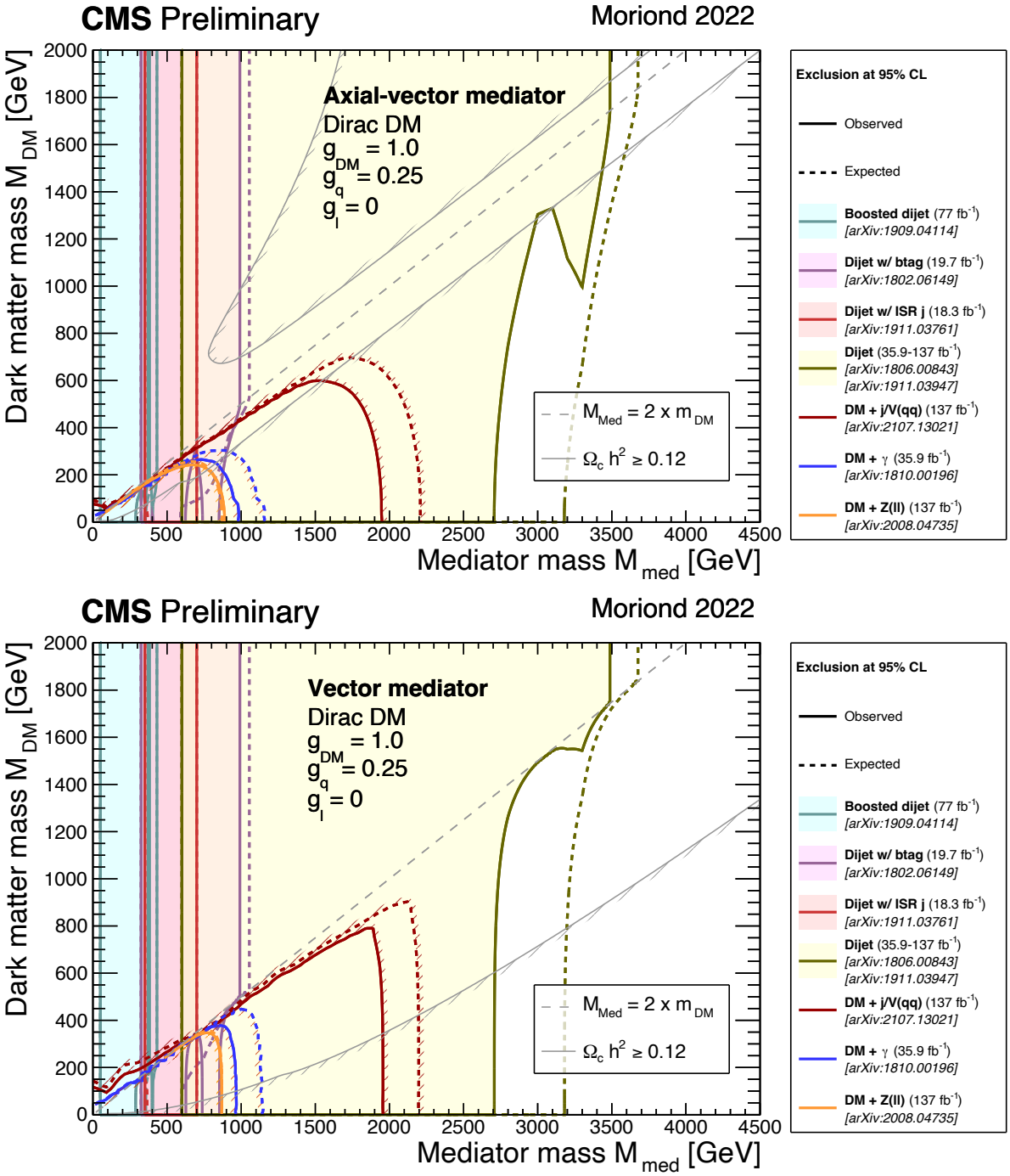

Figure 17 – Exclusion regions at 95%CL computed for a lepto-phobic Axial-vector (top) and vector (bottom) model. Here, the exclusions are computed for a quark coupling of $g_q = 0.25$ and for a DM coupling of $g_{\mathrm{DM}} = 1.0$. These limits are very model and parameter dependent, and usually cannot be applied for other models or choice of couplings [155] The models and couplings were chosen following the recommendations in [54], that also were used for scenarios in this work.

the recommendations by the LHC Dark Matter Working Group [52, 156].

In these studies, the CMS collaboration shows the restriction to a mediator coupling with the dark sector that reaches mass around 2 TeV for DM particles mass of $m_\chi = 1$ GeV

(see Figure 17). Moreover, in this same scenario, constraints on the mediator mass exceed 1.6 TeV even for a DM particle mass approximately of 800 GeV [155]. Exclusive dijet searches, which do not depend on the DM mass, focusing on an invariant mass of a new heavy mediator, have reported mass restrictions that surpass 2.6 TeV in the latest analyses as reported by Ref. [155]. However, it is crucial to recognize the model and parameter dependency of these searches; variations in the model or significant parameter alterations can invalidate these constraints, as noted by Ref. [155].

Interestingly, even when considering an axial-vector type mediator with the same parametrization, i.e. $g_{\mathrm{DM}} = 1$, $g_q = 0.25$, $g_\ell = 0$, the most stringent limits remain consistent with the vector case. Nonetheless, a notable difference emerges in the expected relic density for both cases. Axial-vector mediators exhibit a more restricted parameter space, aligned with the gray curve in Figure 17 defining the overabundance of DM in the early universe, specifically where $\Omega h^2 > 0.120$. Conversely, searches featuring a monophoton as ISR yield less restrictive mediator mass limits, under 1 TeV for both vector and axial-vector mediators, a fact that may favors more significant and detailed searches on this channel, such as those highlighted in the results of this work (see chapter 6).

Similarly, results from the ATLAS Collaboration [157] depicted in Figure 18 with identical coupling parametrization shows that a massive vector mediator is excluded for $M_{\mathrm{med}} \lesssim 2$ TeV at $m_\chi = 1$ GeV for monojet and p_T^{miss} searches, with slightly more stringent results for monophotons than CMS, indicating no detection of a mediator at least $M_{\mathrm{med}} \lesssim 1.5$ TeV for this ISR signal. Exclusive analyses in dijet final states, however, exclude masses below 3.5 TeV, also more stringent than the CMS findings.

However, in many models involving this type of interaction, the mediator is expected to have stronger couplings with the dark sector. Hence, exclusive measurements of Z' interactions with the SM, or any other mediator boson, are not unequivocally determined, due to their strong model dependence. That said, ATLAS results also suggest tighter restrictions in the region corresponding to the correct DM abundance for axial-vector mediators compared to vector ones, echoing the findings by CMS [155] in this matter.

It is worth to note that relic density calculations for massive mediators often overlook resonance production [90, 148], which inspired the pursuit of specific calculations in this regime by our part (see chapter 4). Resonance enhancement presents a compelling scenario for new physics, applicable in both LHC-type accelerators and electron-positron ones, the latter with the possibility of even more promising results, by tuning the center-of-mass energy to values near the invariant mass of the prospected mediator. This resonance-induced enhancement in the cross section could facilitate an increased event rate in this regime, which would favor the obtaining of even more properties about the particle or process under study.

Lastly, for exclusive dijet and dilepton searches in models with non-zero lepton

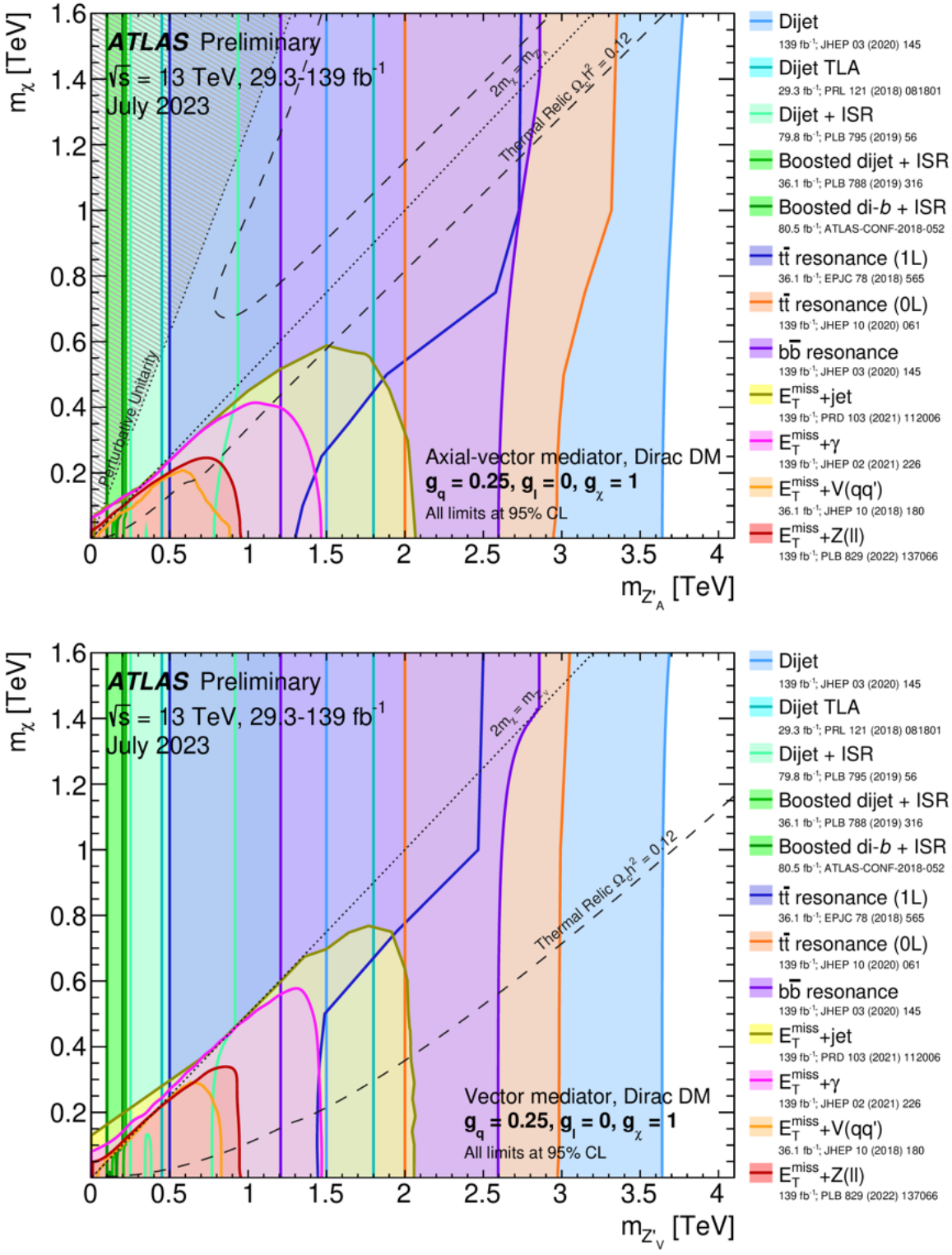

Figure 18 – The figures show excluded regions in the mass plane (M_{med} vs m_χ), at 95% CL by visible and invisible searches, for leptophobic axial-vector (top) and vector (bottom) mediators for simplified models. The couplings set are the same used in Figure 19 and Figure 17. The dashed lines correspond to where these parameter combinations is consistent with $\Omega h^2 = 0.120$ DM density, computed with `MadDM` [157].

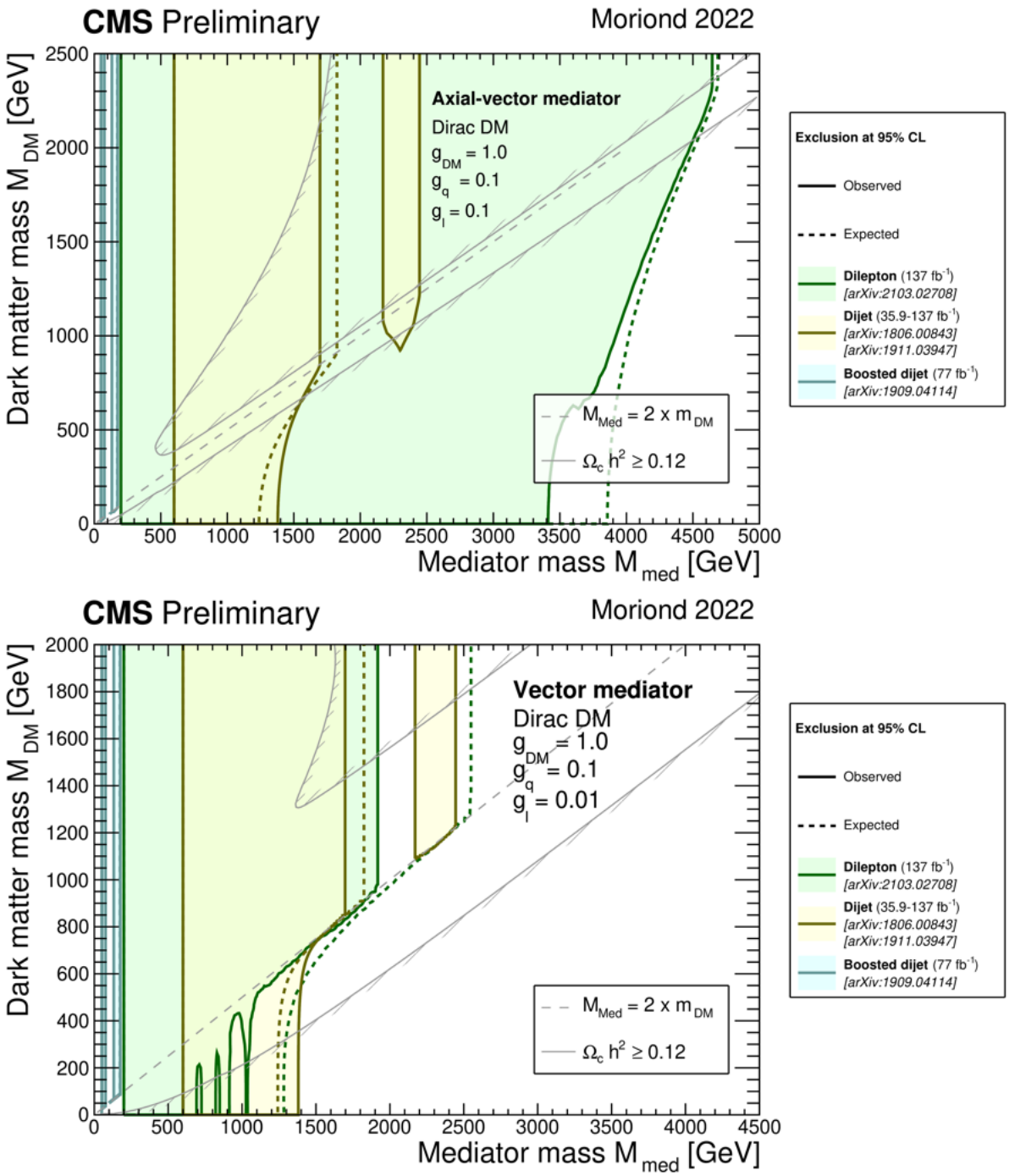

Figure 19 – Exclusion regions at 95%CL computed for a model with minimal couplings to leptons ($g_\ell = 0.01$) also for a Axial-vector (top) and vector (bottom) model. The universal quark couplings were set to $g_q = 0.1$ and for a DM coupling of $g_{\mathrm{DM}} = 1.0$ [155]. These limits, as well as for Figure 17, are very model and parameter dependent. The parameters were chosen following the recommendations in [54], that also were used for scenarios in this work.

coupling, where $g_l = 0.01$ and $g_q = 0.1$, following Refs. [52, 156], vector mediators face constraints at 95% confidence level around ≈ 1.4 TeV for dijets and ≈ 1 TeV for dilepton channels. Axial-vector mediators encounter even more stringent limits, with dijet searches in non-leptophobic models imposing mediator mass restrictions at 3.4 TeV and 1.4 TeV

for dilepton final states. ATLAS searches yielded similar outcomes [157], and variations in relic density remained comparable, given the minor relevance of SM final states compared to the masses and couplings involved with the estimation of the DM relic density.

In conclusion, the meticulous efforts undertaken by collider experiments, notably those from the LHC, have imposed a restrictive landscape in the quest for DM detection. The mono-X search strategies, complemented by the inclusion of multi-jet events, exhibit the complexity and sophistication of current experimental approaches. Despite the inherent challenges posed by background noise and systematic uncertainties, advances in computational techniques and data analysis, such as machine learning, are enhancing the sensitivity and precision of these searches. The comprehensive limits established on mediator masses and DM particle properties, as evidenced by both CMS and ATLAS collaborations, delineates a challenging parameter space for future explorations. With this we hope to illustrate the dynamic interplay between theoretical predictions and experimental constraints, clarifying where opportunities can be found for future investigations that may take into account higher energy collisions, novel detection strategies, or even alternative experimental setups beyond the LHC.

5.1 Computational Framework for HEP

On HEP, specially in new physics and BSM scenarios, utilization of computational tools and software has become indispensable. Theoretical, phenomenological, and experimental calculations in these fields often rely on a variety of software packages. Commonly used tools include `PYTHIA` [158], for simulating particle collisions at high energies and`GEANT4`, for modeling the passage of particles through matter [159]. Yet, particularly on DM searches, softwares as `MadDM` and `micrOMEGAS` are widely used within the community, providing solid results that can serve as benchmarks for various new physics models [160,161]. These software packages are instrumental in simulating complex physical processes, analyzing experimental data, and exploring the theoretical underpinnings of the Universe.

In this work we opted to develop our own code, which both advantages and disadvantages, though the benefits, in our opinion, often significantly impact the work of the researcher. Custom software can be tailored to specific research needs, offering flexibility and the ability to adapt to unique problem sets that off-the-shelf software might not address efficiently. It allows for the introduction of new theoretical models or simulation techniques ahead of the broader adoption of the community, providing a competitive edge in novel research areas. Additionally, developing custom code promotes a deeper understanding of the underlying physics and computational methods, enhancing the skills and insights of the researcher. However, it requires a significant investment of time

and resources, with the potential for bugs and errors that can lead to incorrect results if not meticulously checked. This was the case during much of the development of this work. Despite these drawbacks, the advantages of custom software development often outweigh the risks, especially for cutting-edge research that pushes the boundaries of knowledge.

In this way, computational physics, reinforced by the knowledge gained through both the use of established software and the development of custom code, empowers the researcher to cross disciplinary boundaries. The skills acquired in computational methods, data analysis, and numerical modeling are highly transferable and valuable in a wide range of interdisciplinary fields [162].

In this study, employing the Lagrangians referenced in section 3.5, we have been able to generate Feynman diagrams for the spin-1 mediator resonance in the s-channel, along with their corresponding amplitudes. This was achieved through both traditional Feynman rules and with the support of software tools such as `FeynCalc` and `FeynArts` packages for `Wolfram Mathematica` [163–165]. We present a schematic in Figure 20, illustrating the workflow and components of the software developed and employed throughout this investigation.

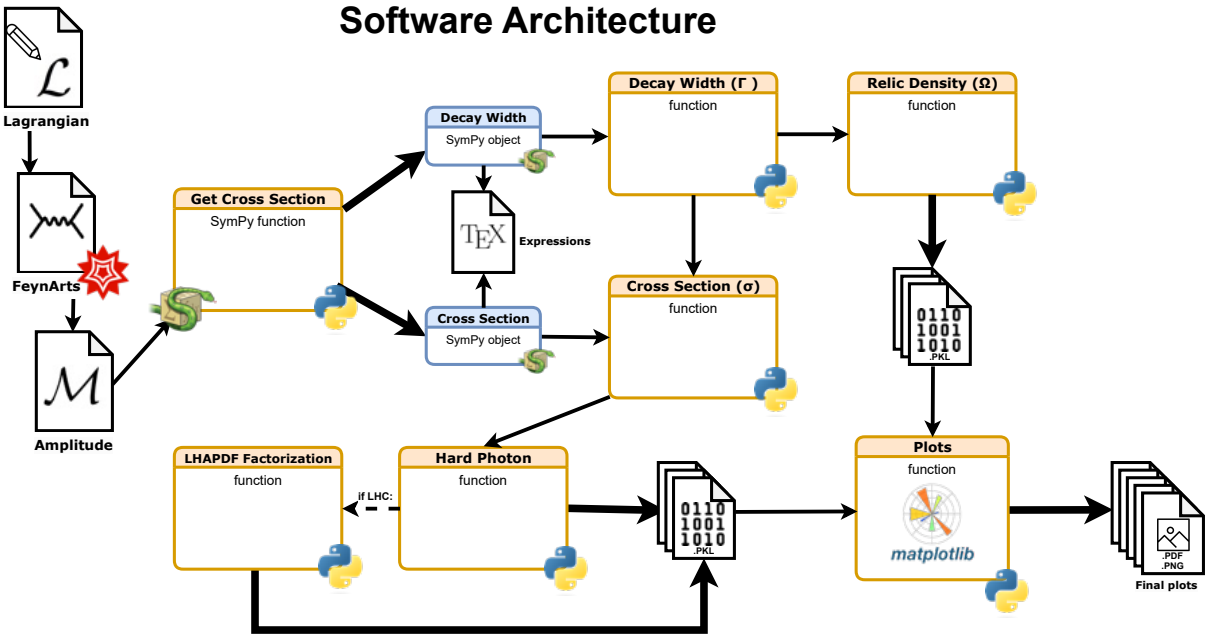

Figure 20 – Description of the software architecture employed to evaluate the models presented, ranging from their interaction Lagrangian to the final figures included in this work. The majority of the code was developed in Python; however, certain sections required the implementation of segments in other languages. All functions depicted in the diagram and utilized in the work were authored independently, except for minor adaptations from third-party codes used in certain sections.

Utilizing the amplitudes derived, we proceeded to compute the total cross sections with the aid of the `SymPy` symbolic manipulation package. The `SymPy` package is an open-

source Python library for symbolic mathematics. It is a computer algebra system which tries to keep the code as simple as possible in order to be comprehensible and provides a powerful environment for symbolic computation, allowing for algebraic operations, calculus, equation solving, discrete mathematics, and more [166]. Additionally, `SymPy` can also output results in LaTeX format, a feature that we took great advantage of to develop this work. Despite its relatively infrequent use in HEP, `SymPy` enables the performance of complex calculations essential for our field. For that, we used a pre-developed package designed for intuitive HEP calculations by Professor Christoph Berger [167, 168]. The functions and methods devised in it played a crucial role in validating various calculations previously attempted by other means, achieving satisfactory crosschecks that consolidated the confidence in our results.

We then developed specific functions for calculating the cross sections and decay widths for each scenario examined. This included functions for parton density and ISR factorizations based on the parameters of the studied processes, as well as functions for computing the relic density, incorporating all necessary integrations as described in chapter 4.

Finally, we prepared the figures for publication and discussed our results, benchmarking them against other significant findings in the literature (see Appendix A [138], Appendix B [139] and Appendix C [140]) This included comparisons with outcomes derived from other software and tools like `micrOMEGAS` for relic density calculations and `MadGraph` for total cross section computations [160, 169]. While computational limitations sometimes constrained the resolution within the parameter space, requiring models to run for several hours for each scenario and steps, the results remained coherent.

We believe that beyond the comprehensive control and precision gained in calculating the presented models, this methodology offered excellent training for us. It ensured our proficiency with computational physics techniques increasingly employed within the community, and we also anticipate that the software developed, shared with the community via a `GitHub` repository that can be found in Ref. [170], will contribute to further research to come. It could serve as both a crosscheck and benchmark for future investigations in the field, highlighting the importance of computational tools in advancing theoretical and experimental physics.

6 Results and Discussions

The complete discussion of the results of these investigations is detailed in the Appendices, which present the content of the scientific articles resulted from this work. In particular, the results from Appendix A [138] and Appendix B [139] convey the main findings of this thesis.

The first article focuses on the analysis of scalar and fermion DM candidates. This article has been submitted to and accepted for publication in the European Physical Journal C (EPJC). It delineates the implications of employing a simplified model for DM, alongside providing descriptive graphs for the accurate calculation of relic density, parameter selection for initial state radiation (ISR) calibration, and expressions and graphs for the total cross section of the processes described.

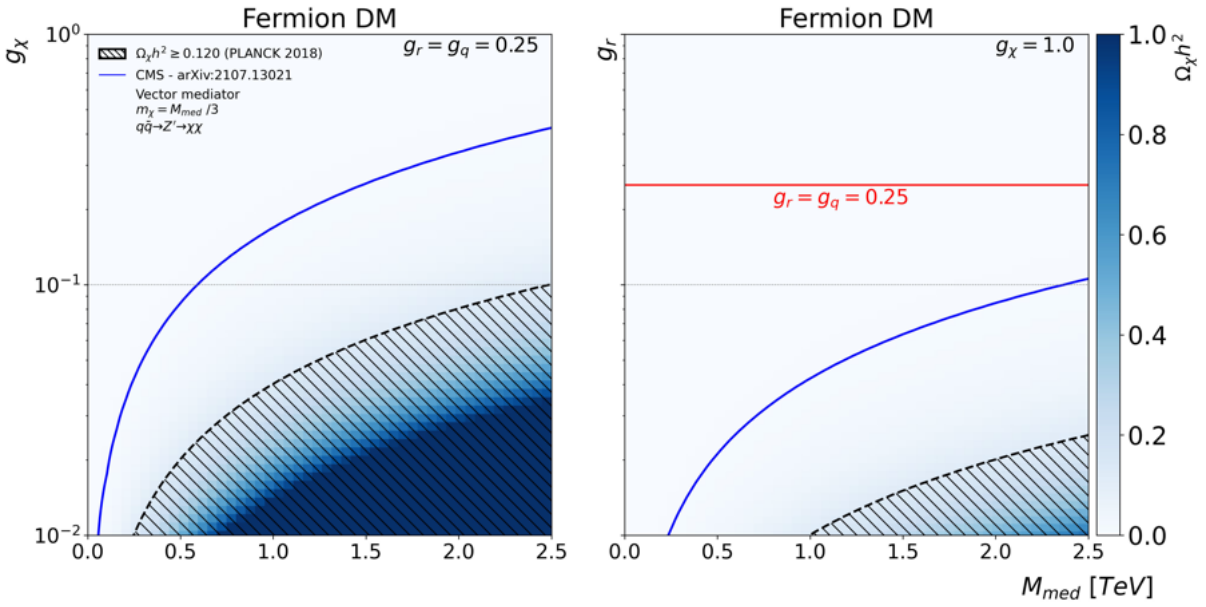

Figure 21 – Dimensionless density parameter $\Omega_\chi h^2$ for DM produced via Z' mediator with $M_{med} \equiv M_{Z'}$ [114] and DM pairs with mass $m_\chi = M_{Z'}/3$ in the s-channel taken for $q\bar{q}$ scenarios, where we scan over different values of g_r and g_χ, fixing (left panel) $g_r = 0.25$ as a leptophobic context ($g_\ell = 0$), and (right panel) $g_\chi = 1$ [138].

One of the main results achieved in this paper points to Figure 21, a plot that is akin to the one depicted in Figure 14, clearly demonstrating how the calculated relic density in a resonant process modifies the outcomes typically achieved through the standard numerical approximation referenced in [114] (solid blue line). In the scenario depicted by Figure 21, the relic density computation utilized a DM fermion, with the mediator mass set to $m_\chi = M_{Z'}/3$. Our findings indicate a pronounced suppression in the constrained area for values of $\Omega_\chi h^2 \geq 0.120$. This reduction is primarily attributed to the conventional

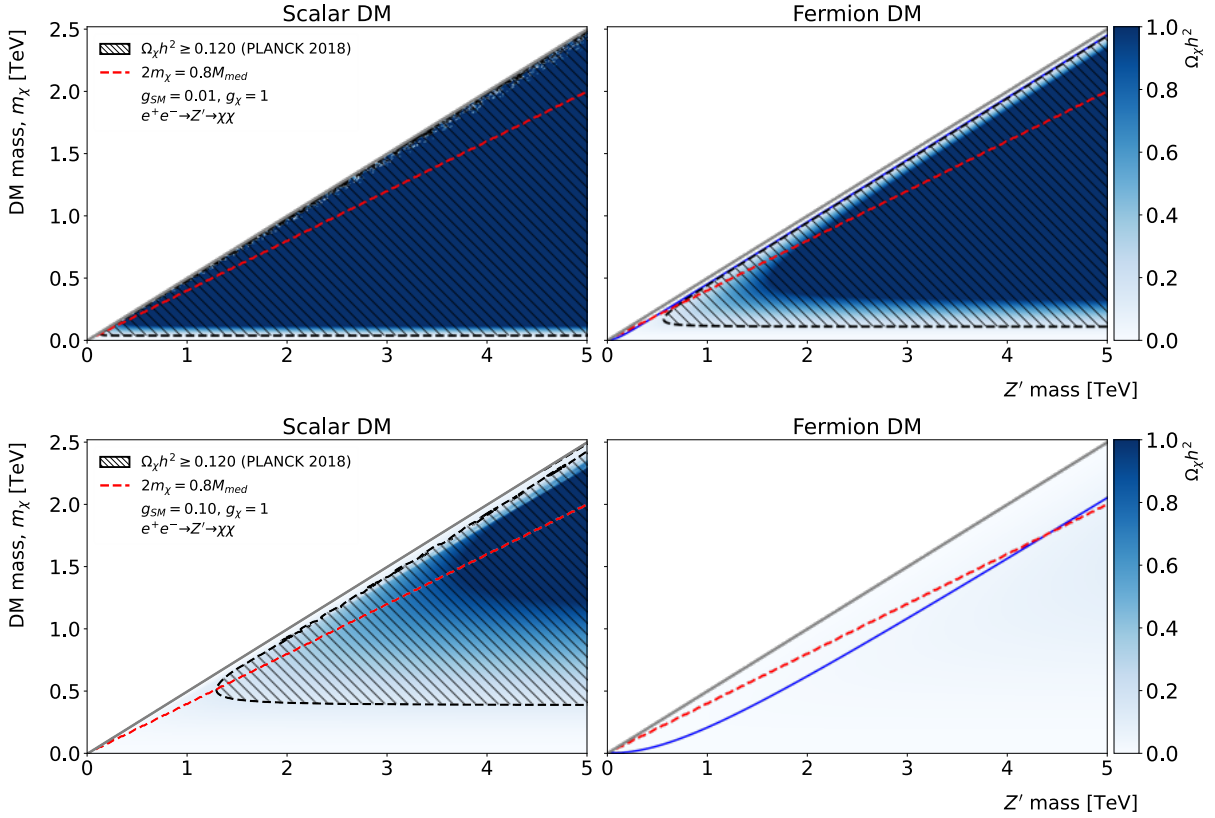

Figure 22 – Dimensionless density parameter $\Omega_\chi h^2$ for DM produced via Z' mediator with mass $M_{Z'}$ and DM pairs with mass m_χ taken for e^+e^- collisions, whereas a Z' couples with all six SM leptons pairs in the final state. The hatched area shows the regions with DM overabundance compared to the observed CDM abundance, which are excluded. The diagonal solid line represents the kinematic limit with $m_\chi = M_{Z'}/2$. For the upper plot, $g_r = 0.01$ and $g_\chi = 1$, while $g_r = 0.1$ and $g_\chi = 1$ for the bottom one. The red dashed lines show the threshold of the m_χ to produce the resonance with thermal energy while the blue solid lines on the fermion DM plots indicate the naive approach for relic density calculations, as in Ref. [52, 138].

calculation of relic density not accounting for resonance effects, which tends to overestimate the values for $\Omega_\chi h^2 \geq 0.120$, as demonstrated by our figures. This suggests that even lower couplings for the dark sector (g_χ and g_q) might be viable without breaching cosmological constraints on DM abundance. The limits and exclusion lines displayed in the plots consider the analytical values only, without taking into account statistical tests or the number of events of these processes. We chose to proceed this way considering the phenomenological nature of the study, but we understand that subsequent analyses taking into account more experimental characteristics of these models can enrich the work.

Furthermore, Figure 22 presents results from a non-leptophobic model consistent with the guidelines of Ref. [52], showing a substantial reduction in the area constrained by the primordial abundance of DM, especially when the coupling of the mediator to the dark sector is around $g_{\mathrm{SM}} = 0.1$ for a DM candidate that is a fermion. However, in this

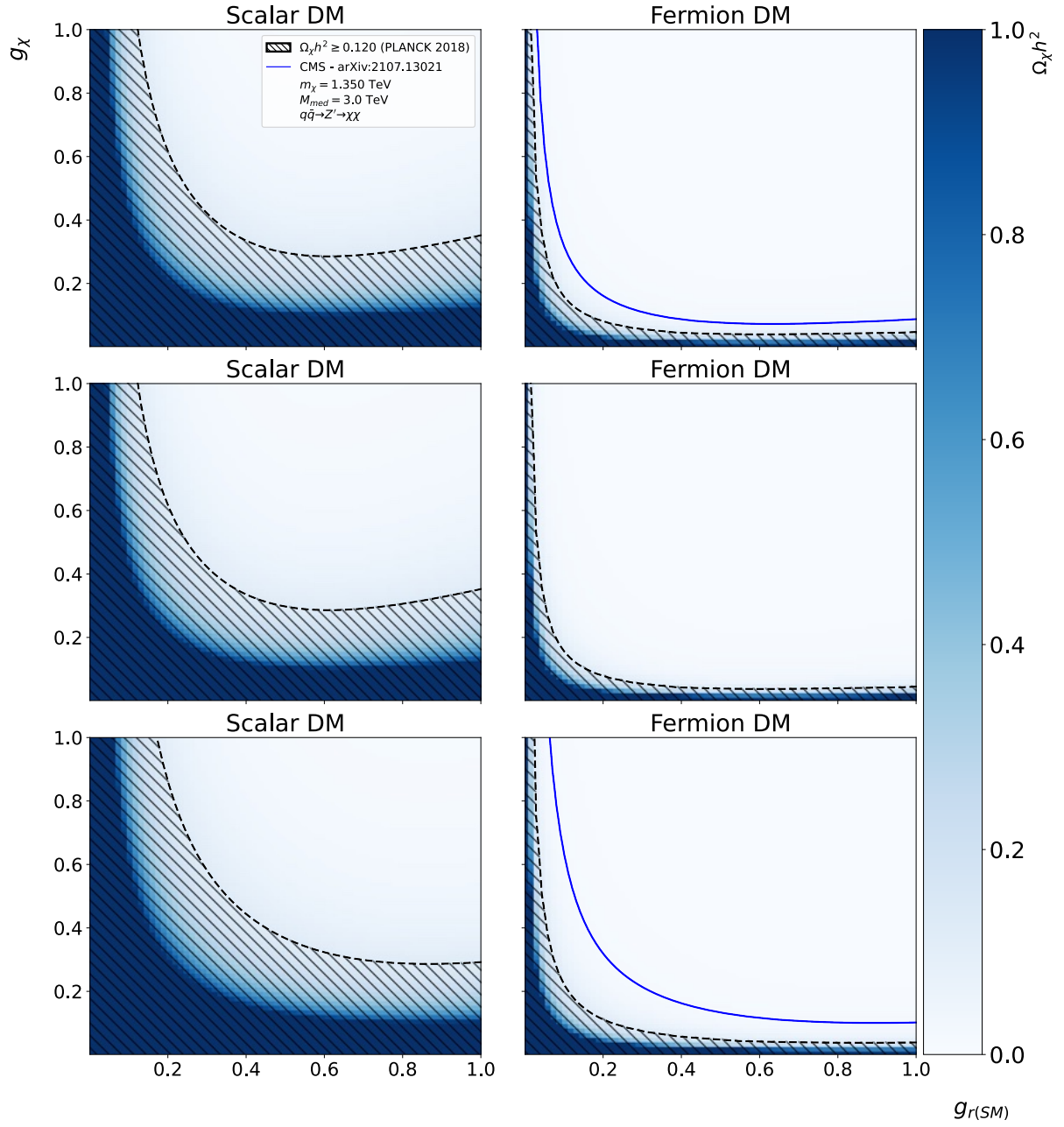

Figure 23 – Dimensionless density parameter $\Omega_\chi h^2$ for DM produced by a resonance with mass $M_{Z'} = 3$ TeV and decaying into DM pairs of mass 1350 GeV, whereas a Z' couples with all six SM leptons pairs in the final state. The region with a cross section smaller than that needed to produce the observed CDM abundance is shown beveled in black. We have vector couplings in the first row, axial-vector couplings in the second, and chiral (right) in the third one [138].

same scenario, a model predicting scalar-type DM (yet to be directly compared with other experimental outcomes) still faces significant restrictions in the phase space on the $M_{Z'}$ versus m_χ plane.

Additionally, in Appendix A [138], we discuss how variations in the couplings alone impact DM abundance, highlighting the importance of this parameter as demonstrated

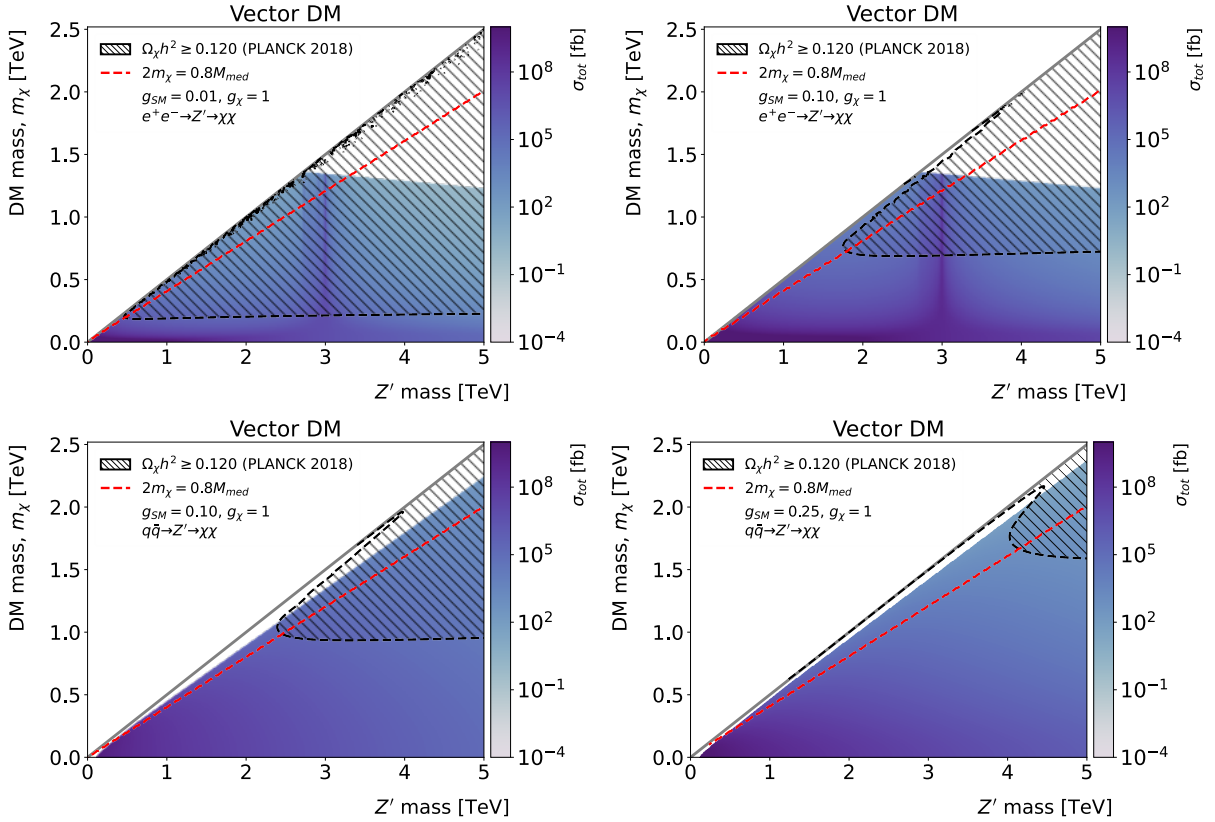

Figure 24 – Scan of the total cross section, including ISR contributions, as a function of DM (m_χ) and boson Z' ($M_{Z'}$) masses in e^+e^- (top) and pp (bottom) collision. The red dashed line indicates the threshold for examining the mass range close to the resonance, where the relic density is less suppressed. Plots differ by the use of the g_r coupling to leptons or quarks depending on the scenario [139].

in the previous figures. In Figure 23, we adjust the couplings of the vector, axial-vector, and chiral mediator from 0 to 1, observing the same reduction in constraints previously imposed by other studies, as we delve into more detail in Appendix A.

Results from Appendix B [139] explores a more elusive candidate within the same framework, characterized by an exclusively vector DM final state. Its primary distinction, besides the inherently more complex analytical calculation, is its inversely proportional dependence on the mass of the final state. This variance significantly alters the results by orders of magnitude, especially concerning the expected cross section. Therefore, it is plausible to assert that such a candidate should have already been observed in the kinetic regimes available at experiments, even though parameter space may still allow for potential observation.

Figure 24 demonstrates that the non-hatched area, indicative of regions not cosmologically constrained, is small and varies proportionally with the models proposed for scalar and fermion DM. In the context of a leptophobic model, we observe that the allowed region of phase space—characterized in this instance by the total cross-section in pb units of the process, already incorporating the observation of a monophoton in the initial

state—is more favorable than models involving mediator interactions with leptons, which were evaluated at smaller mediator couplings. However, for processes where production is exclusively through resonance channels, the inverse proportionality with m_χ is of minor relevance, considering the defined limit of $m_\chi = M_{Z'}/2$ (red dotted line) for the condition of producing resonant processes in the s-channel.

Lastly, Appendix C [140] pertains to an early phase of this study, evaluating exclusively the production cross sections of the three processes without considering initial state radiation or the correct calculation for relic density. Here, the DM abundance is estimated based on the *naive* approach widely disseminated in the literature (see chapter 4). Despite its preliminary nature, we believe this work is relevant as it showcases variations in the parameters explored in this research. It presents a version that can be more directly compared with first-principle calculations for the new physics under study here, without adding complexities beyond the calculation of cross sections and decay widths themselves.

In both works, the elucidation of models is evident, and we demonstrate how the selection of free parameters, and calculations derived from these simplified models can significantly impact expected results when in comparison with analogous findings in the literature, particularly regarding the final states of the DM candidates we examine, the initial photon that characterizes the proposed signal for such events, as well as details of calculations in resonance processes. These aspects allow for a more detailed evaluation of the parameters related to DM production.

7 Conclusion

There are a large set of observational clues that DM is present in our Universe. The analysis of radial velocities through the redshift of stars and galaxy clusters compellingly suggests the necessity of an additional non-baryonic matter to provide the gravitational pull required for the stability of such structures over extensive periods. Gravitational lensing effects and CMB measurements also corroborate to a DM hypothesis. The most recent data indicates that 26.4% of the energy-density, or 84.4% of the total matter is composed by a dark component, unlike anything present in the SM of elementary particles.

In this work, we have embarked on a comprehensive study of DM production mechanisms, particularly focusing on resonant process, its cosmological and phenomenological implications. Our investigation into the resonant production of DM through a new spin-1 mediator has not only clarified aspects of DM production in the primordial Universe but also provided a framework for calculating the appropriate relic density in such scenarios for the first time in the literature. Through the application of simplified models, we aimed to explore the potential observables that could signal the presence of DM in future and contemporary collider experiments, such as those conducted at the LHC.

By sweeping through the possible parameter space for DM production, we have constructed phenomenological models of the DM candidates under study, targeting future experimental data, especially in the upcoming Run-3 of the LHC and next generation electron-positron colliders. The comparison of our results with existing literature on analogous processes has been instrumental in delineating the potential of our proposed models to contribute and narrow the parameter space of DM searches. Radiative corrections, especially those involving high energy photon emissions, play a crucial role in identifying DM signals at these colliders. The methodological advancements in calculating these corrections enhance our ability to predict and identify DM signatures amidst numerous background processes.

In this study, with results published in Appendix A [138], Appendix B [139] and Appendix C [140], we demonstrate that with the proper relic abundance estimation, detecting new physics that could be DM in e^+e^- collisions presents significant challenges, with only a narrow phase space region potentially viable for fermion DM, particularly near the resonance if DM possesses couplings to SM leptons on the order of $\mathcal{O}(10^{-1})$. Conversely, for pp collisions, we identify a more promising detection landscape for resonances that could act as portals for DM production. For example, there is a promising detection region for larger vector DM couplings in the LHC energy regime. This is also true for fermion DM candidates, while scalar DM final states show little or no room for current

detection, taking into account the constraints and benchmark parameters applied in the literature. Nonetheless, we emphasize that our analysis of the relic density in proximity to a resonance must to be taken in forecasting LHC outcomes, as it reveals still-accessible regions for resonance production that align with both cosmological and collider constraints. Importantly, we find that near-resonance enhancements in $\langle \sigma v \rangle$ narrow the exclusion parameters, allowing for a 2-4 fold increase in accessible coupling constants, notably within the LHC kinematic regime. This indicates that experimental constraints on the mediator mass of DM could be refined beyond simple relic density calculations.

This research contributes to narrowing down the parameter space, with a focus on the mediator mass range, laying the groundwork for future searches of massive mediators through resonant s-channel production. However, it is important to note that should DM traces be detected in collider experiments, it would not immediately imply that such DM is identical to that inferred from cosmological gravitational effects. Moreover, cross-analyzing data from various experiments usually depends on specific DM models, highlighting the challenge of independent comparisons [1, 102]. Our findings underscore that monophoton production with significant missing momentum could serve as a competitive experimental signature for DM detection at the LHC, potentially unveiling the nature of a vector mediator for DM near its resonance.

A future work could prioritize the deduction of current constraints in direct detection methods, such as DM-nucleon interactions, to enhance our understanding and detection capabilities for experiments other than colliders. Additionally, we believe it is also important to explore the implications of mixing terms between these models, as well with another SM particles and potential more complex dark sectors that could include self-interactions or the formation of bound states.

In conclusion, our work contributes to the ongoing efforts to detect and understand DM by providing a theoretical and phenomenological basis for its study through collider physics and cosmological observations. While we have made significant advances in modeling DM interactions and predicting their observable signatures, the elusive nature of DM continues to challenge our understanding, given the lack of direct evidence for it until the date of writing this work. Future experimental data from the LHC and other observational platforms will be crucial in testing the models proposed and moving closer to uncover DM. The journey to fully comprehend DM is far from over, but each step forward, as delineated in this work, brings us closer to understanding the fundamental constituents of our Universe.

Bibliography

1 WORKMAN, R. L. et al. Review of Particle Physics. *PTEP*, v. 2022, p. 083C01, 2022. Cited 21 time in pages 9, 10, 21, 31, 32, 33, 34, 35, 36, 37, 40, 42, 43, 44, 45, 46, 47, 53, 55, 56, and 77.

2 AGHANIM, N. et al. Planck 2018 results. VI. Cosmological parameters. *Astron. Astrophys.*, v. 641, p. A6, 2020. [Erratum: Astron.Astrophys. 652, C4 (2021)]. Cited 5 time in pages 9, 21, 32, 33, and 34.

3 ZWICKY, F. Die Rotverschiebung von extragalaktischen Nebeln. *Helv. Phys. Acta*, v. 6, p. 110–127, 1933. Cited 2 time in pages 21 and 25.

4 ZWICKY, F. On the Masses of Nebulae and of Clusters of Nebulae. *The Astrophysical Journal*, v. 86, p. 217, out. 1937. Disponível em: <http://adsabs.harvard.edu/abs/1937ApJ....86..217Z>. Cited in page 21.

5 RYDEN, B. *Introduction to Cosmology*. Addison-Wesley, 2002. ISBN 0805389121. Disponível em: <https://www.xarg.org/ref/a/0805389121/>. Cited 10 time in pages 9, 21, 25, 29, 30, 32, 33, 34, 35, and 56.

6 CARR, B.; KüHNEL, F. Primordial black holes as dark matter: Recent developments. *Annual Review of Nuclear and Particle Science*, v. 70, n. 1, p. 355–394, 2020. Disponível em: <https://doi.org/10.1146/annurev-nucl-050520-125911>. Cited 4 time in pages 10, 21, 45, and 47.

7 CARR, B.; KUHNEL, F. Primordial Black Holes as Dark Matter Candidates. *SciPost Phys. Lect. Notes*, SciPost, p. 48, 2022. Disponível em: <https://scipost.org/10.21468/SciPostPhysLectNotes.48>. Cited 2 time in pages 21 and 45.

8 SASAKI, M. et al. Primordial Black Hole Scenario for the Gravitational-Wave Event GW150914. *Phys. Rev. Lett.*, v. 117, n. 6, p. 061101, 2016. [Erratum: Phys.Rev.Lett. 121, 059901 (2018)]. Cited in page 21.

9 FENG, J. L. Dark Matter Candidates from Particle Physics and Methods of Detection. *Ann. Rev. Astron. Astrophys.*, v. 48, p. 495–545, 2010. Cited 2 time in pages 21 and 22.

10 BOVEIA, A.; DOGLIONI, C. Dark Matter Searches at Colliders. *Ann. Rev. Nucl. Part. Sci.*, v. 68, p. 429–459, 2018. Cited in page 21.

11 BRÜNING, O. et al. The scientific potential and technological challenges of the High-Luminosity Large Hadron Collider program. *Rept. Prog. Phys.*, v. 85, n. 4, p. 046201, 2022. Cited in page 21.

12 SCHUMANN, M. Direct Detection of WIMP Dark Matter: Concepts and Status. *J. Phys. G*, v. 46, n. 10, p. 103003, 2019. Cited in page 21.

13 HEROS, C. Pérez de los. Status, Challenges and Directions in Indirect Dark Matter Searches. *Symmetry*, v. 12, n. 10, p. 1648, 2020. Cited in page 21.

14 AALTONEN, T. et al. High-precision measurement of the W boson mass with the CDF II detector. *Science*, v. 376, n. 6589, p. 170–176, 2022. Cited in page 22.

15 BOER, W. de. Grand unified theories and supersymmetry in particle physics and cosmology. *Prog. Part. Nucl. Phys.*, v. 33, p. 201–302, 1994. Cited in page 22.

16 HOOPER, D.; PROFUMO, S. Dark Matter and Collider Phenomenology of Universal Extra Dimensions. *Phys. Rept.*, v. 453, p. 29–115, 2007. Cited in page 22.

17 BIRKEDAL, A. et al. Little Higgs dark matter. *Phys. Rev.*, D74, p. 035002, 2006. Cited in page 22.

18 PARTICLE Dark Matter: Observations, Models and Searches. [S.l.]: Cambridge University Press, 2010. Cited in page 22.

19 MANOHAR, A. V. Introduction to Effective Field Theories. 4 2018. Cited in page 22.

20 BAEK, S.; KO, P.; PARK, W.-I. Search for the Higgs portal to a singlet fermionic dark matter at the LHC. *JHEP*, v. 02, p. 047, 2012. Cited in page 22.

21 JUNIOR, M. de S. M.; SILVEIRA, G. G. da. *Investigação da natureza de um mediador vetorial massivo para a matéria escura por meio de colisões e^+e^-*. Dissertação (Mestrado) — Universidade Federal do Rio Grande do Sul, Porto Alegre, Brasil, 2020. Disponível em: <https://lume.ufrgs.br/handle/10183/211546>. Acesso em: 01 ago. 2022. Cited 7 time in pages 22, 32, 33, 35, 38, 39, and 44.

22 BRITTO, A. L. M. *Oscilação de Neutrinos Produzidos por Aniquilação de Matéria Escura no Sol*. Dissertação (Mestrado em Ciências) — Universidade de São Paulo, 2014. Cited 2 time in pages 25 and 26.

23 LUBIN, L. M. Gas mass and total mass in clusters of galaxies. *AIP Conf. Proc.*, v. 336, p. 208–211, 1995. Cited in page 26.

24 MILGROM, M. MOND vs. dark matter in light of historical parallels. *Stud. Hist. Phil. Sci. B*, v. 71, p. 170–195, 2020. Cited in page 26.

25 JOHNSON JR., J. *Fritz Zwicky: Part eccentric, part genius, completely uncontained*. 2019. Disponível em: <https://www.sciencefocus.com/space/fritz-zwicky-part-eccentric-part-genius-completely-uncontained/>. Cited in page 27.

26 RUBIN, V. C.; FORD JR., W. K. Rotation of the Andromeda Nebula from a Spectroscopic Survey of Emission Regions. *Astrophys. J.*, v. 159, p. 379–403, 1970. Cited in page 27.

27 CARIGNAN, C. et al. Extended hi rotation curve and mass distribution of m31. *Astrophys. J. Lett.*, v. 641, p. L109–L112, 2006. Cited 2 time in pages 9 and 28.

28 MARTÍN, B. *Cem anos do eclipse de Sobral que deu razão a Einstein*. 2019. Disponível em: <https://brasil.elpais.com/brasil/2019/05/25/ciencia/1558801243_807178.html>. Cited in page 28.

29 WILLIAMS, M. Universe Today, 2023. Original images: NASA/ESA/D. Player (STScI) and NASA/ESA/STSc/T.Treu/Judy Schmidt. Disponível em: <https://www.universetoday.com/161198/gravitational-lensing-is-helping-to-nail-down-dark-matter/>. Cited 2 time in pages 9 and 29.

30 NOVATI, S. C. et al. Microlensing towards the SMC: a new analysis of OGLE and EROS results. *Mon. Not. Roy. Astron. Soc.*, v. 435, p. 1582, 2013. Cited in page 29.

31 GRIEST, K.; CIEPLAK, A. M.; LEHNER, M. J. New Limits on Primordial Black Hole Dark Matter from an Analysis of Kepler Source Microlensing Data. *Phys. Rev. Lett.*, v. 111, n. 18, p. 181302, 2013. Cited in page 29.

32 ABBOTT, B. P. et al. Search for Subsolar-Mass Ultracompact Binaries in Advanced LIGO's First Observing Run. *Phys. Rev. Lett.*, v. 121, n. 23, p. 231103, 2018. Cited in page 30.

33 AGENCY, E. E. S. *The bullet cluster*. NASA/CXC/CfA/M.Markevitch, 2007. Disponível em: <https://www.esa.int/ESA_Multimedia/Images/2007/07/The_Bullet_Cluster2>. Cited 2 time in pages 9 and 31.

34 HARVEY, D. et al. The non-gravitational interactions of dark matter in colliding galaxy clusters. *Science*, v. 347, p. 1462–1465, 2015. Cited 2 time in pages 9 and 31.

35 WANG, W.; ZHANG, M.; ZHAO, J. Higgs exotic decays in general NMSSM with self-interacting dark matter. *Int. J. Mod. Phys. A*, v. 33, n. 11, p. 1841002, 2018. Cited in page 30.

36 WEINBERG, D. H. et al. Cold dark matter: controversies on small scales. *Proc. Nat. Acad. Sci.*, v. 112, p. 12249–12255, 2015. Cited in page 30.

37 THOMPSON, R.; DAVÉ, R.; NAGAMINE, K. The rise and fall of a challenger: the Bullet Cluster in Λ cold dark matter simulations. *Mon. Not. Roy. Astron. Soc.*, v. 452, n. 3, p. 3030–3037, 2015. Cited in page 31.

38 ROBERTSON, A.; MASSEY, R.; EKE, V. What does the Bullet Cluster tell us about self-interacting dark matter? *Mon. Not. Roy. Astron. Soc.*, v. 465, n. 1, p. 569–587, 2017. Cited in page 31.

39 AGHANIM, N. et al. Planck 2018 results. I. Overview and the cosmological legacy of Planck. *Astron. Astrophys.*, v. 641, p. A1, 2020. Cited in page 33.

40 SACHS, R. K.; WOLFE, A. M. Perturbations of a cosmological model and angular variations of the microwave background. *The Astrophysical Journal*, American Astronomical Society, v. 147, p. 73, jan. 1967. ISSN 1538-4357. Disponível em: <http://dx.doi.org/10.1086/148982>. Cited in page 33.

41 COLLESS, M. et al. The 2df galaxy redshift survey: Spectra and redshifts. 2001. Disponível em: <https://arxiv.org/abs/astro-ph/0106498>. Cited in page 35.

42 BULLOCK, J. S.; BOYLAN-KOLCHIN, M. Small-Scale Challenges to the ΛCDM Paradigm. *Ann. Rev. Astron. Astrophys.*, v. 55, p. 343–387, 2017. Cited 2 time in pages 35 and 36.

43 ALLISON, K. *The standard model to the Planck scale*. Tese (Doutorado) — Balliol Coll., Oxford, 2014. Cited in page 37.

44 ROSS, G. *Grand unified theories*. Redwood City, Calif: Addison-Wesley, the Advanced Book Program, 1990. ISBN 978-0-8053-6968-7. Cited in page 37.

45 CSÁKI, C.; LOMBARDO, S.; TELEM, O. TASI Lectures on Non-supersymmetric BSM Models. In: _____. *Proceedings, Theoretical Advanced Study Institute in Elementary Particle Physics : Anticipating the Next Discoveries in Particle Physics (TASI 2016): Boulder, CO, USA, June 6-July 1, 2016*. [S.l.]: WSP, 2018. p. 501–570. Cited in page 37.

46 COLLINS, J. et al. Lorentz invariance and quantum gravity: an additional fine-tuning problem? *Phys. Rev. Lett.*, v. 93, p. 191301, 2004. Cited in page 37.

47 BLANKE, M. Flavour Physics from Present to Future Colliders. In: *Strong dynamics for physics within and beyond the Standard Model at LHC and Future Colliders*. [S.l.: s.n.], 2019. p. 116–123. Cited in page 37.

48 *The Meaning of anomalous couplings*, C960625. NEW176 p. [1063(1996)]. Cited in page 38.

49 ALVES, D. Simplified Models for LHC New Physics Searches. *J. Phys. G*, v. 39, p. 105005, 2012. Cited 2 time in pages 38 and 52.

50 SCHMEIER, D. Master thesis, *Effective Models for Dark Matter at the International Linear Collider*. 2013. ArXiv:1308.4409[hep-ph]. Cited 4 time in pages 38, 52, 53, and 54.

51 ABDALLAH, J. et al. Simplified models for dark matter searches at the lhc. *Physics of the Dark Universe*, v. 9-10, p. 8–23, 2015. ISSN 2212-6864. Cited 4 time in pages 38, 39, 52, and 53.

52 ALBERT, A. et al. Recommendations of the LHC Dark Matter Working Group: Comparing LHC searches for dark matter mediators in visible and invisible decay channels and calculations of the thermal relic density. *Phys. Dark Univ.*, v. 26, p. 100377, 2019. Cited 6 time in pages 12, 38, 52, 64, 67, and 72.

53 ABERCROMBIE, D.; AKCHURIN, N.; AL., E. A. et. Dark matter benchmark models for early lhc run-2 searches: Report of the atlas/cms dark matter forum. *Physics of the Dark Universe*, v. 27, p. 100371, 2020. ISSN 2212-6864. Disponível em: <https://www.sciencedirect.com/science/article/pii/S2212686419301712>. Cited 2 time in pages 38 and 52.

54 BOVEIA, A. et al. Recommendations on presenting LHC searches for missing transverse energy signals using simplified s-channel models of dark matter. *Phys. Dark Univ.*, v. 27, p. 100365, 2020. Cited 5 time in pages 11, 38, 52, 64, and 67.

55 LANGACKER, P. The Physics of Heavy Z' Gauge Bosons. *Rev. Mod. Phys.*, v. 81, p. 1199–1228, 2009. Cited 3 time in pages 38, 39, and 53.

56 ARCADI, G. et al. The waning of the WIMP? A review of models, searches, and constraints. *Eur. Phys. J. C*, v. 78, n. 3, p. 203, 2018. Cited 3 time in pages 39, 53, and 63.

57 BERTONE, G.; HOOPER, D. History of dark matter. *Reviews of Modern Physics*, 2016. Cited 2 time in pages 39 and 40.

58 ABE, T. et al. Lhc dark matter working group: Next-generation spin-0 dark matter models. *Physics of the Dark Universe*, 2018. Cited in page 39.

59 RUHDORFER, M.; SALVIONI, E.; WEILER, A. A Global View of the Off-Shell Higgs Portal. *SciPost Phys.*, v. 8, p. 027, 2020. Cited 2 time in pages 39 and 53.

60 D'ONOFRIO, M.; FISCHER, O.; WANG, Z. S. Searching for Dark Photons at the LHeC and FCC-he. *Phys. Rev. D*, v. 101, n. 1, p. 015020, 2020. Cited in page 39.

61 FRANK, M.; HUITU, K.; MONDAL, S. Dark matter and Collider signals in supersymmetric $U(1)'$ models with non-universal Z' couplings. *Phys. Rev. D*, v. 100, n. 11, p. 115018, 2019. Cited in page 39.

62 BALÁZS, C. et al. Sensitivity of the Cherenkov Telescope Array to the detection of a dark matter signal in comparison to direct detection and collider experiments. *Phys. Rev. D*, v. 96, n. 8, p. 083002, 2017. Cited in page 39.

63 BELYAEV, A. et al. Interplay of the LHC and non-LHC Dark Matter searches in the Effective Field Theory approach. *Phys. Rev. D*, v. 99, n. 1, p. 015006, 2019. Cited in page 39.

64 BUSONI, G. et al. On the Validity of the Effective Field Theory for Dark Matter Searches at the LHC. *Phys. Lett. B*, v. 728, p. 412–421, 2014. Cited in page 39.

65 PECCEI, R. D.; QUINN, H. R. CP Conservation in the Presence of Instantons. *Phys. Rev. Lett.*, v. 38, p. 1440–1443, 1977. Cited in page 39.

66 CORSICO, A. H. et al. The Potential of the variable DA white dwarf G117 - B15A as a tool for fundamental physics. *New Astron.*, v. 6, p. 197–213, 2001. Cited in page 39.

67 SANTOS, A. L. dos. *Matéria Escura como uma Extensão Higgs-Stuckelberg do Modelo Padrão*. Tese (Doutorado) — Universidade Federal do Rio Grande do Sul, Porto Alegre, Brasil, 2015. Disponível em: <https://lume.ufrgs.br/handle/10183/130087>. Acesso em: 28 dez. 2019. Cited in page 39.

68 BERTONE, G.; HOOPER, D.; SILK, J. Particle dark matter: Evidence, candidates and constraints. *Phys. Rept.*, v. 405, p. 279–390, 2005. Cited 4 time in pages 39, 41, 42, and 53.

69 CASTRO, L. B.; ALLOY, M. D.; MENEZES, D. P. Mass radius relation of compact stars in the braneworld. *JCAP*, v. 08, p. 047, 2014. Cited in page 39.

70 CORNELL, J. M.; PROFUMO, S.; SHEPHERD, W. Dark matter in minimal universal extra dimensions with a stable vacuum and the "right" Higgs boson. *Phys. Rev. D*, v. 89, n. 5, p. 056005, 2014. Cited 2 time in pages 39 and 53.

71 RANDALL, L.; SUNDRUM, R. A Large mass hierarchy from a small extra dimension. *Phys. Rev. Lett.*, v. 83, p. 3370–3373, 1999. Cited in page 39.

72 ABBOTT, B. P. et al. Observation of Gravitational Waves from a Binary Black Hole Merger. *Phys. Rev. Lett.*, v. 116, n. 6, p. 061102, 2016. Cited in page 40.

73 ABBOTT, B. P. et al. GW170817: Observation of Gravitational Waves from a Binary Neutron Star Inspiral. *Phys. Rev. Lett.*, v. 119, n. 16, p. 161101, 2017. Cited in page 40.

74 KOLB, E. W.; LONG, A. J. Superheavy dark matter through Higgs portal operators. *Phys. Rev. D*, v. 96, n. 10, p. 103540, 2017. Cited in page 40.

75 HERMS, J.; IBARRA, A. Probing multicomponent FIMP scenarios with gamma-ray telescopes. *JCAP*, v. 03, p. 026, 2020. Cited in page 40.

76 MOHANTY, S.; PATRA, A.; SRIVASTAVA, T. MeV scale model of SIMP dark matter, neutrino mass and leptogenesis. *JCAP*, v. 03, p. 027, 2020. Cited in page 40.

77 FEDDERKE, M. A.; GRAHAM, P. W.; RAJENDRAN, S. White dwarf bounds on charged massive particles. *Phys. Rev. D*, v. 101, n. 11, p. 115021, 2020. Cited in page 40.

78 BAUER, M.; PLEHN, T. *Yet Another Introduction to Dark Matter: The Particle Physics Approach*. [S.l.]: Springer, 2019. v. 959. (Lecture Notes in Physics, v. 959). Cited 7 time in pages 40, 44, 45, 47, 52, 56, and 57.

79 O'HARE, C. A. J. New Definition of the Neutrino Floor for Direct Dark Matter Searches. *Phys. Rev. Lett.*, v. 127, n. 25, p. 251802, 2021. Cited 3 time in pages 10, 40, and 43.

80 OUELLET, J. L. et al. First Results from ABRACADABRA-10 cm: A Search for Sub-μeV Axion Dark Matter. *Phys. Rev. Lett.*, v. 122, n. 12, p. 121802, 2019. Cited in page 42.

81 ASZTALOS, S. J. et al. A SQUID-based microwave cavity search for dark-matter axions. *Phys. Rev. Lett.*, v. 104, p. 041301, 2010. Cited in page 42.

82 AGUILAR-AREVALO, A. et al. Constraints on Light Dark Matter Particles Interacting with Electrons from DAMIC at SNOLAB. *Phys. Rev. Lett.*, v. 123, n. 18, p. 181802, 2019. Cited in page 42.

83 ARNAUD, Q. et al. First results from the NEWS-G direct dark matter search experiment at the LSM. *Astropart. Phys.*, v. 97, p. 54–62, 2018. Cited in page 42.

84 APRILE, E. et al. The XENON1T Dark Matter Experiment. *Eur. Phys. J. C*, v. 77, n. 12, p. 881, 2017. Cited in page 42.

85 APRILE, E. et al. Search for New Physics in Electronic Recoil Data from XENONnT. *Phys. Rev. Lett.*, v. 129, n. 16, p. 161805, 2022. Cited in page 42.

86 BERNABEI, R. et al. First model independent results from DAMA/LIBRA-phase2. *Nucl. Phys. Atom. Energy*, v. 19, n. 4, p. 307–325, 2018. Cited in page 42.

87 ANTONELLO, M. et al. Monte Carlo simulation of the SABRE PoP background. *Astropart. Phys.*, v. 106, p. 1–9, 2019. Cited in page 42.

88 FENG, J. L. et al. Planning the Future of U.S. Particle Physics (Snowmass 2013): Chapter 4: Cosmic Frontier. In: *Snowmass 2013: Snowmass on the Mississippi*. [S.l.: s.n.], 2014. Cited in page 43.

89 LIN, T. Dark matter models and direct detection. *PoS*, v. 333, p. 009, 2019. Cited in page 43.

90 GONDOLO, P.; GELMINI, G. Cosmic abundances of stable particles: Improved analysis. *Nucl. Phys. B*, v. 360, p. 145–179, 1991. Cited 11 time in pages 44, 48, 52, 56, 57, 58, 59, 60, 61, 62, and 65.

91 AGUILAR, M. et al. Towards Understanding the Origin of Cosmic-Ray Positrons. *Phys. Rev. Lett.*, v. 122, n. 4, p. 041102, 2019. Cited 3 time in pages 10, 44, and 45.

92 DAYLAN, T. et al. The characterization of the gamma-ray signal from the central milky way: A compelling case for annihilating dark matter. 2014. Disponível em: <https://arxiv.org/abs/1402.6703>. Cited in page 45.

93 CALORE, F.; CHOLIS, I.; WENIGER, C. Background Model Systematics for the Fermi GeV Excess. *JCAP*, v. 03, p. 038, 2015. Cited in page 45.

94 PROFUMO, S.; QUEIROZ, F.; SIQUEIRA, C. Has AMS-02 Observed Two-Component Dark Matter? *J. Phys. G*, v. 48, n. 1, p. 015006, 2020. Cited in page 45.

95 FALKOWSKI, A. et al. Flavourful Z' portal for vector-like neutrino Dark Matter and $R_{K^{(*)}}$. *JHEP*, v. 08, p. 061, 2018. Cited 2 time in pages 10 and 46.

96 COLAFRANCESCO, S.; PROFUMO, S.; ULLIO, P. Multi-frequency analysis of neutralino dark matter annihilations in the Coma cluster. *Astron. Astrophys.*, v. 455, p. 21, 2006. Cited in page 45.

97 COLAFRANCESCO, S.; PROFUMO, S.; ULLIO, P. Detecting dark matter WIMPs in the Draco dwarf: A multi-wavelength perspective. *Phys. Rev. D*, v. 75, p. 023513, 2007. Cited in page 45.

98 ABELL, P. A. et al. LSST Science Book, Version 2.0. 12 2009. Cited in page 45.

99 CERN. *Longer term LHC schedule*. 2023. Disponível em: <https://lhc-commissioning.web.cern.ch/schedule/LHC-long-term.htm>. Cited in page 47.

100 TODESCO, E. et al. A First Baseline for the Magnets in the High Luminosity LHC Insertion Regions. *IEEE Trans. Appl. Supercond.*, v. 24, n. 3, p. 4003305, 2014. Cited in page 47.

101 FERNANDEZ, I. Z. et al. High-Luminosity Large Hadron Collider (HL-LHC): Technical design report. v. 10/2020, 12 2020. Cited in page 47.

102 TREVISANI, N. Collider Searches for Dark Matter (ATLAS + CMS). *Universe*, v. 4, n. 11, p. 131, 2018. Cited 2 time in pages 47 and 77.

103 CHATRCHYAN, S. et al. Observation of a New Boson at a Mass of 125 GeV with the CMS Experiment at the LHC. *Phys. Lett. B*, v. 716, p. 30–61, 2012. Cited in page 48.

104 AAD, G. et al. Observation of a new particle in the search for the Standard Model Higgs boson with the ATLAS detector at the LHC. *Phys. Lett. B*, v. 716, p. 1–29, 2012. Cited in page 48.

105 GRIFFITHS, D. *Introduction to elementary particles*. 2. ed. Weinheim, Germany: Wiley-VCH Verlag, 2008. Cited in page 48.

106 ABADA, A. et al. FCC-ee: The Lepton Collider. *Eur. Phys. J. ST*, v. 228, n. 2, p. 261–623, 2019. Cited in page 49.

107 CEPC Study Group. Cepc conceptual design report: Volume 1 - accelerator. 9 2018. Cited in page 49.

108 ADOLPHSEN, C. et al. The International Linear Collider Technical Design Report - Volume 3.II: Accelerator Baseline Design. 2013. Disponível em: <https://arxiv.org/abs/1306.6328>. Cited in page 49.

109 LINSSEN, L. et al. Physics and Detectors at CLIC: CLIC Conceptual Design Report. 2012. Disponível em: <https://arxiv.org/abs/1202.5940>. Cited in page 49.

110 TUMASYAN, A. et al. Search for resonant production of strongly coupled dark matter in proton-proton collisions at 13 TeV. *JHEP*, v. 06, p. 156, 2022. Cited 3 time in pages 49, 50, and 51.

111 HALZEN, F. *Quarks and leptons : an introductory course in modern particle physics*. New York: Wiley, 1984. ISBN 978-0471887416. Cited in page 49.

112 SIRUNYAN, A. M. et al. Search for resonant and nonresonant new phenomena in high-mass dilepton final states at $\sqrt{s} = 13$ TeV. *JHEP*, v. 07, p. 208, 2021. Cited in page 50.

113 SIRUNYAN, A. M. et al. Search for high mass dijet resonances with a new background prediction method in proton-proton collisions at $\sqrt{s} = 13$ TeV. *JHEP*, v. 05, p. 033, 2020. Cited in page 50.

114 TUMASYAN, A. et al. Search for new particles in events with energetic jets and large missing transverse momentum in proton-proton collisions at $\sqrt{s} = 13$ TeV. *JHEP*, v. 11, p. 153, 2021. Cited 9 time in pages 10, 11, 12, 50, 51, 52, 53, 63, and 71.

115 CHATRCHYAN, S. et al. Search for New Physics with a Mono-Jet and Missing Transverse Energy in *pp* Collisions at $\sqrt{s} = 7$ TeV. *Phys. Rev. Lett.*, v. 107, p. 201804, 2011. Cited in page 51.

116 CHATRCHYAN, S. et al. Search for Dark Matter and Large Extra Dimensions in Monojet Events in *pp* Collisions at $\sqrt{s} = 7$ TeV. *JHEP*, v. 09, p. 094, 2012. Cited in page 51.

117 KHACHATRYAN, V. et al. Search for dark matter, extra dimensions, and unparticles in monojet events in proton–proton collisions at $\sqrt{s} = 8$ TeV. *Eur. Phys. J.*, C75, n. 5, p. 235, 2015. Cited in page 51.

118 AAD, G. et al. Search for new phenomena with the monojet and missing transverse momentum signature using the ATLAS detector in $\sqrt{s} = 7$ TeV proton-proton collisions. *Phys. Lett.*, B705, p. 294–312, 2011. Cited in page 51.

119 KHACHATRYAN, V. et al. Search for new phenomena in monophoton final states in proton-proton collisions at $\sqrt{s} = 8$ TeV. *Phys. Lett.*, B755, p. 102–124, 2016. Cited in page 51.

120 SIRUNYAN, A. M. et al. Search for new physics in the monophoton final state in proton-proton collisions at $\sqrt{s} = 13$ TeV. *JHEP*, v. 10, p. 073, 2017. Cited in page 51.

121 COLLABORATION, C. Search for Dark Matter Produced in Association with a Higgs Boson Decaying to Two Photons. 2017. Cited in page 51.

122 SIRUNYAN, A. M. et al. Search for associated production of dark matter with a Higgs boson decaying to $b\bar{b}$ or $\gamma\gamma$ at $\sqrt{s} = 13$ TeV. *JHEP*, v. 10, p. 180, 2017. Cited in page 51.

123 SIRUNYAN, A. M. et al. Search for dark matter produced in association with a Higgs boson decaying to $\gamma\gamma$ or $\tau^+\tau^-$ at $\sqrt{s} = 13$ TeV. *JHEP*, v. 09, p. 046, 2018. Cited in page 51.

124 SIRUNYAN, A. M. et al. Search for dark matter produced in association with a Higgs boson decaying to a pair of bottom quarks in proton–proton collisions at $\sqrt{s} = 13$ TeV. *Eur. Phys. J.*, C79, n. 3, p. 280, 2019. Cited in page 51.

125 KHACHATRYAN, V. et al. Search for dark matter and unparticles produced in association with a Z boson in proton-proton collisions at $\sqrt{s} = 8$ TeV. *Phys. Rev.*, D93, n. 5, p. 052011, 2016. [Erratum: Phys. Rev.D97,no.9,099903(2018)]. Cited in page 51.

126 KHACHATRYAN, V. et al. Search for dark matter in proton-proton collisions at 8 TeV with missing transverse momentum and vector boson tagged jets. *JHEP*, v. 12, p. 083, 2016. [Erratum: JHEP08,035(2017)]. Cited in page 51.

127 SIRUNYAN, A. M. et al. Search for dark matter produced with an energetic jet or a hadronically decaying W or Z boson at $\sqrt{s} = 13$ TeV. *JHEP*, v. 07, p. 014, 2017. Cited in page 51.

128 SIRUNYAN, A. M. et al. Search for dark matter and unparticles in events with a Z boson and missing transverse momentum in proton-proton collisions at $\sqrt{s} = 13$ TeV. *JHEP*, v. 03, p. 061, 2017. [Erratum: JHEP09,106(2017)]. Cited in page 51.

129 KHACHATRYAN, V. et al. Search for Monotop Signatures in Proton-Proton Collisions at $\sqrt{s} = 8$ TeV. *Phys. Rev. Lett.*, v. 114, n. 10, p. 101801, 2015. Cited in page 51.

130 SIRUNYAN, A. M. et al. Search for dark matter produced in association with a single top quark or a top quark pair in proton-proton collisions at $\sqrt{s} = 13$ TeV. *JHEP*, v. 03, p. 141, 2019. Cited in page 51.

131 FELDSTEIN, B.; FITZPATRICK, A. L.; KATZ, E. Form Factor Dark Matter. *JCAP*, v. 01, p. 020, 2010. Cited in page 53.

132 CUI, Y. et al. Candidates for Inelastic Dark Matter. *JHEP*, v. 05, p. 076, 2009. Cited in page 53.

133 CHANG, C.-F.; HE, X.-G.; TANDEAN, J. Two-Higgs-Doublet-Portal Dark-Matter Models in Light of Direct Search and LHC Data. *JHEP*, v. 04, p. 107, 2017. Cited in page 53.

134 ARCADI, G.; DJOUADI, A.; RAIDAL, M. Dark Matter through the Higgs portal. *Phys. Rept.*, v. 842, p. 1–180, 2020. Cited in page 53.

135 ROSZKOWSKI, L.; SESSOLO, E. M.; TROJANOWSKI, S. WIMP dark matter candidates and searches - current status and future prospects. *Rept. Prog. Phys.*, v. 81, n. 6, p. 066201, 2018. Cited in page 53.

136 BOYARSKY, A. et al. Sterile neutrino Dark Matter. *Prog. Part. Nucl. Phys.*, v. 104, p. 1–45, 2019. Cited in page 53.

137 AGRAWAL, P. et al. A Classification of Dark Matter Candidates with Primarily Spin-Dependent Interactions with Matter. *UMD-PP-10-004, RUNHETC-2010-07*, 2010. ArXiv:1003.1912[hep-ph]. Cited in page 54.

138 SILVEIRA, G. G. da; MATEUS, M. S. Investigation of scalar and fermion dark matter in mono-photon production at high-energy colliders. *Eur. Phys. J. C*, v. 84, n. 2, p. 181, 2024. Cited 10 time in pages 12, 54, 57, 61, 62, 70, 71, 72, 73, and 76.

139 SILVEIRA, G. G. da; MATEUS, M. S. Resonant production of vector dm states characterized by monophoton isr at high-energy colliders. Unpublished manuscript. 2024. Cited 9 time in pages 12, 54, 57, 61, 62, 70, 71, 74, and 76.

140 MATEUS, M.; SILVEIRA, G. G. da. Investigation of the nature of a massive vector mediator for dark matter through e^+e^- collisions. *Astron. Nachr.*, v. 342, n. 1-2, p. 411–415, 2021. Cited 4 time in pages 54, 70, 75, and 76.

141 GARCIA, M. A. G.; PIERRE, M.; VERNER, S. Scalar dark matter production from preheating and structure formation constraints. *Phys. Rev. D*, v. 107, n. 4, p. 043530, 2023. Cited in page 55.

142 HAWKING, S. Gravitationally collapsed objects of very low mass. *Mon. Not. Roy. Astron. Soc.*, v. 152, p. 75, 1971. Cited in page 55.

143 D'ERAMO, F.; FERNANDEZ, N.; PROFUMO, S. Dark Matter Freeze-in Production in Fast-Expanding Universes. *JCAP*, v. 02, p. 046, 2018. Cited in page 55.

144 MEEHAN, M. T.; WHITTINGHAM, I. B. Asymmetric dark matter in braneworld cosmology. *JCAP*, v. 06, p. 018, 2014. Cited in page 55.

145 ZUREK, K. M. Asymmetric Dark Matter: Theories, Signatures, and Constraints. *Phys. Rept.*, v. 537, p. 91–121, 2014. Cited in page 55.

146 PETRAKI, K. Slides presentation, *Dark matter candidates*. 2018. <https://indico.cern.ch/event/653314/contributions/2681551/attachments/1604718/2545530/Petraki_DarkMatterCandidates.pdf>. Accessed: 2024-02-18. Cited 2 time in pages 11 and 58.

147 BAE, K. J.; PARK, M.; ZHANG, M. Demystifying freeze-in dark matter at the LHC. *Phys. Rev. D*, v. 101, n. 11, p. 115036, 2020. Cited in page 60.

148 GRIEST, K.; SECKEL, D. Three exceptions in the calculation of relic abundances. *Phys. Rev. D*, v. 43, p. 3191–3203, 1991. Cited 2 time in pages 62 and 65.

149 BONNEAU, G.; MARTIN, F. Hard photon emission in e+ e- reactions. *Nucl. Phys. B*, v. 27, p. 381–397, 1971. Cited in page 63.

150 SIRUNYAN, A. M. et al. Search for new particles decaying to a jet and an emerging jet. *JHEP*, v. 02, p. 179, 2019. Cited in page 63.

151 AAD, G. et al. Search for new phenomena in events with an energetic jet and missing transverse momentum in pp collisions at $\sqrt{s}$ =13 TeV with the ATLAS detector. *Phys. Rev. D*, v. 103, n. 11, p. 112006, 2021. Cited in page 63.

152 COLLABORATION, C. Search for resonant and nonresonant new phenomena in high-mass dilepton final states at $\sqrt{s} = 13$ tev. *JHEP 07 (2021) 208*, 2021. Cited in page 63.

153 ORZARI, B. et al. LHC hadronic jet generation using convolutional variational autoencoders with normalizing flows. *Mach. Learn. Sci. Tech.*, v. 4, p. 045023, 2023. Cited in page 63.

154 KANSAL, R. et al. Evaluating generative models in high energy physics. *Phys. Rev. D*, v. 107, n. 7, p. 076017, 2023. Cited in page 63.

155 COLLABORATION, C. Compilation of plots, *Summary Plots EXO 13 TeV*. 2024. <https://twiki.cern.ch/twiki/bin/view/CMSPublic/SummaryPlotsEXO13TeV>. Accessed: 2024-02-18. Cited 4 time in pages 11, 64, 65, and 67.

156 ALVES, D. Simplified Models for LHC New Physics Searches. *J. Phys.*, G39, p. 105005, 2012. Cited 2 time in pages 64 and 67.

157 COLLABORATION, A. Compilation of plots, *Dark matter summary plots for s-channel, 2HDM+a, Higgs Portal and Dark Higgs models*. 2024. <https://atlas.web.cern.ch/Atlas/GROUPS/PHYSICS/PUBNOTES/ATL-PHYS-PUB-2023-018/>. Accessed: 2024-02-18. Cited 4 time in pages 11, 65, 66, and 68.

158 SJÖSTRAND, T. et al. An introduction to PYTHIA 8.2. *Comput. Phys. Commun.*, v. 191, p. 159–177, 2015. Cited in page 68.

159 AGOSTINELLI, S. et al. GEANT4–a simulation toolkit. *Nucl. Instrum. Meth. A*, v. 506, p. 250–303, 2003. Cited in page 68.

160 ALGUERO, G. et al. micrOMEGAs 6.0: N-component dark matter. 12 2023. Cited 2 time in pages 68 and 70.

161 ARINA, C. et al. Studying dark matter with MadDM 3.1: a short user guide. *PoS*, TOOLS2020, p. 009, 2021. Cited in page 68.

162 SANTORO, M.; BIERLY, P. Facilitators of knowledge transfer in university-industry collaborations: A knowledge-based perspective. *IEEE Transactions on Engineering Management*, v. 53, p. 495–507, 2006. Cited in page 69.

163 HAHN, T. Generating Feynman diagrams and amplitudes with FeynArts 3. *Comput. Phys. Commun.*, v. 140, p. 418–431, 2001. Cited in page 69.

164 SHTABOVENKO, V.; MERTIG, R.; ORELLANA, F. FeynCalc 9.3: New features and improvements. *Comput. Phys. Commun.*, v. 256, p. 107478, 2020. Cited in page 69.

165 INC., W. R. *Mathematica, Version 13.2*. 2022. Champaign, IL. Disponível em: <https://www.wolfram.com/mathematica>. Cited in page 69.

166 MEURER, A. et al. SymPy: symbolic computing in Python. *PeerJ Comput. Sci.*, v. 3, p. e103, 2017. Cited in page 70.

167 BERGER, C. *Elementarteilchenphysik: Von den Grundlagen zu den modernen Experimenten*. Springer Berlin Heidelberg, 2014. ISSN 0937-7433. ISBN 9783642417535. Disponível em: <http://dx.doi.org/10.1007/978-3-642-41753-5>. Cited in page 70.

168 BERGER, C. *Particle physics using Python/Sympy*. 2018. Website. Available online at <https://profchristophberger.com/lehrbuch-elementarteilchenphysik/python/> [Accessed Date: 2024-02-18]. Cited in page 70.

169 ALWALL, J. et al. The automated computation of tree-level and next-to-leading order differential cross sections, and their matching to parton shower simulations. *JHEP*, v. 07, p. 079, 2014. Cited in page 70.

170 JR, M. S. M. *resonant-dm-relic*. 2023. GitHub repository. Disponível em: <https://github.com/mardesoushi/resonant-dm-relic>. Cited in page 70.

APPENDIX A – Investigation of scalar and fermion dark matter in mono-photon production at high-energy colliders

Eur. Phys. J. C (2024) 84:181
https://doi.org/10.1140/epjc/s10052-024-12528-9

THE EUROPEAN PHYSICAL JOURNAL C

Regular Article - Theoretical Physics

Investigation of scalar and fermion dark matter in mono-photon production at high-energy colliders

G. Gil da Silveira[1,2,a], **M. S. Mateus Jr.**[2,b]

[1] PH Department, CERN, 1211 Geneva, Switzerland
[2] Group of Analysis and Simulation of Particles (GASP), IF-UFRGS, Caixa Postal 15051, Porto Alegre, RS CEP 91501-970, Brazil

Received: 8 July 2023 / Accepted: 7 February 2024

Abstract Many theories about dark matter have emerged due to its strong theoretical appeal in explaining astrophysical phenomena. However, experimental and theoretical particle physics have yet not provided evidence that dark matter is part of the observable Universe. Our work aims to investigate the interaction between Standard Model (SM) fermions and different species of dark matter (DM) particles in high-energy collisions through interaction of a new massive vector mediator, Z'. The production of scalar and fermion DM pairs via fermion annihilation into the new vector boson is investigated near a resonance ($m_\chi \sim M_{Z'}/2$), where a SM signal from hard photon emission is considered as initial state radiation, namely a mono-photon production. Values of coupling constants between the DM and the SM particles are mapped in contrast to the Planck satellite data for thermal relic density DM computed in the correct framework for the relic density near a resonance, where a weaker suppression of the relic density is expected. We show for the CLIC and LHC kinematic regimes that certain mass ranges and coupling constants of these DM particles are in agreement with the expected relic density near a resonance and are not excluded by collider and astrophysical limits.

1 Introduction

The Standard Model (SM) of the elementary particle interactions has been tested for a variety of phenomena in particle physics at great precision. Nevertheless, there is no (currently) particle in the SM that satisfies the characteristics of the dark matter (DM), i.e., a suitable candidate to explain astrophysical phenomena at cosmological, galaxy cluster and galactic scales. Neutrinos, for example, known to have non-zero mass [1], would be an ideal candidate for DM, however their mass is too small to account for large structure formation [2,3]. It is reasonable, therefore, to conceive extensions of the SM that could include new particles and interactions that are consistent with an even more complete description of nature. Several studies have been proposed to investigate the DM and to decipher its origin and nature [2–9], where distinct approaches aim to understand how DM interacts, with itself and with the SM particles, and what could be the possible mechanisms of detecting it.

Following Refs. [3,10–12], our work assumes a simplified model where the interaction of any Weakly Interactive Massive Particle (WIMP) with the SM is mediated by a new massive boson at GeV–TeV scale, which we will indicate hereafter by Z' [12–15]. This Z' boson then acts as a mediator in the production of primordial DM until the *freeze-out* is reached [16]. A higher mass mediator is preferred due to strong experimental constraints in the search for a resonance at lower masses, then we show that a massive vector mediator on the TeV scale would be accessible even with the restrictions imposed on phase space by the current collider searches. Unlike the cases analyzed in Refs. [10,11], we do not assume a priori any effective model and proceed with the calculation of the total cross section, σ_{tot}, using the Feynman rules obtained from the simplified model Lagrangian, where the templates for couplings and vertices remain very similar to those in the SM for massive gauge bosons. Hence, we are not only interested in parameters related to the final state of the particles, such as their mass and spin, but also on the characteristics for a mediator Z' and their couplings with the initial state fermions, ψ, and the DM particle, χ, in final state.

In this context, we could attempt to recreate it with the use of particle colliders with sufficient high energies if DM was produced by a thermal process that has gone through a freeze-out [16]. An arbitrary coupling of DM with ordinary

[a] e-mail: gustavo.silveira@cern.ch (corresponding author)
[b] e-mail: msmateusjr@gmail.com

Published online: 22 February 2024

matter is hence assumed, expressed in the form of an arbitrary gauge coupling, which would represent a direct dark sector coupling to leptons and/or quarks [3,17–19]. Nonetheless, the detection of DM particles poses a major experimental challenge, since DM-related couplings are expected to be very weak [20], e.g., as much or even more than those with neutrinos, and exclusion limits have been recently imposed on massive vector mediators up to the TeV scale [21–23]. In general, searches in high-energy colliders focus in the observation of DM signatures in the form of missing transverse momentum or missing transverse energy [24–26]. Such a signal would occur if the DM particles are invisible to the detector or a possible charged DM particle has a sufficiently long lifetime to pass through the detector volume and leave a characteristic trace of charged particles, decaying shortly into particles too light to generate any signs on the detector calorimeters.

In this work we investigate the Z' production via monophoton production process in electron-positron annihilation (e^+e^-) at CLIC at $\sqrt{s} = 3$ TeV [27] and for proton-proton (pp) collisions at the LHC at $\sqrt{s} = 14$ TeV in the scenario where the invisible decay products of the Z' mediator, i.e. DM particles, have invariant masses close to the resonance and the photon is the SM signal to be triggered. Considering the limits already imposed by the searches performed by the ATLAS and the CMS Collaboration of DM mediator mass above 2 TeV [28,29], we focus this study in a Z' mass of 3 TeV in both CLIC and LHC. As a result, one has to properly account for the viability of the DM model candidate by accounting for the expected relic density, and this calculation cannot rely on the usual framework usually done away from resonances. As shown in Refs. [30,31], the proper treatment of the relic density near a resonance results in a weaker reduction of the expected relic density. Hence, we compare our predictions for the production cross sections with the proper evaluation of the relic density for DM species for the first time in the literature.

This paper is organized as follows: in Sect. 2 we describe the theoretical modeling of the Z' mediator, with some motivations for a scalar and fermion final DM states,[1] nonetheless a richer dark sector can be studied in the TeV scale in a subsequent analysis, as proposed by [33]. In Sect. 3 we present the evaluation of the relic density near a resonance. This approach enables effective comparisons with results in the literature typically obtained without taking the resonance into account. In Sect. 4 we discuss how this model could be perceived with a ISR assuming a hard-photon emitted by the an incoming fermion [34] and present the results obtained for the mass and coupling constant regions available at the high-energy CLIC and LHC colliders. Finally, we present our conclusions in Sect. 5.

2 Theoretical framework

Extensions of the SM can usually be studied using effective, simplified, or (so to say) complete models [1,3]. Still, we can make several claims regarding the nature of the kind of New Physics we expect to find even with the simplest effective models [35]. These models are a starting point for studying New Physics, given their simplicity on describing the particles and interactions involved using only a small number of parameters that can be directly related to experimental observations, such as: mass of the particles involved, their decay widths, production cross sections of these new processes, among others [36]. One can apply a simplified model in trying to explain some New Physics results through functions of the variables involved in its description, excluding certain values based on different experimental constraints [37].

We start with interaction Lagrangians describing a SM extension with some new symmetry group $U_\chi(1)$ acting as a vector portal for DM. The use of a $U_\chi(1)$ symmetry for investigating interactions between DM and SM has been widely proposed [1,17,38,39] and very tightly constrained at low and high masses have been imposed mostly by collider experiments (e.g., see Refs. [28,29]). This work explores a framework to probe the limits and to analyze parameters for the DM thermal production through a process that involves interactions of the SM with the dark sector mediated by a new massive boson mediator (Z') described with a Breit–Wigner (BW) resonance. Such mediator couples to scalar and fermion fields as candidates for DM. Feynman diagrams representing the s-channel Z'_μ exchange with DM candidates, χ, are shown in Fig. 1, where $g_{r/l}$ and g_χ are the couplings of this new spin-1 boson to the SM and the different DM fields, respectively. Here we investigate the different final DM states as separated cases; details of the implications of the simultaneous existence of these final states for DM and possible interactions between them are beyond the scope of this work. These possible states would be an aspect of a even more complete model where further studies could be performed with a experimental observation. We then focus on the evaluation of the cross section and in turn analyze the parameter space more comprehensively. As widely followed in the literature, we do not focus on how the Z' boson acquires its mass, nor we delve into details regarding the gauge regularization of the presented Lagrangians, which does not hinder the derivation of our results or similar studies [40] that follows this same methodology. More comprehensive models on spin-1 mediators and the related final states that prescribe their gauge

[1] Here we assume that each kind of DM final state composes all the DM relic abundance observed by the PLANCK satellite [32].

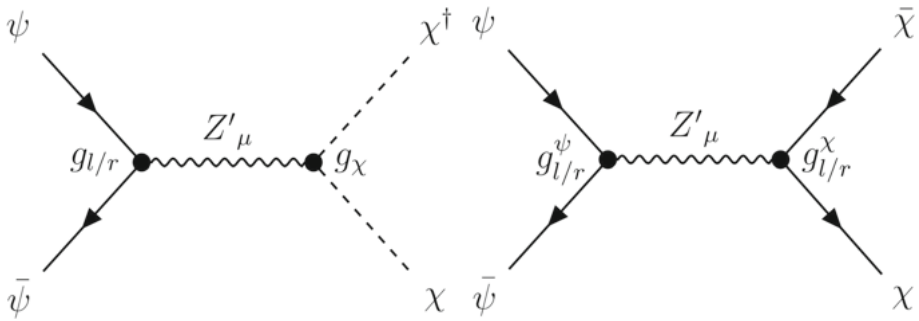

Fig. 1 Feynman diagrams for the interaction of SM fermions, ψ, with a scalar (left), fermion (right) χ, field through a Z' boson. The couplings $g_{r/l}$ and g_χ represents the coupling of the Z' boson with the SM and the DM fields, respectively

invariance are described in Refs. [1,2,9,12,17,29,38,41–44].

2.1 Tree-level process with s-channel resonance

Let ψ be any SM fermion spinor and Z'_μ a real vector[2] field corresponding to an on-shell massive spin-1 mediator coupling to scalar particles representing the DM fields [Fig. 1 (left)]. An extension interaction Lagrangian of this process can be written as

$$\mathcal{L}^{\text{scalar}}_{\text{int}} \supset \bar{\psi}\gamma^\mu \left(g_l P_L + g_r P_R\right) \psi Z'_\mu + g_\chi \left(\chi^\dagger \partial_\mu \chi - \chi \partial_\mu \chi^\dagger\right) Z'^\mu, \quad (1)$$

where we use $M_{Z'}$ for the mediator mass and γ^μ are the usual Dirac matrices. The P_L and P_R operators refer to left and right-handed operators, respectively, defined by $P_L \equiv \frac{1}{2}(1-\gamma^5)$ and $P_R \equiv \frac{1}{2}(1+\gamma^5)$, with g_l and g_r representing chiral coupling magnitudes. The final DM scalar state is well motivated both in simplified effective models and more complete models containing sometimes a Higgs doublet [9,41,42] that can act as a mediator between or be the main composition of a dark sector. In most of the literature, masses below a few GeV are largely excluded by different experimental DM detection pathways [45–47], hence we discuss the production of scalar DM where the final state mass is on the TeV scale.

For a DM particle characterized as a Majorana fermion (Fig. 1, right), the interaction Lagrangian has the form

$$\mathcal{L}^{\text{fermion}}_{\text{int}} \supset \left[\bar{\psi}\gamma^\mu \left(g_l P_L + g_r P_R\right) \psi + \bar{\chi}\gamma^\mu \left(g_\chi P_L + g_\chi P_R\right) \chi\right] Z'_\mu, \quad (2)$$

where we adopt $g_{l/r} \neq g_\chi$ and $g_{\chi,r} = g_{\chi,l} = g_\chi$ due to the Majorana condition for the spinor components. Moreover, we see that the interaction of the Z' boson with the DM field is given by the operators in the last term of Eq. 2, which also contains the adjoint spinor for the DM particle $\bar{\chi}$ and once again the chiral operators and couplings.

[2] Depending on the chosen coupling configuration, this mediator can function as an (axial)vector or a chiral vector. Refer to Table 1 for further details.

Fermion DM is well motivated through the literature and seen as one of the main candidates for WIMP DM in many different models [1,2,29,38]. For instance, a well-studied case in minimal supersymmetric models (MSSM) [48] would be the existence of a long lived particle (LLP) in the form of a neutralino, Dirac or Majorana fermion coming from the symmetry of the neutral mediators of the SM. However, in the case of the LLP, as well as other candidates, the manifestation in any experiments would not necessarily classify this new particle as dark matter itself. Further investigations would be required to identify its properties to trace it as new physics that explains any of the open problems in contemporary physics, including the issue of dark matter in astrophysical observations [12,29]. Furthermore, universal extra-dimensional models [43] as well as models with sterile neutrino [44] introduce candidates in the form of a fermion final state, sometimes discussed in another mass scale though. We emphasize that we deal with masses at the TeV scale, an accessible mass window in searches at high-energy collider experiments.

2.2 Production cross section and decay widths

The cross sections for all process in Fig. 1 are obtained with the help of `FeynCalc` [49] and `FeynArts` [50] packages available for the `Wolfram Mathematica` software [51]. From the Lagrangians and Feynman diagrams, scattering amplitudes are obtained and evaluated using Feynman rules and appropriate kinematic variables for these packages. Once the expression for the total cross section of the process $2 \to 2$ is obtained, the mass and couplings of the particles involved in the process are treated as free parameters and evaluated separately.

The total cross section, $\hat{\sigma}_{\text{tot}}$, for a process $2 \to 2$ in the center-of-momentum (CM) frame can be calculated in terms of the Mandelstam variable s, averaging over the spin of the initial states of those processes and the square of weighted scattering amplitude over all initial spin states. Thus we obtain the total cross section for these processes:

Table 1 Categorization of SM couplings following the definition given in Ref. [10]

Coupling type	Definition
Vector	$g_l = g_r$
Axial-vector	$g_l = -g_r$
Right (*chiral*)	$g_l = 0$

$$\hat{\sigma}_{\text{tot}}^{\text{scalar}} = \frac{g_\chi^2 \left(g_l^2 + g_r^2\right)\left[s(s-4m_\chi^2)\right]^{3/2}}{192\pi s^2\left[\left(s - M_{Z'}^2\right)^2 + \Gamma^2 M_{Z'}^2\right]}, \tag{3a}$$

$$\hat{\sigma}_{\text{tot}}^{\text{fermion}} = \frac{g_\chi^2\sqrt{s-4m_\chi^2}\left[g_l^2\left(s-m_\chi^2\right) + 6g_l g_r m_\chi^2 + g_r^2\left(s-m_\chi^2\right)\right]}{48\pi\sqrt{s}\left[\left(s - M_{Z'}^2\right)^2 + \Gamma^2 M_{Z'}^2\right]}. \tag{3b}$$

The terms for the BW width ($\Gamma^2 M_{Z'}^2$) in the denominator of the scattering amplitudes correspond to the mediator exchange of a s-channel resonance.

As we will deal with the cross section of a process involving a massive spin-1 mediator, we need to compute the decay widths. The Z' decay into both species of DM particles are evaluated to determine the decay width, Γ^{i}, at which it can decay into two DM particles of identical masses m_χ. The calculation is performed in the same way as for any $1 \to 2+3$ process, where the decay width Γ takes the form:

$$\Gamma_{a\to b+c} = \frac{|\vec{p}_f|}{8\pi M^2}\frac{|\mathcal{M}_{1\to 2}|^2}{3}, \tag{4}$$

resulting in the respective decays widths for each DM final state:

$$\Gamma^{\text{scalar}} = \frac{g_\chi^2\left(M_{Z'}^2 - 4m_\chi^2\right)\sqrt{1-4m_\chi^2/M_{Z'}^2}}{48\pi M_{Z'}}, \tag{5}$$

$$\Gamma^{\text{fermion}} = \frac{N_f\left[g_{l\chi}^2\left(M_{Z'}^2 - m_\chi^2\right) + 6g_{l\chi}g_{r\chi}m_\chi^2 + g_{r\chi}^2\left(M_{Z'}^2 - m_\chi^2\right)\right]\sqrt{1-4m_\chi^2/M_{Z'}^2}}{24\pi M_{Z'}}. \tag{6}$$

In this context, the parameter N_f represents the count of fermions with which Z' can decay within the SM sector. Specifically, we set $N_f = 6$ for e^+e^- collisions, where Z' exclusively couples with leptons, and $N_f = 18$ when Z' couples solely with quarks. We can separate the SM coupling in different types due to the nature of the mediator. From left and right projection operators, the Z' mediator can be vector, axial-vector, or chiral, with coupling constants according to Table 1, where we use $g_{l\chi} = g_{r\chi} = 1$ in the fermion case [10].

2.3 Initial-state photon radiation

The experimental detection of DM is a hard task given the unknown characteristics of its interaction with ordinary matter, hence ways of detecting it is a topic of intense research [52], typically leading to the search of events with missing transverse energy (MET), $\vec{E}_T$. One way of observing a DM event with MET is to consider the emission of SM particles as initial state radiation (ISR). As such, different particles can be emitted from the initial colliding particles, collectively known as mono-X searches. The search for a photon as ISR is natural as electromagnetic radiation is perhaps one of the simplest to be measured with precision at experiments in particle colliders. Also, it can have a very broad spectrum, on scales from keV to TeV, depending on the invisible event that one want to characterize [39,53–55].

Radiative corrections to the tree-level DM process are necessary to account for DM production via mono-photon process. While most of the studies in the literature are given in terms of an approximation with a soft photon or calculated numerically for a $3 \to 2$ process [56–58], we choose here to account for the radiative correction with emission of a hard photon as discussed in the classical approach by Ref. [34] which also were used in subsequent works [59–63] in non-exclusive DM contexts. This framework proposes a factorization in terms of lower order processes where $\psi\bar{\psi}$ reactions generate a final state with the emission of a hard photon in the event. This particular approach uses a rigorous calculation of higher order corrections together with a more precise evaluation of the phase space of the emitted photon. Such precautions are necessary due to the high energy involved and the emitted photon itself, which would disqualify a process containing only one ISR of a low energy or soft collinear photon, as in the Weizsäcker–Williams (WW) approximation [10,64]. We employ this framework by using the appropriate factorization to obtain the total cross section

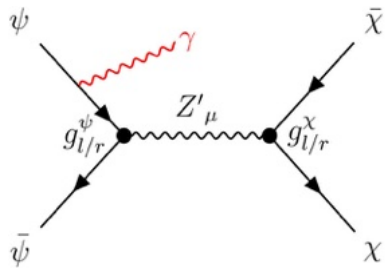

Fig. 2 A representation of a Feynman diagram with the emission of a photon as ISR, in red wiggly line, in the case of fermion DM production

for a mono-photon process, as represented in Fig. 2:

$$\sigma'_{\rm tot}(\psi\bar{\psi} \to Z'\gamma \to \gamma\chi\bar{\chi}) = \hat{\sigma}_{\rm tot}(\psi\bar{\psi} \to Z' \to \chi\bar{\chi})(1+\delta), \tag{7}$$

with $\hat{\sigma}$ given by Eq. 3 integrated over the scattering amplitude squared for each DM species and

$$\delta = \frac{2\alpha}{\pi}\left\{\left(-1+2\log\frac{\sqrt{\hat{s}}}{m_\psi}\right)\left[\log x_\gamma^{\rm min} + \frac{13}{12} + \int_{x_\gamma^{\rm min}}^{x_\gamma^{\rm max}} {\rm d}x_\gamma\, \xi(x_\gamma)\right] - \frac{17}{36} + \frac{\pi^2}{6}\right\}, \tag{8}$$

$$\xi(x_\gamma) = \frac{1}{x_\gamma}\left(1 - x_\gamma + \frac{x_\gamma^2}{2}\right)\frac{\hat{\sigma}(\hat{s}-\hat{s}x_\gamma)}{\hat{\sigma}(\hat{s})}, \tag{9}$$

where $\alpha = 1/137$ is the electromagnetic fine structure constant, q_γ is the momentum carried by the photon from ISR, and $\hat{\sigma}(\sqrt{\hat{s}})$ is the total cross section of the $2 \to 2$ process, with energy $\sqrt{\hat{s}}$. Function $\xi(x_\gamma)$ takes into account the available center-of-mass energy for producing the DM pair plus a hard photon, which decreases for more energetic photons. This can be seen in Fig. 3 (top panel) where the function $\xi(x_\gamma)$ is shown, which depends on the partonic cross section with and without ISR, for all DM species. The shape of the distribution is very similar for all mediator couplings, although the fermion DM a little enhancement in the tail towards high x_γ. A typical photon spectrum in particle detectors starts at a few GeV where isolation and reconstruction efficiencies are above 90%.

Considering a usual efficiency turn-on curve in trigger selection, we employ $x_\gamma = q_\gamma/E_{beam}$ with a minimum photon energy of 60 GeV, or $x_\gamma = 0.04$ for a beam of 1.5 TeV, motivated by the identification capabilities expected at CLIC dp [65] and assessed in the LHC experiments [66]. Figure 3 (bottom panel) shows the distribution of the ratio between the total cross sections with and without ISR in terms of the minimum photon energy $x_\gamma^{\rm min}$, which illustrate the contribution of the δ term in Eq. 7. Although the shape of $\xi(x_\gamma)$ decreases rapidly with increasing photon energy fraction, the radiative corrections improve the production cross section at higher photon energies up to $\sim 7\%$, which is independent of the dark sector parameters, such as masses and coupling constants. Also, the dip structure occurring around $x_\gamma^{\rm min} \approx 0.02$ reveals the effect of the corrections for very low photon energies. The ratio reaches a value of 1 at $x_\gamma^{\rm min} \approx 0.06$, marking the starting point at which the radiative corrections enhance the total cross-section. Although the chosen value of 0.04 as minimum photon energy in this study is located in a region where the cross section is slightly suppressed, we aim to investigate the kinematic region expected for the photon identification in experiments, especially at CLIC dp.

As shown in Ref. [67], the production cross section of DM pairs plus hard photon are $\mathcal{O}$(fb), making its observation possible with an integrated luminosity of the order of ab^{-1}. Similar simulations also indicate high visibility in the emission and consequent detection of mono-photons from invisible decays, with significant cross section and transverse momentum fraction of the emitted photon [54]. The detection of such mono-photon event can be made with the usual signature of high-p_T photon plus MET, where MET will peak around the resonance mass of the mediator.

3 Calculation of the DM relic density near a resonance

The DM abundance and, consequently, the cross sections involved in its primordial production, are typically calculated taking into account processes in equilibrium and away from poles or production resonances of a given species. When considering a resonant production processes, like the one investigated in this work, one cannot simply apply the usual solution of the Boltzmann equation in terms of $\langle\sigma v\rangle$. We address this issue by following the steps described in Ref. [30] and write $\langle\sigma v\rangle$ as a non-relativistic BW resonance (like it is the case for a cold DM candidate in the LCDM model) in the following form

$$\langle\sigma v\rangle_{\rm res} = \frac{16\pi}{m_\chi^2}\frac{(2J+1)}{(2S+1)^2}x^{3/2}\pi^{1/2}\frac{M_{Z'}\Gamma_{Z'}}{m_\chi^2}B_i(1-B_i) \times \sum_{l=0}^{\infty}\frac{b_R^{(l)}}{l!}F_l(z_R;x), \tag{10}$$

where $x = m_\chi/T$ and the quantities J and B_i are, respectively, the spin and resonance branching fraction of the initial state, whereas S and m_χ are the spin and mass of the DM particle, respectively. Here we consider the annihilation of DM particles into SM ones via the resonant mediator Z' in the relic density calculation, hence the initial state particles are the DM candidates themselves in the cosmological context of this equation. The terms $b_R^{(l)}$ are the coefficients of the expansion of a function involving the branching fraction B_i of the form

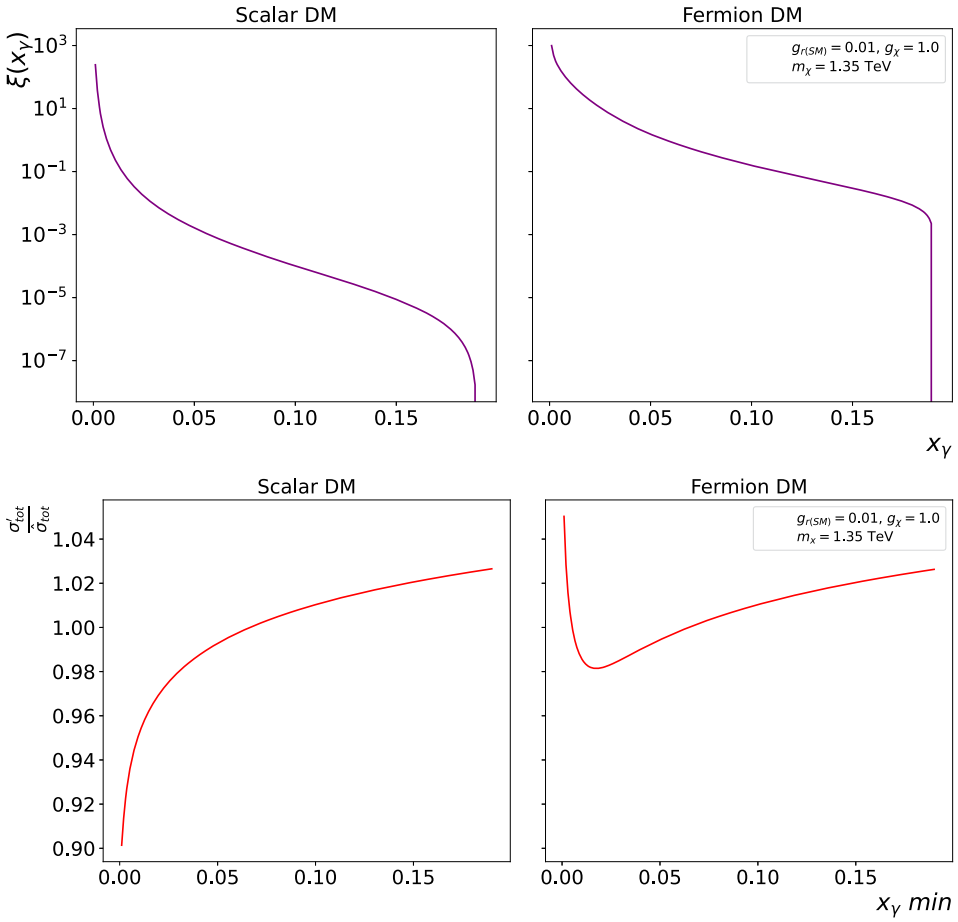

Fig. 3 (Top panel) Correction $\xi(x_\gamma)$ in terms of the photon energy fraction, which account for radiative corrections. (Bottom panel) The ratio of the cross section with ISR, σ'_{tot}, and without ISR, $\hat{\sigma}_{\text{tot}}$, that represents $1+\delta$ of Eq. 7 carrying all radiative corrections. In both cases the cross sections are computed with $M_{Z'} = 3$ TeV and $m_\chi = 1$ GeV

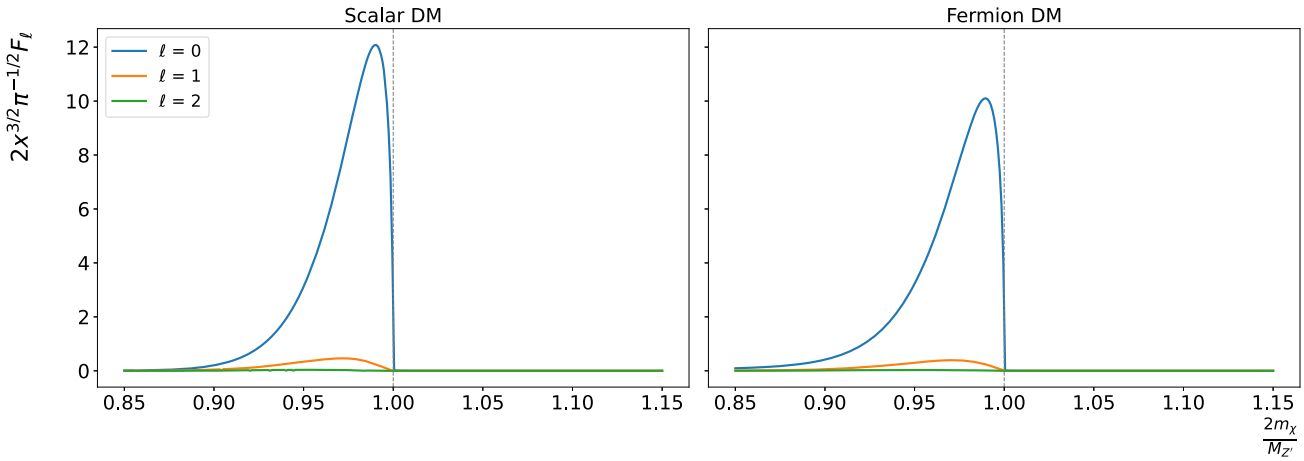

Fig. 4 Profile of the thermal average, $\Sigma(z_R; x)$, near the Z' resonance for $l = 0, 1, 2$

$$b_R(\epsilon) \equiv \frac{B_i(1-B_i)(1+\epsilon)^{1/2}}{\epsilon^{1/2}(1+2\epsilon)} = \sum_{l=0}^{\infty} \frac{b_R^{(l)}}{l!}\epsilon^l, \tag{11}$$

in terms of ϵ, which is the energy per unit mass of the process as a whole defined by

$$\epsilon = \frac{s - m_\chi^2}{m_\chi^2}. \tag{12}$$

Lastly, the $F_l(z_R; x)$ term results from the thermal average of σv with integration over the energy per unit mass ϵ

$$F_l(z_R; x) = \text{Re}\frac{i}{\pi}\int_0^\infty \frac{\epsilon^{(l+1/2)}e^{-x\epsilon}}{(z_R - \epsilon)}\text{d}\epsilon, \tag{13}$$

with a ϵ^l factor from Eq. 11 and an auxiliary variable in terms of the masses and decay widths of the particles involved

$$z_R = \frac{M_{Z'}^2 - m_\chi^2}{m_\chi^2} + i\frac{M_{Z'}\Gamma_{Z'}}{m_\chi^2}. \tag{14}$$

We can investigate with these results the profile of the thermal average near the resonance computed in the proper framework for the expansion of the BW cross section. As we can see in Fig. 4, the profile defined as

$$\Sigma(z_R; x) = 2x^{3/2}\pi^{-1/2}F_l(z_R; x) \tag{15}$$

shows the relative masses where the enhancement in the thermal average arises near the Z' resonance, for relative masses above 0.8. For relative masses below threshold the thermal average is very similar if compared to the usual, non-resonant calculation of the thermal average. The enhancement peak is positioned at DM masses below the resonance mass given the fact that there is enough thermal energy to produce a heavier resonance during the equilibrium phase. Also, the profile does not extend beyond the resonance mass since we are taking into account a narrow resonances for the Z' boson for both scalar and fermion DM (both $\Gamma_{Z'}/M_{Z'} \sim 10^{-2}$). DM particle with masses above the resonance mass would be possible for wider resonances, where low energy tail would allow a non-zero thermal average for DM particles with relative mass above the resonance mass. As a result, we consider in this study m_χ masses with relative mass in the range $0.8 < 2m_\chi/M_{Z'} < 1.0$ in order to probe the region where the thermal average is enhanced by the Z' resonance: together with the relic density, results will contain a (red dashed) line delimiting the threshold relative to $2m_\chi/M_{Z'} = 0.8$. Taking for instance a resonance of 3 TeV, the threshold of m_χ with enough thermal energy to produce a Z' starts at 1350 GeV – we use this mass value as reference.

Nonetheless, Eqs. 11 and 13 can be combined to express $F_l(z_R; x)$ without the expansion in l terms as

$$F(z_R; x) = \mathrm{Re}\frac{i}{\pi}\int_0^\infty \frac{(1+\epsilon)^{1/2}e^{-x\epsilon}}{(1+2\epsilon)(z_R-\epsilon)}\mathrm{d}\epsilon. \tag{16}$$

This way we can rewrite Eq. 10 in a simpler form without relying on the expansion in terms of ϵ^l as done in Ref. [30]. This, in turn, has been evaluated by means of the following expression

$$\langle\sigma v\rangle_{\mathrm{res}} = \frac{16\pi}{m_\chi^2}\frac{(2J+1)}{(2S+1)^2}x^{3/2}\pi^{1/2} \times\frac{M_{Z'}\Gamma_{Z'}}{m_\chi^2}B_i(1-B_i)\,F(z_R; x), \tag{17}$$

which allows us to numerically estimate the dimensionless density parameter referring to the primordial DM fraction as [30,40]

$$\Omega_\chi h^2 \approx 8.76\times10^{-11}\,\mathrm{GeV}^{-2}\left[\int_{T_0}^{T_f} g_*^{1/2}\langle\sigma v\rangle_{\mathrm{res}}\frac{\mathrm{d}T}{m_\chi}\right]^{-1}, \tag{18}$$

being T_0 and T_f the current and at *freeze-out* temperatures, respectively, and g_* are the particles degrees of freedom in the same epoch.

The production process with ISR photon needs to probe the enhanced region above $\sqrt{s} = 0.8M_{Z'}$. Thus, the reduced beam energy resulting from the photon emission cannot go below this threshold if we want to investigate the mass region near the Z' resonance, restricting the photon energy for possible searches of DM production. In this work we consider a photon irradiation from an incoming fermion with energies ranging from 60 GeV up to $0.2M_{Z'}$, allowing to evaluate the production cross section where the relic density will be lesser suppressed near the resonance.

As a result of the proper calculation of the relic density with usual SM-DM and DM-DM coupling found in the literature, namely $g_\chi = 1.0$ and $g_{r/l} = 0.25$, an extension of the available parameter space is expected in comparison the usual calculation outside resonance regions (namely the "naive" approach as used by Ref. [30]). This extended region can be seen in Fig. 5 by the reduced exclusion region in contrast to the usual calculation performed by experimental searches, such as the one by the CMS Collaboration in Ref. [29], where all phase space below the blue solid line is excluded. These results are an improvement of a factor of 3–4 in g_χ and a factor ~ 2 in $g_{r/l}$ within the LHC kinematics. We note that the regions in the mass scan differ significantly from those shown in other works that do not take into account processes near or at the resonance peak of a massive mediator, even though numerically calculated for analogous processes [13,28]. This corroborates the assertion by the authors in Ref. [30] that the incorrect evaluation of resonance results in a reduction of $\langle\sigma v\rangle$, the velocity-weighted cross-section. Consequently, the naive approach overestimates the relic density and the proper calculation reduced the exclusion regions in the parameter space. These findings motivate us to investigate this approach in more detail.

Following the recommendations in the literature [13–15,28,29,65,68–70], we opted to analyze two scenarios for each studied initial state, where the coupling of the mediator with the SM is fixed: $g_{r/l} = 0.01$ and 0.1 for the $\ell\ell Z'$ coupling in e^+e^- collisions and $g_{r/l} = 0.10$ and 0.25 for the $q\bar{q}Z'$ coupling in pp collisions, whereas the coupling of Z' with the dark sector is set at $g_\chi = 1$ for all cases.

In the case where the mediator Z' is a pure vector, we can indeed obtain a scenario where the coupling with quarks is much greater than with leptons at tree level, and the coupling with the latter occurs only through the loop mixing of Z' with the other neutral bosons of the SM. This can naturally lead to an expected ratio of ~ 0.1 between $g_{Z'\ell\ell}/g_{Z'qq}$ [13]. All these discussed scenarios and particular values tend to be highly dependent on the specifics of the model at hand. However, considering only the scenario for massive mediators on the TeV scale, we can assume larger couplings

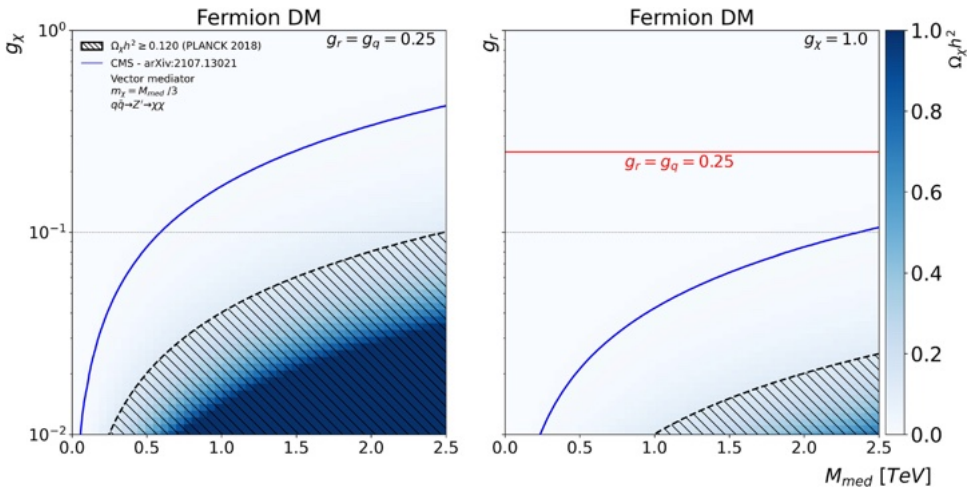

Fig. 5 Dimensionless density parameter $\Omega_\chi h^2$ for DM produced via Z' mediator with $M_{med} \equiv M_{Z'}$ [29] and DM pairs with mass $m_\chi = M_{Z'}/3$ in the s-channel taken for $q\bar{q}$ scenarios, where we scan over different values of g_r and g_χ, fixing (left panel) $g_r = 0.25$ as a leptophobic context ($g_\ell = 0$), and (right panel) $g_\chi = 1$, following Refs. [12–15,28,29,68], and overlaying the curve for the naive approach evaluated by the CMS Collaboration in Refs. [13,29]

($g_{Z'ff} \geq 0.1 \sim 0.3$) considering that one may possible evade the constraints imposed by direct and indirect detection experiments in this mass regime [6,7]. Also, larger couplings could be explored if a specific model imposes multi-TeV masses on the mediator, which would further escape direct detection constraints, particularly those related to the coupling, a significant restriction in interaction models via Z'. In general, smaller coupling values favor collider searches as they become more sensitive (as more data is collected), given the clear reduction in the magnitude of such processes. However, very low coupling values disadvantage thermal DM production scenarios, as the calculated relic abundance of such processes increases considerably [30,31].

Figures 6 and 7 show how the DM overabundance regions, behave in the mass scans $m_\chi \times M_{Z'}$, parameterized by the dimensionless density $\Omega_\chi h^2$ obtained with Eq. 18. The region that comprises the limit with $\Omega_\chi h^2 \geq 0.120$ corresponds to the hatched area and is used in all results indicating the region of excess primordial DM production. These results show that the proper calculation of these limits is essential to evaluate the available regions to probe the mass of the mediator and the DM particles taking into account the limits obtained from astrophysical observations. When the $\ell\ell Z'$ coupling is set to $g_r = 0.01$, most mass regions are largely excluded for the CLIC energy regime, as seen in the top panels of Fig. 6. However, for larger values of the g_r coupling in the bottom panels of Fig. 6, we observe a significant reduction in the area corresponding DM overabundance, which favors resonance searches in e^+e^- accelerators like CLIC and ILC [65,71,72]. This is because results from these experiments evade the limits imposed by the LHC, especially in scenarios with leptophilic models without couplings to quarks at tree-level. Similarly, the LHC kinematics shown in Fig. 7 reveals opportunities for probing new mediators, due to the area corresponding to the region excluded being quite small as well. In these cases, significantly smaller regions of the phase space are excluded for scalar DM, while remaining entirely accessible for fermion DM. Besides, the mass scan for fermion DM shows that the limits evaluated in the naive approach (below blue solid line) produce significant exclusion regions which are not really limitations if the proper calculation near a resonance is considered.

In order to verify the complete available regions in the parameter space, Figs. 8 and 9 present the scans of couplings $g_r \times g_\chi$ for both CLIC and LHC kinematics. They show very similar shapes of the exclusion regions for both DM species and coupling possibilities (as detailed in Table 1), differing mainly in terms of the exclusion area that aligns with the observed relic density, however show quite different results between e^+e^- and pp collisions. The region of overabundance for e^+e^- collisions seen in Fig. 6 for $g_r = 0.01$ chosen for the $\ell\ell Z'$ coupling is within the excluded region even considering the enhancement due to the resonance. On the other hand, it becomes largely accessible with varying the fermion DM and mediator masses with $g_r = 0.1$ and very restricted for scalar DM, inaccessible at CLIC at 3 TeV. However, larger values of the $\ell\ell Z'$ coupling need to be analyzed considering a possible leptophobic behavior of the mediator, where more restrictive limits may or may not be imposed when resonance searches in di-leptons are included [68,69]. The same does not happen for the LHC energy regime, where the $g_r = 0.1$ or $g_r = 0.25$ lies close to but above the limit of overabundance of the relic density and largely accessible within the current collider experiments. As already mentioned, the mediator is

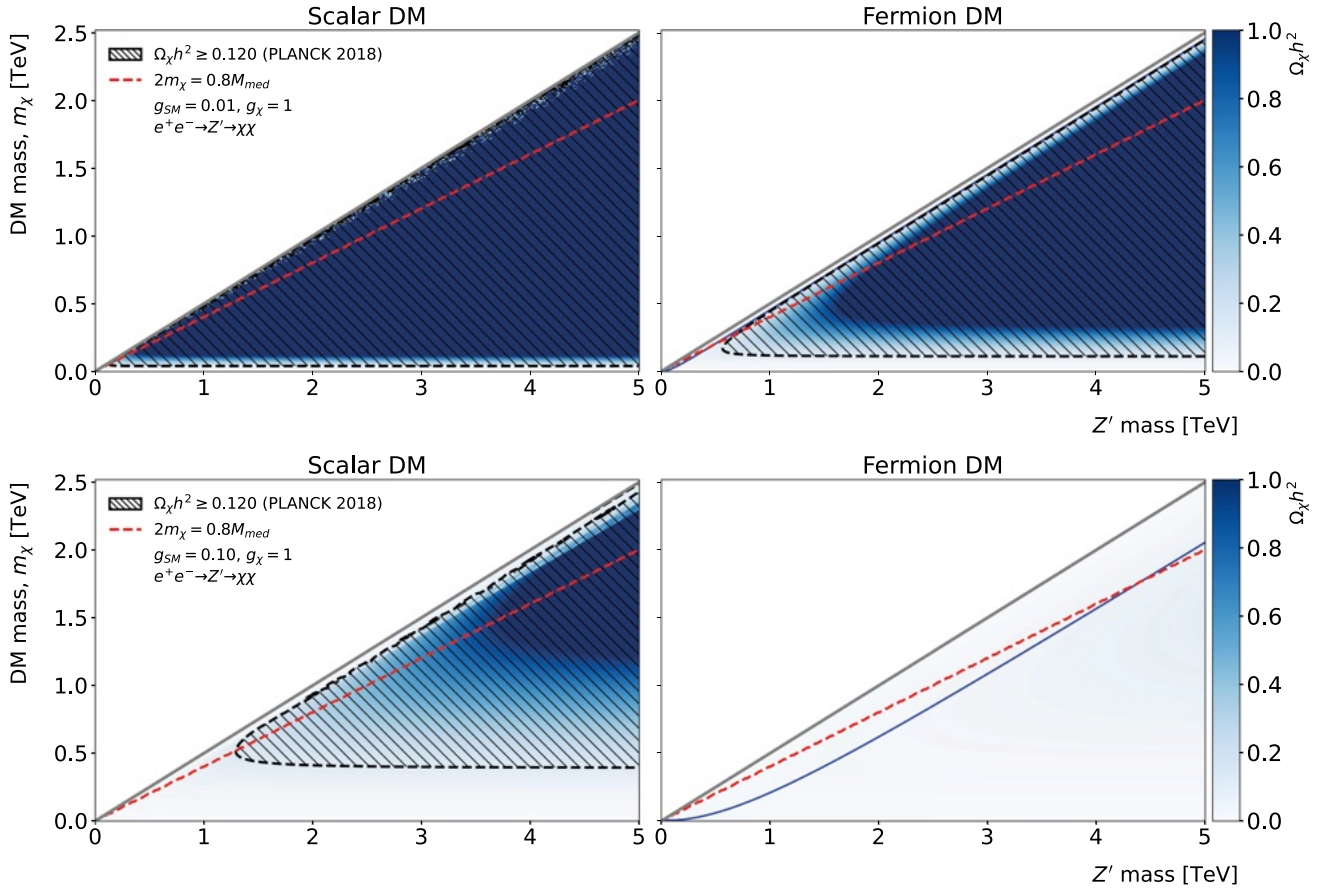

Fig. 6 Dimensionless density parameter $\Omega_\chi h^2$ for DM produced via Z' mediator with mass $M_{Z'}$ and DM pairs with mass m_χ taken for e^+e^- collisions, whereas a Z' couples with all six SM leptons pairs ($N_f = 6$) in the final state. The hatched area shows the regions with DM overabundance compared to the observed CDM abundance, which are excluded. The diagonal solid line represents the kinematic limit with $m_\chi = M_{Z'}/2$. For the upper plot, $g_r = 0.01$ and $g_\chi = 1$, while $g_r = 0.1$ and $g_\chi = 1$ for the bottom one. The red dashed lines show the threshold of the m_χ to produce the resonance with thermal energy while the blue solid lines on the fermion DM plots indicate the naive approach for relic density calculations, as in Ref. [13], i.e., line for $\Omega_\chi h^2 = 0.120$ with all region below the line being excluded

independent, and its coupling is restricted either with leptons or with quarks, then limits in searches for resonances with di-leptons do not directly apply. We shall stress here the fact that the calculation with the proper evaluation of the relic density near a resonance has produced shorted limitations in the parameter space, especially in the LHC energy regime as seen in Fig. 9. These results show that the limits imposed on the mass of the potential spin-1 mediator by analyses of the data from LHC experiments should take it properly into account.

4 Results and discussion

The DM production is very distinctive between lepton and hadron colliders given the available beam energies and detector coverage. We investigate the feasibility of DM production at CLIC and the LHC considering the calorimeter detectors planned/available for photon isolation and reconstruction. The production of DM may be detected by the emission of SM particles in an initial interaction state, where only SM particles and its respective couplings are involved [12,14]. Searches known as *mono-X* may indicate the associated production of jets, vector bosons (H,Z), photons, among others as initial state radiations (ISR). For instance, the future experiments at CLIC will be especially sensitive to wide searches of DM in mono-photon production [65]. In this work we investigate the DM production rates over scalar and fermion DM final states, where a massive mediator acts as a portal with the dark sector in s-channel processes with mono-photon ISR at high-energy colliders.

Hence, we scan the parameter space and find exclusion regions based on the relic density abundance, which shows possible scenarios in the dark sector by means of the sensibility for different species of DM particles. One of the advantage of using particle colliders for the DM searches is that detec-

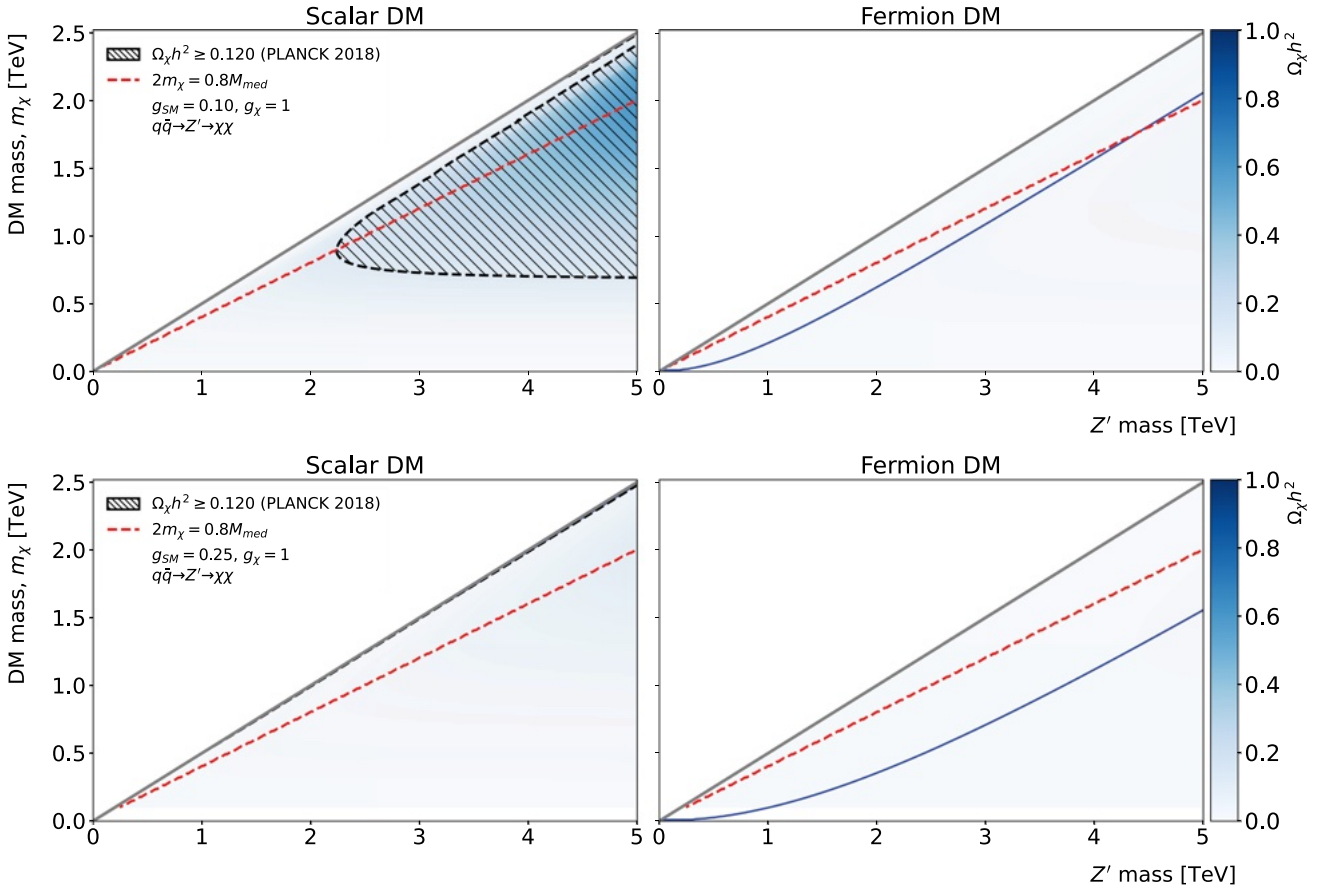

Fig. 7 Same as Fig. 6, but with Z' coupling to quark only ($N_f = 18$) as final states and with a $g_r = 0.10$ (top panel) and $g_r = 0.25$ (bottom panel)

tors may be designed to be *multipurpose*, that is, they make it possible to measure a large number of observables within the expected production processes. Furthermore, the high integrated luminosity ($\int \mathcal{L}dt$) achieved in such colliders reduce the statistical uncertainties for the search of evidence of New Physics. This huge number of events comes together, however, with a large number of background events, but may be subtracted from experimental data with a set of selection criteria and good control of uncertainties and systematic errors, which can be simulated and studied separately [3].

4.1 Kinematics in lepton and hadron colliders

We start investigating the partonic cross section of DM particle production (Eq. 3) in e^+e^- annihilation at CLIC [71,73] at $\sqrt{s} = 3$ TeV and next pp collisions at the LHC at $\sqrt{s} = 14$ TeV, with the initial state fermion mass $m_\psi = m_e$ and $m_\psi = m_q$, respectively. The predictions for CLIC are straightforward given the beam-beam annihilation and resonance production. The mono-photon production in e^+e^- collisions is obtained by the convolution of the partonic cross section and the ISR photon,

$$\sigma'_{\rm tot}(e^+e^- \to Z'\gamma \to \gamma\chi\bar{\chi}) = \hat{\sigma}_{\rm tot}(\psi\bar{\psi} \to Z' \to \chi\bar{\chi})(1+\delta), \tag{19}$$

with δ given by Eq. 8. On the other hand, one needs to employ collinear factorization for a typical Drell–Yan-like process to evaluate the cross section in pp collisions, as shown in Fig. 10. In this framework we have for the cross section given by

$$\sigma_{\rm tot} = \int_0^1 \int_{\tau/x_1}^1 P_{q,\bar{q}}(x_1, x_2)\hat{\sigma}_{\rm tot}(q\bar{q} \to Z' \to \chi\bar{\chi}) \times \delta(\tau s - M^2_{Z'})\, {\rm d}x_2 {\rm d}x_1, \tag{20}$$

where x_i are the longitudinal momentum fractions of the proton carried by the partons with $\tau = x_1x_2 = M^2_{Z'}/s$ and

$$P_{q,\bar{q}}(x_1, x_2) = \sum_{q=1}^{N_f} \Big[f_q(x_1, Q^2) f_{\bar{q}}(x_2, Q^2) + f_{\bar{q}}(x_1, Q^2) f_q(x_2, Q^2) \Big], \tag{21}$$

is the probability that each quark has a fraction x_i of the total proton momentum. In this work we use the parametrization

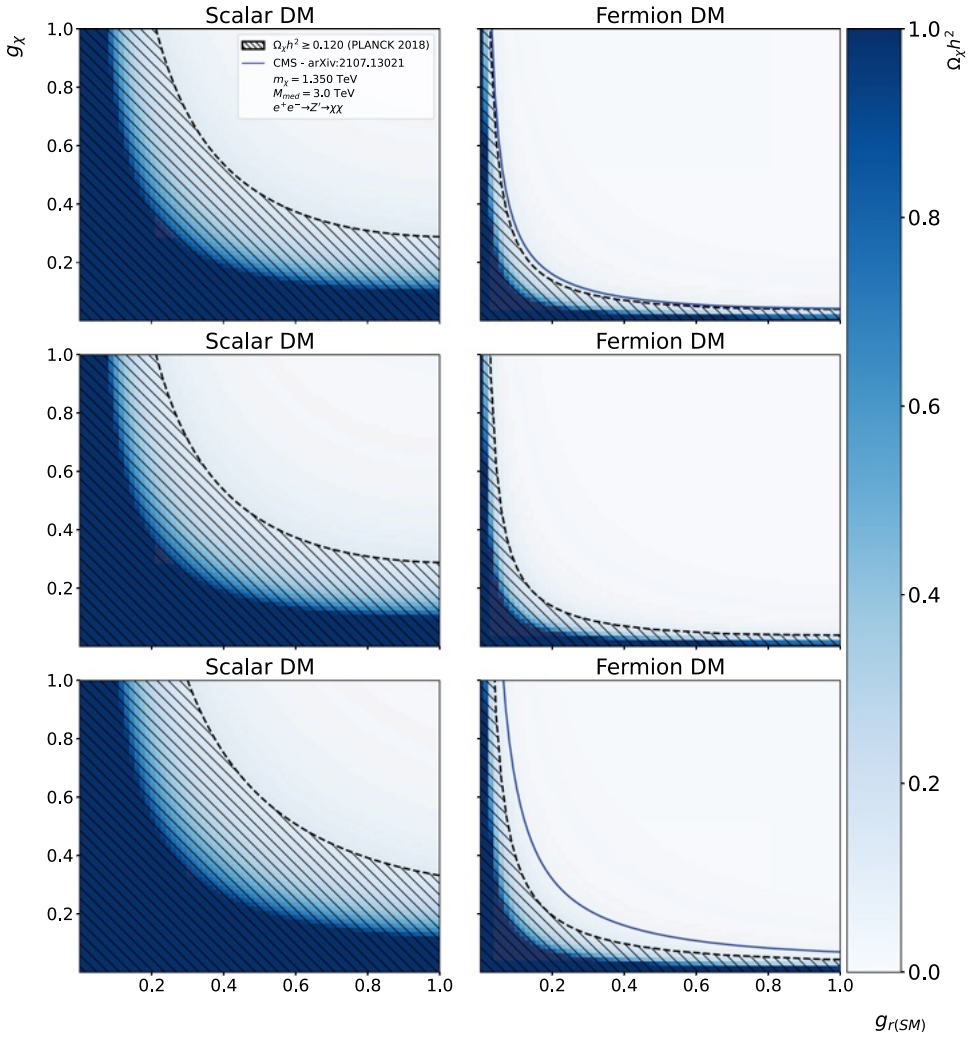

Fig. 8 Dimensionless density parameter $\Omega_\chi h^2$ for DM produced by a resonance with mass $M_{Z'} = 3$ TeV and decaying into DM pairs of mass 1350 GeV, whereas a Z' couples with all six SM leptons pairs ($N_f = 6$) in the final state. The results shown here were obtained using Eq. 18. The region with a cross section smaller than that needed to produce the observed CDM abundance is shown beveled in black. We have vector couplings in the first row, axial-vector couplings in the second, and chiral (right) in the third one

`NNPDF31_lo_as_0118` [74] to model the parton density functions (PDF) within `LHAPDF` [75], where we consider contributions from u, d, and s quarks. Considering that we are interested in the cross section near the resonance, we can write the hadronic cross section as function of τ, such as

$$M^2 \frac{\mathrm{d}\sigma}{\mathrm{d}M^2}\bigg|_{M=M_{Z'}} = \tau \int_\tau^1 f_q(x_1, Q^2) f_{\bar{q}}(\tau/x1, Q^2) \hat{\sigma}_{\mathrm{tot}}(\tau s) \times \frac{\mathrm{d}x_1}{x_1}, \tag{22}$$

with the mass fixed at the dark mediator mass.

The production cross section in pp collisions needs to incorporate the photon ISR within the partonic cross section $\hat{\sigma}_{\mathrm{tot}}$ given that the momentum loss by the quark after the photon emission has to be taken into account. Thus, the corresponding production cross section in pp collisions has the form:

$$\sigma'_{\mathrm{tot}}(pp \to Z'\gamma \to \gamma\chi\bar{\chi}) \equiv M^2 \frac{\mathrm{d}\sigma}{\mathrm{d}M^2}\bigg|_{M=M_{Z'}} = \tau \int_\tau^1 f_q(x_1, Q^2) f_{\bar{q}}(\tau/x_1, Q^2) \hat{\sigma}'_{\mathrm{tot}}(\tau s) \frac{\mathrm{d}x_1}{x_1}, \tag{23}$$

$$\hat{\sigma}'_{\mathrm{tot}}(q\bar{q} \to Z'\gamma \to \gamma\chi\bar{\chi}) = \hat{\sigma}_{\mathrm{tot}}(q\bar{q} \to Z' \to \chi\bar{\chi})(1+\delta). \tag{24}$$

We are interested in the SM signal coming from the mono-photon production mechanism in order to observe such an event in the electromagnetic calorimeters. Thus, the photon spectrum is the main experimental signature for searching the DM production. In Fig. 11 we show the normalized differential cross section for both e^+e^- and pp collisions as function of the photon energy fraction for both DM species considered in this work. One can clearly see that the fermion DM case produces a harder photon spectrum than the scalar

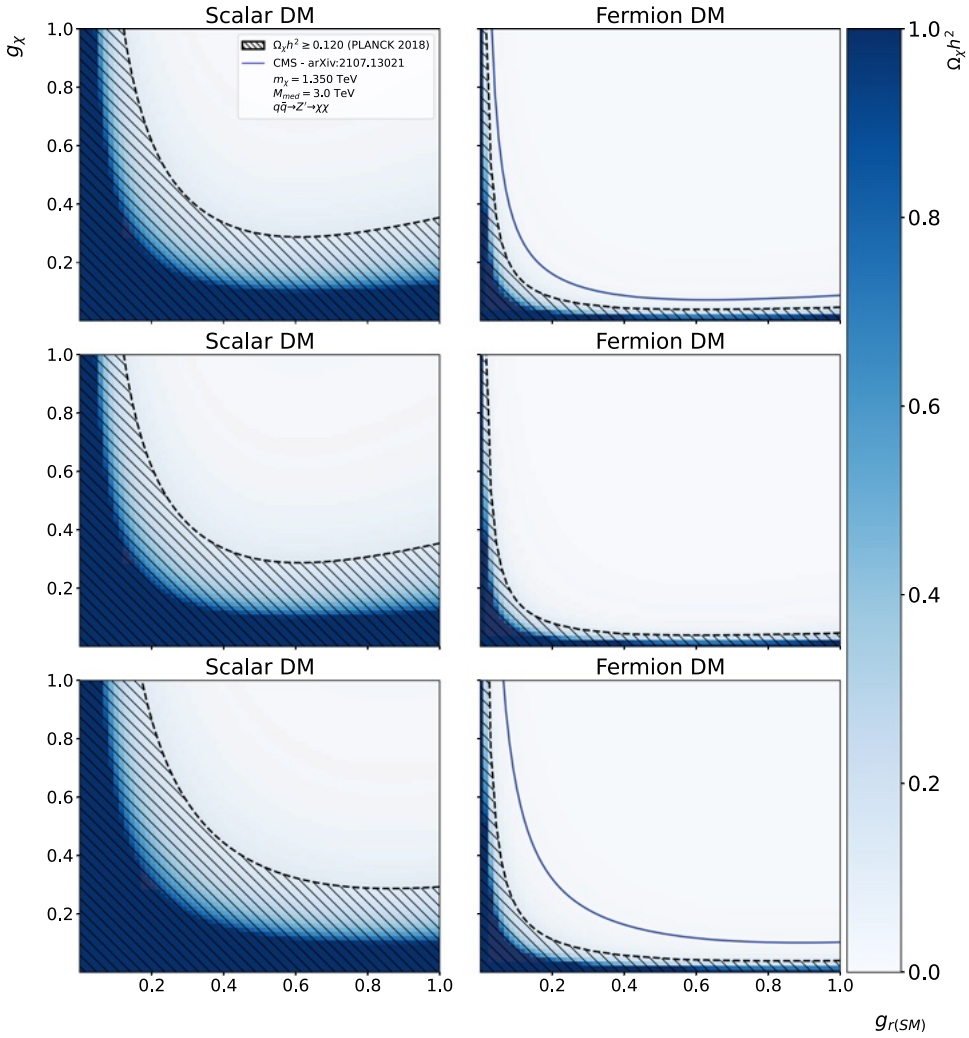

Fig. 9 Same as Fig. 8, but with Z' coupling solely with quark pairs ($N_f = 18$) as final states

DM case within the photon energy range near the resonance, which could be a hint for DM production as a experimental signature. Beyond 0.1 the normalized cross section tends to 1.

4.2 DM parameter scan

As we are mainly interested in the DM observation via production by resonances in the s-channel, Figs. 12 and 13 show the mass scan in terms of the DM production near the mediator resonance of mass $M_{Z'}$ decaying into DM particles of mass m_χ for both e^+e^- and pp collisions. Given that CLIC will operate with a fixed energy, we scan the masses in Fig. 12 with the resonant cross section with $\sqrt{s}$ at the Z' peak at 3 TeV and varying m_χ. Besides the kinematic limit of $m_\chi \leq M_{Z'}/2$, the photon ISR restricts the growth of the cross-section with m_χ, resulting in a slightly decreasing upper bound in m_χ beyond $M_{Z'} > 3$ TeV. Instead, LHC probes different invariant masses and the cross section in Fig. 13 is then free to vary with both $M_{Z'}$ and m_χ, and the restriction imposed **by** the ISR appears as a decreasing cross section right below the diagonal for $m_\chi = M_{Z'}/2$. As stated before, the coupling of the mediator with the SM is fixed to

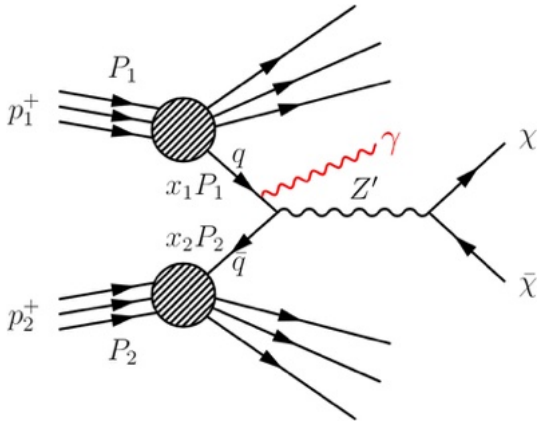

Fig. 10 A representation of a Drell–Yan-like process mediated by a massive resonance and decaying into DM final states. The same representation is used for different DM species; here shown for the fermion DM case

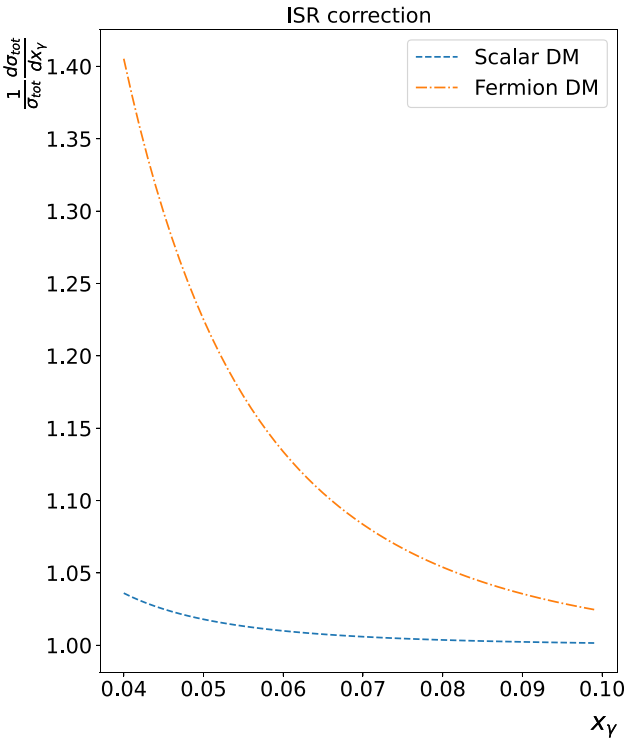

Fig. 11 Differential distributions for the ISR factorized cross section as function of the photon energy fraction, $x_\gamma = q_\gamma / E_{beam}$, normalized by the total integrated cross section. Here we use $M_{Z'} = 3$ TeV and $m_\chi = 1350$ GeV

$g_{r/l} = 0.01$ and 0.1 for the $\ell\ell Z'$ and $g_{r/l} = 0.1$ and 0.25 to $q\bar{q}Z'$ and $g_\chi = 1$ in both cases.

The hatched areas show the regions with relic overabundance and thus excluded and the red dashed line limits the region with a minimum m_χ in agreement with the relic calculation near the Z' resonance, where we note that the cross section for scalar and fermion DM are of the same order of magnitude. As we can see in Fig. 12, nearly all the mass region is excluded for the CLIC energy regime by the relic overabundance or kinematic reach for $g_r = 0.01$. Only the case of fermion DM with $g_r = 0.1$ leaves a tiny mass range available very close to the Z' peak, making it very challenging for observation at CLIC. The results for the LHC, on the other hand, show a much lesser stringent exclusion region **for** both scalar and fermion DM. Hence, the allowed region above the red dashed line results in a fully available m_χ for fermion DM and scalar DM with $g_r = 0.1$.

Considering the potential for observation at particle colliders, if any, one can see very distinctive possibilities within the DM species. The scalar and fermion DM have a significant cross section for smaller m_χ and $M_{Z'}$ masses. However, according to Refs. [28,29], massive mediators in the region below 2 TeV are already excluded with a 95% confidence level, which favors searches for regions of even higher masses. Besides, a reasonable prediction for the number of expected events needs to take into account the efficiency of identifying invisible final states and the impact of background signals, which are neglected in this work given the specifics of each detector. Hence, the observed event rate will be reduced from these predictions, but still competitive for observation, especially at the High-Luminosity LHC.

The predicted cross section for scalar and fermion DM in both e^+e^- and pp collisions resides at $\sim 10^1$–10^3 fb, which would be reduced considering detector efficiencies and background rejection to the level applied in current data analyses, however the expected event rate would be still consistent with the lack of observation as reported by the LHC experiments. Furthermore, in the spectrum chosen for the hard photon emitted as ISR, we noticed little variation in the absolute values of the cross section despite the fact that there is an evident kinematic constraint near the limit $M_{Z'} = 2m_\chi$, which indicates that, even in the case of a higher order process, this ends up not disfavoring possible future observations.

The regions not excluded by the relic density in both e^+e^- and pp collisions are very distinct and at very much different scales. Regions of DM production consistent with cosmological observations are strongly excluded for scalar DM due to the very nature of the resonant production process applied here according to Ref. [30]. This can be seen in the e^+e^- collisions at CLIC, while the restriction is much less stringent in pp collisions. Besides, regions of low DM mass are not accessible in e^+e^- collisions – neglecting the low m_χ masses far from the resonance region –, the pp ones can access the higher DM mass region at TeV scale. The cross section, and correspondingly the event rate, is comparable within the scalar and fermion DM, excluding a tiny region at higher DM mass in the scalar DM case, however this exclusion region depends on the range of photon energy which drives how DM mass in reachable in particle colliders.

Figures 14 and 15 present the distributions in terms of g_r and g_χ couplings with conventional matter and the dark sector for e^+e^- and pp collisions taking into account the photon ISR. We show the cross sections with mediator mass of $M_{Z'} = 3$ TeV and DM mass of $m_\chi = 1350$ GeV so that we are able to see more clearly the regions where the DM mass near the resonance allows the DM relic abundance production to conform with cosmological limits. We can notice that a large part of the phase space for scalar DM is excluded by the relic density, while the fermion DM is the one that presents the best observation opportunity due to its higher cross section. In addition, we see a small effect by changing the type of coupling between the SM particles and the dark mediator due to the small contribution of the coupling constants in the cross sections. One can noticed that the chiral coupling results in a slightly larger exclusion region given the nature of the g_l coupling in the cross sections and decay widths.

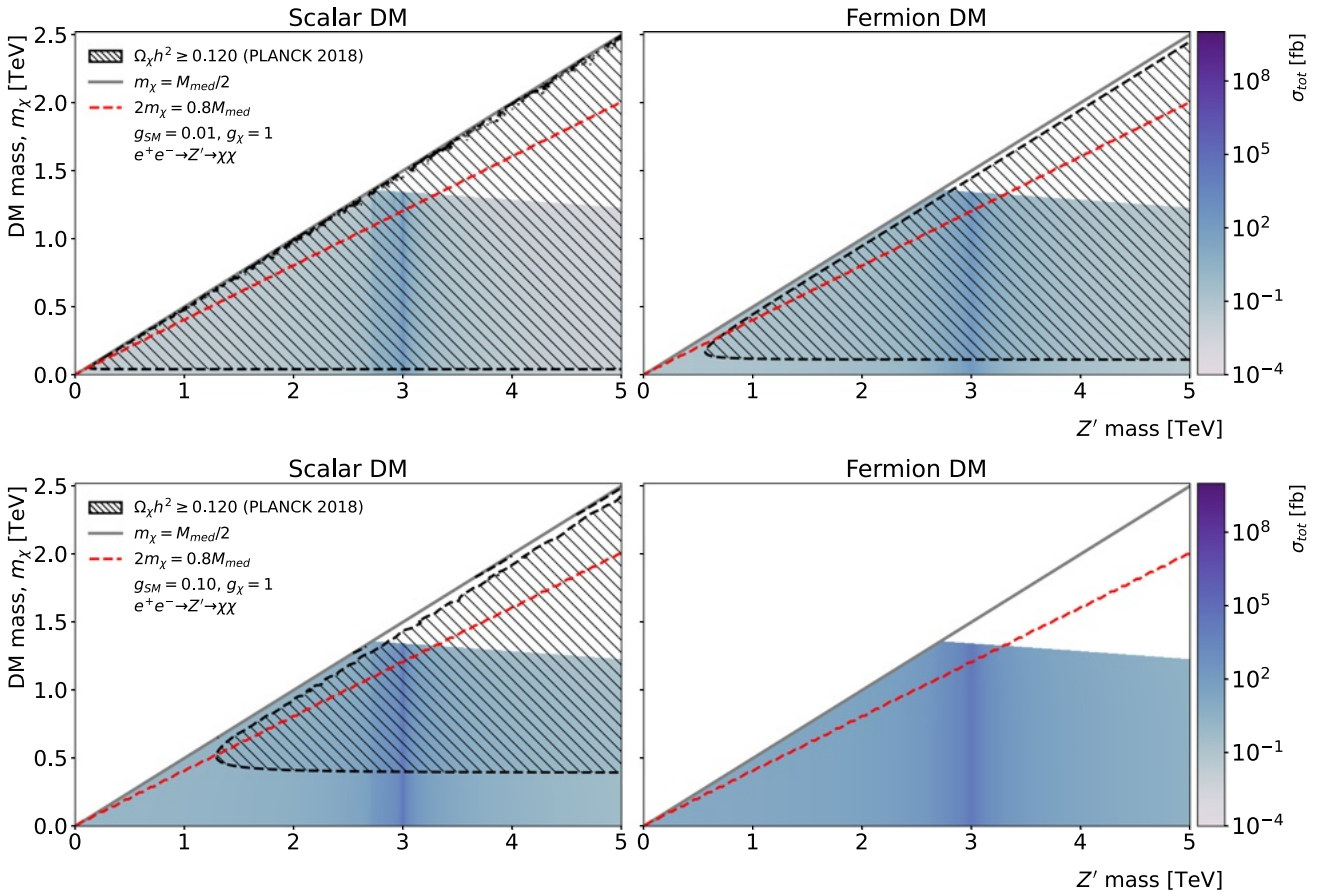

Fig. 12 Scan of the total cross section with ISR contribution as a function of the DM particle mass m_χ and mass of the mediator $M_{Z'}$ for e^+e^- collisions at CLIC at 3 TeV. The top panel illustrates the Z' coupling with the SM as $g_r = 0.01$ while the bottom panel shows the results for $g_r = 0.1$. The red dashed line draws the threshold for probing the mass range near the Z' resonance where the relic density is lesser suppressed as result of this work

5 Conclusion

We present a simplified SM extension with a new renormalizable symmetry group $U_\chi(1)$ acting as a (axial)vector portal for dark sector, which can be distinguished by the composition of its fields, i.e., scalar or fermion, by two respective possible interaction Lagrangians. We evaluated the relic density near this resonance of the Z' mediator for the first time in the literature, which drives the exclusion regions in the mass and parameter scans. As a result, we are able to define a region where the relic density is lesser suppressed, providing proper exclusion limits for DM production mediated by a Z' vector boson at TeV scale, showing that our simplified model are within the parameter space probed in the experimental and cosmological limits, excluding a significant region of coupling constants.

In this work we show that the potential for DM observation in e^+e^- collisions is very challenging, with a tiny region of the phase space still available for fermion DM very close to the resonance in case DM has a $\mathcal{O}(10^{-1})$ coupling to SM leptons. For pp collisions we can see that there is still a promising region for detection of resonances that can serve as a portal for the DM production, especially for fermion DM as a candidate in the LHC energy regime under these assumptions. Our calculation of the relic density near a resonance region is an important factor for obtaining predictions for the LHC and we showed that there still available regions for this resonance production in agreement with cosmological and collider constraints. We show that the enhancement of $\langle \sigma v \rangle$ near a resonance shrinks the exclusion regions in the parameter space when this calculation is carried out with the appropriate approach, extending the accessible coupling constants by a factor 2–4, especially at the LHC kinematic regime. This result demonstrate the experimental limits imposed on the DM mediator mass could be improved in comparison to the naive calculation of the relic density. This work aims to further narrow the parameter space, especially the mass range of the mediator mass, to establish grounds for the search of massive mediators in the resonant s-channel production. The search for New Physics, specifically the production of DM in pp colliders, is promising, even in regions already covered

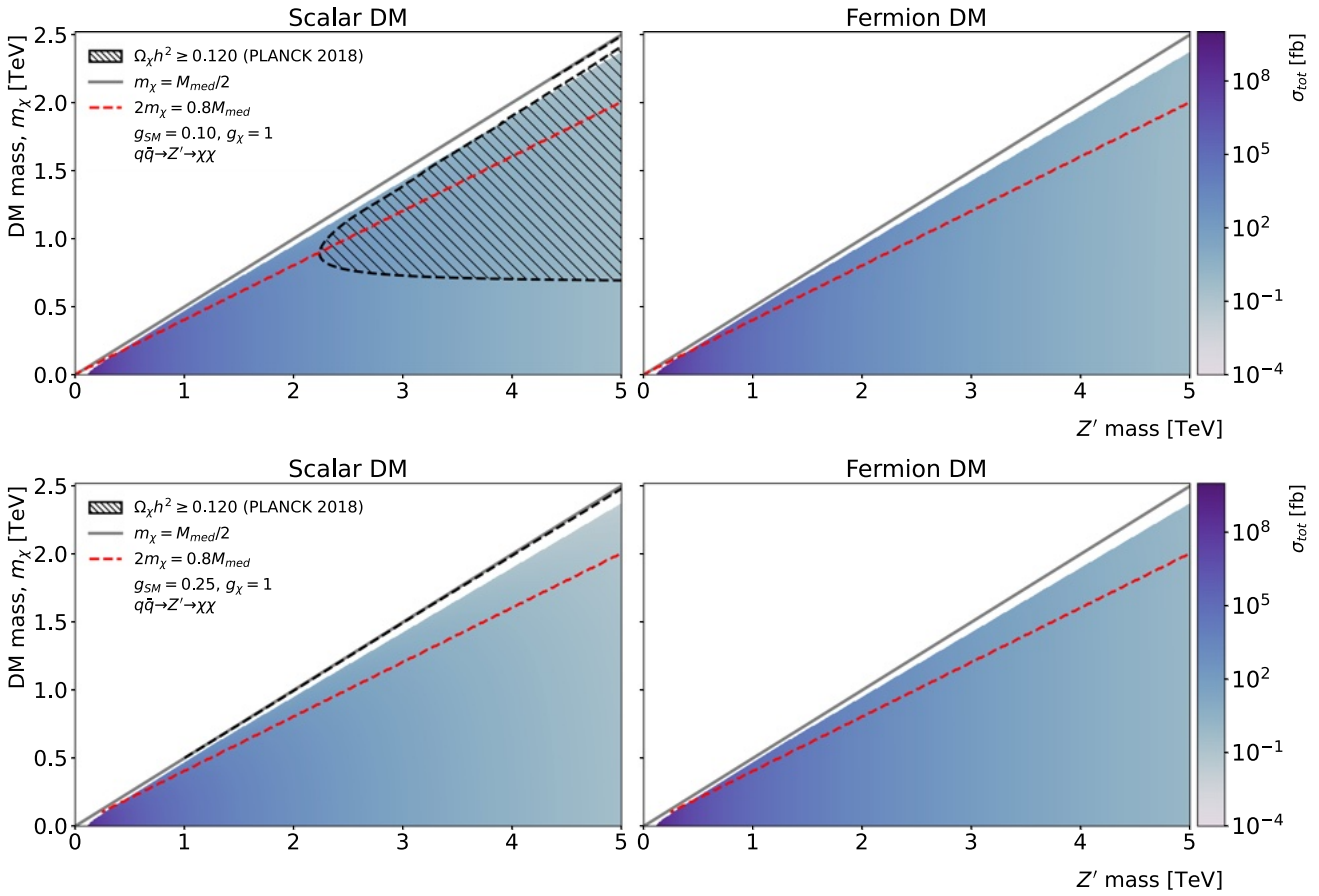

Fig. 13 Same as Fig. 12, but for pp collisions at the LHC at 14 TeV and $g_r = 0.1$ (top) and $g_r = 0.25$ (bottom)

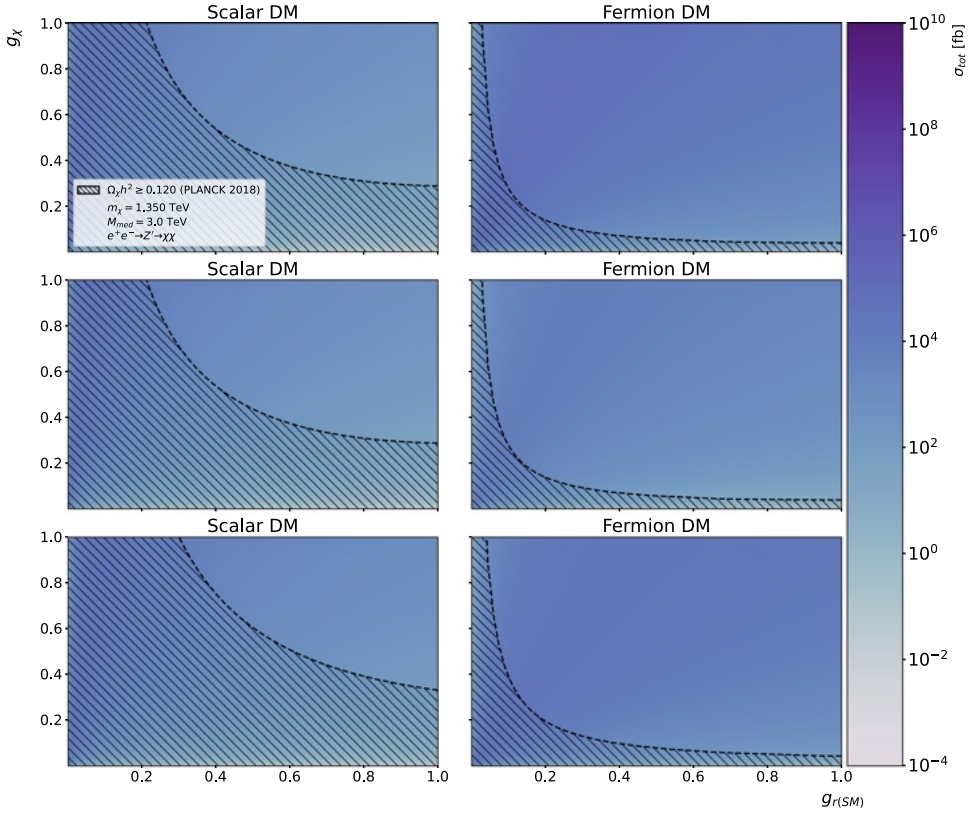

Fig. 14 Parameter scan showing the total cross section in e^+e^- collisions at CLIC at 3 TeV for each type of coupling with the SM: vector (top), axial-vector (middle), and chiral (bottom panel). The DM particle mass and the mediator mass are fixed to $m_\chi = 1350$ GeV and $M_{Z'} = 3$ TeV, respectively

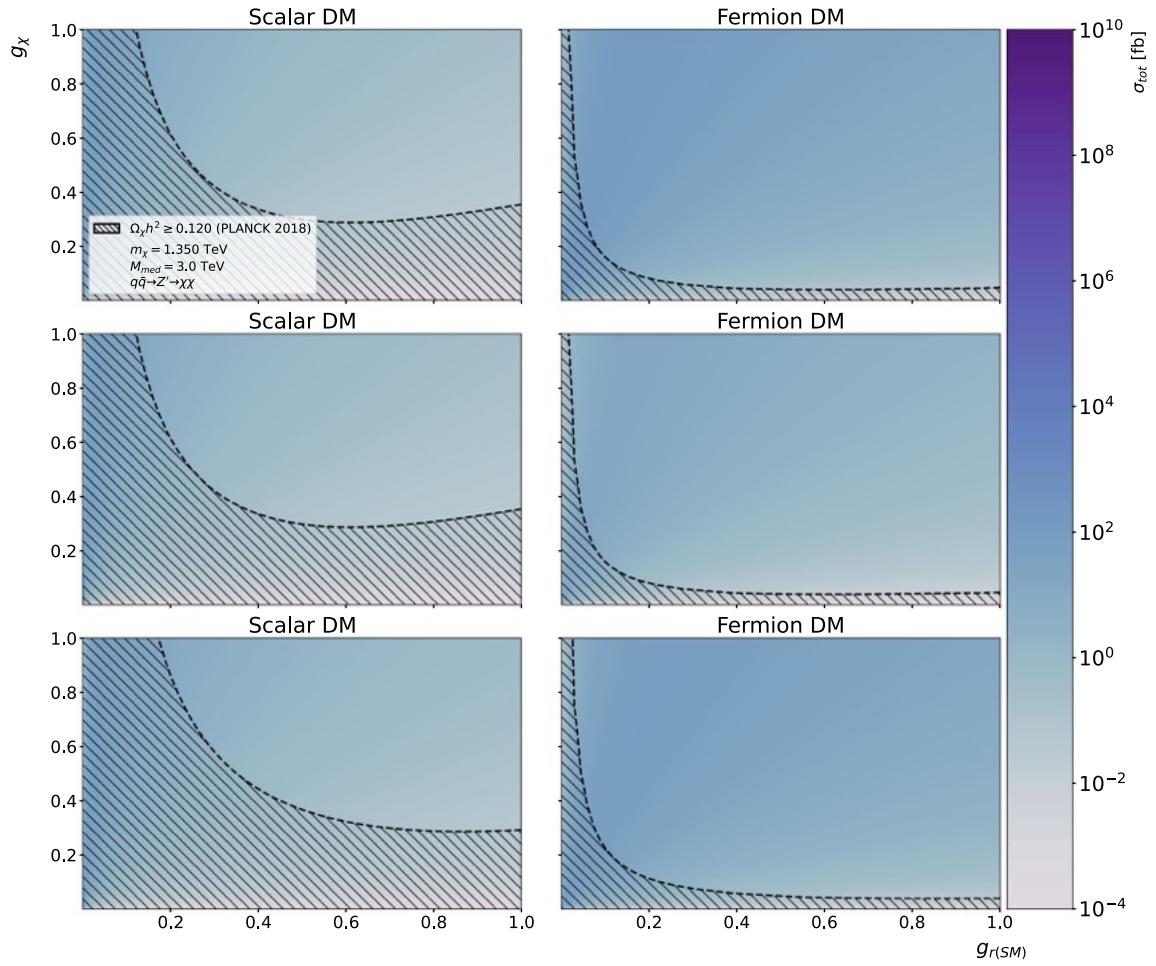

Fig. 15 Same as Fig. 14, but in *pp* collisions at the LHC at 14 TeV

by the energy and luminosity of the LHC as well as in future accelerators.

Differently from what happens in direct and indirect searches, if any DM trace have been detected in collider experiments, it would not be possible to state that the observed DM would be the same that has its gravitational effects observed at cosmological levels. This is because the time of flight of a particle to traverse all detector dependencies is not comparable to the cosmological lifetime of a stable primordial DM particle. In addition, cross-analysis of data from different experiments almost always takes some dependence on specific DM models, due to the difficulty of comparing such results independently [1,76]. The experimental viability of DM observation through these processes are focused in the use of disappearing tracks, as already done by the experiments at the LHC [77]. Therefore, our results show that searches of mono-photon production with large missing energy can be a competitive experimental signature for observing evidence of DM particles at the LHC, with the potential of characterizing the nature of a DM vector mediator in production near its resonance.

Acknowledgements This work was partially financed by the Brazilian funding agencies FAPERGS, CAPES and CNPq. This study was financed in part by the Coordenação de Aperfeiçoamento de Pessoal de Nível Superior – Brasil (CAPES) – Finance Code 001. GGS acknowledges funding from the Brazilian agency Conselho Nacional de Desenvolvimento Científico e Tecnológico (CNPq) with grant CNPq/311851/2020-7.

Data Availability Statement This manuscript has no associated data or the data will not be deposited. [Authors' comment: This is a phenomenological study and has no experimental data associated to it.]

References

1. R.L. Workman et al., Review of particle physics. PTEP **2022**, 083C01 (2022). https://doi.org/10.1093/ptep/ptac097
2. G. Bertone, D. Hooper, J. Silk, Particle dark matter: evidence, candidates and constraints. Phys. Rep. **405**, 279–390 (2005). https://doi.org/10.1016/j.physrep.2004.08.031
3. M. Bauer, T. Plehn, *Yet Another Introduction to Dark Matter: The Particle Physics Approach. Lecture Notes in Physics*, vol. 959 (Springer, Berlin, 2019). https://doi.org/10.1007/978-3-030-16234-4
4. M. Klasen, K. Kovarik, S. Schmiemann, Direct detection of neutralino dark matter with DM@NLO. PoS **EPS-HEP2017**, 068 (2017). https://doi.org/10.22323/1.314.0068
5. M. Duerr, K. Schmidt-Hoberg, S. Wild, Self-interacting dark matter with a stable vector mediator. JCAP **09**, 033 (2018). https://doi.org/10.1088/1475-7516/2018/09/033
6. M. Schumann, Direct detection of wimp dark matter: concepts and status. J. Phys. G **46**(10), 103003 (2019). https://doi.org/10.1088/1361-6471/ab2ea5
7. C.P. de los Heros, Status, challenges and directions in indirect dark matter searches. Symmetry **12**(10), 1648 (2020). https://doi.org/10.3390/sym12101648
8. R. Catena, L. Covi, SUSY dark matter(s). Eur. Phys. J. C **74**, 2703 (2014). https://doi.org/10.1140/epjc/s10052-013-2703-4
9. G. Arcadi, A. Djouadi, M. Raidal, Dark matter through the Higgs portal. Phys. Rep. **842**, 1–180 (2020). https://doi.org/10.1016/j.physrep.2019.11.003
10. D. Schmeier, Effective models for dark matter at the international linear collider (2013). https://doi.org/10.48550/arXiv.1308.4409
11. P. Agrawal, Z. Chacko, C. Kilic, R.K. Mishra, A classification of dark matter candidates with primarily spin-dependent interactions with matter. UMD-PP-10-004, RUNHETC-2010-07 (2010). arXiv:1003.1912 [hep-ph]
12. J. Abdallah et al., Simplified models for dark matter searches at the lhc. Phys. Dark Universe **9–10**, 8–23 (2015). ISSN:2212-6864. https://doi.org/10.1016/j.dark.2015.08.001
13. A. Albert et al., Recommendations of the LHC Dark Matter Working Group: comparing LHC searches for dark matter mediators in visible and invisible decay channels and calculations of the thermal relic density. Phys. Dark Universe **26**, 100377 (2019). https://doi.org/10.1016/j.dark.2019.100377
14. D. Abercrombie, N. Akchurin, E. Akilli et al., Dark matter benchmark models for early LHC run-2 searches: report of the ATLAS/CMS dark matter forum. Phys. Dark Universe **27**, 100371 (2020). ISSN:2212-6864. https://doi.org/10.1016/j.dark.2019.100371
15. A. Boveia et al., Recommendations on presenting LHC searches for missing transverse energy signals using simplified s-channel models of dark matter. Phys. Dark Universe **27**, 100365 (2020). https://doi.org/10.1016/j.dark.2019.100365
16. E.W. Kolb, M.S. Turner, *The Early Universe*, vol. 69 (CRC Press, Boca Raton, 1990). ISBN:978-0-201-62674-2. https://doi.org/10.1201/9780429492860
17. P. Langacker, The physics of heavy Z' gauge bosons. Rev. Mod. Phys. **81**, 1199–1228 (2009). https://doi.org/10.1103/RevModPhys.81.1199
18. M. Frank, K. Huitu, S. Mondal, Dark matter and collider signals in supersymmetric $U(1)'$ models with non-universal Z' couplings. Phys. Rev. D **100**(11), 115018 (2019). https://doi.org/10.1103/PhysRevD.100.115018
19. O. Buchmueller, M.J. Dolan, S.A. Malik, C. McCabe, Characterising dark matter searches at colliders and direct detection experiments: vector mediators. JHEP **01**, 037 (2015). https://doi.org/10.1007/JHEP01(2015)037
20. A. Boveia, C. Doglioni, Dark matter searches at colliders. Annu. Rev. Nucl. Part. Sci. **68**, 429–459 (2018). https://doi.org/10.1146/annurev-nucl-101917-021008
21. A.M. Sirunyan et al., Search for new physics in final states with an energetic jet or a hadronically decaying W or Z boson and transverse momentum imbalance at $\sqrt{s} = 13$ TeV. Phys. Rev. D **97**(9), 092005 (2018). https://doi.org/10.1103/PhysRevD.97.092005
22. A.M. Sirunyan et al., Search for narrow and broad dijet resonances in proton–proton collisions at $\sqrt{s} = 13$ TeV and constraints on dark matter mediators and other new particles. JHEP **08**, 130 (2018). https://doi.org/10.1007/JHEP08(2018)130
23. M. Aaboud et al., Search for dark matter and other new phenomena in events with an energetic jet and large missing transverse momentum using the ATLAS detector. JHEP **01**, 126 (2018). https://doi.org/10.1007/JHEP01(2018)126
24. L. Linssen, A. Miyamoto, M. Stanitzki, H. Weerts, Physics and detectors at CLIC: CLIC conceptual design report (2012). https://doi.org/10.5170/CERN-2012-003
25. K. Kadota, A. Spray, Electroweak multiplet dark matter at future lepton colliders. JHEP **02**, 017 (2019). https://doi.org/10.1007/JHEP02(2019)017
26. P.J. Fox, R. Harnik, J. Kopp, Y. Tsai, Missing energy signatures of dark matter at the LHC. Phys. Rev. D **85**, 056011 (2012). https://doi.org/10.1103/PhysRevD.85.056011
27. J. de Blas et al., The CLIC potential for new physics. CERN-TH-2018-267, CERN-2018-009-M (2018). https://doi.org/10.23731/CYRM-2018-003
28. G. Aad et al., Search for new phenomena in events with an energetic jet and missing transverse momentum in pp collisions at $\sqrt{s} = 13$ TeV with the ATLAS detector. Phys. Rev. D **103**(11), 112006 (2021). https://doi.org/10.1103/PhysRevD.103.112006
29. A. Tumasyan et al., Search for new particles in events with energetic jets and large missing transverse momentum in proton–proton collisions at $\sqrt{s} = 13$ TeV. JHEP **11**, 153 (2021). https://doi.org/10.1007/JHEP11(2021)153
30. P. Gondolo, G. Gelmini, Cosmic abundances of stable particles: improved analysis. Nucl. Phys. B **360**, 145–179 (1991). https://doi.org/10.1016/0550-3213(91)90438-4
31. K. Griest, D. Seckel, Three exceptions in the calculation of relic abundances. Phys. Rev. D **43**(10), 3191–3203 (1991). https://doi.org/10.1103/physrevd.43.3191
32. N. Aghanim et al., Planck 2018 results. VI. Cosmological parameters. Astron. Astrophys. **641**, A6 (2020). https://doi.org/10.1051/0004-6361/201833910. [Erratum: Astron. Astrophys. **652**, C4 (2021)]
33. R. Oncala, K. Petraki, Bound states of WIMP dark matter in Higgs-portal models. Part I. Cross-sections and transition rates. JHEP **06**, 124 (2021). https://doi.org/10.1007/JHEP06(2021)124
34. G. Bonneau, F. Martin, Hard photon emission in e^+e^- reactions. Nucl. Phys. B **27**, 381–397 (1971). https://doi.org/10.1016/0550-3213(71)90102-7
35. J. Wudka, *The Meaning of Anomalous Couplings*, vol. C960625 (1996). https://doi.org/10.48550/arXiv.hep-ph/9606478
36. D. Alves, Simplified models for LHC new physics searches. J. Phys. G **39**, 105005 (2012). https://doi.org/10.1088/0954-3899/39/10/105005
37. D. Abercrombie et al., Dark matter benchmark models for early LHC Run-2 searches: report of the ATLAS/CMS dark matter forum. Phys. Dark Universe **27**, 100371 (2020). https://doi.org/10.1016/j.dark.2019.100371
38. L. Roszkowski, E.M. Sessolo, S. Trojanowski, WIMP dark matter candidates and searches—current status and future prospects. Rep. Prog. Phys. **81**(6), 066201 (2018). https://doi.org/10.1088/1361-6633/aab913
39. A.C. Kopecky, A search for dark matter in the monophoton final state at CMS. PhD thesis, UC, Davis (2012)

40. G. Arcadi, M. Dutra, P. Ghosh, M. Lindner, Y. Mambrini, M. Pierre, S. Profumo, F.S. Queiroz, The waning of the WIMP? A review of models, searches, and constraints. Eur. Phys. J. C **78**(3), 203 (2018). https://doi.org/10.1140/epjc/s10052-018-5662-y
41. C.-F. Chang, X.-G. He, J. Tandean, Two-Higgs-doublet-portal dark-matter models in light of direct search and LHC data. JHEP **04**, 107 (2017). https://doi.org/10.1007/JHEP04(2017)107
42. M. Ruhdorfer, E. Salvioni, A. Weiler, A global view of the off-shell Higgs portal. SciPost Phys. **8**, 027 (2020). https://doi.org/10.21468/SciPostPhys.8.2.027
43. J.M. Cornell, S. Profumo, W. Shepherd, Dark matter in minimal universal extra dimensions with a stable vacuum and the "right" Higgs boson. Phys. Rev. D **89**(5), 056005 (2014). https://doi.org/10.1103/PhysRevD.89.056005
44. A. Boyarsky, M. Drewes, T. Lasserre, S. Mertens, O. Ruchayskiy, Sterile neutrino dark matter. Prog. Part. Nucl. Phys. **104**, 1–45 (2019). https://doi.org/10.1016/j.ppnp.2018.07.004
45. E. Aprile et al., The XENON1T dark matter experiment. Eur. Phys. J. C **77**(12), 881 (2017). https://doi.org/10.1140/epjc/s10052-017-5326-3
46. E. Aprile et al., Search for new physics in electronic recoil data from XENONnT. Phys. Rev. Lett. **129**(16), 161805 (2022). https://doi.org/10.1103/PhysRevLett.129.161805
47. A. Falkowski, S.F. King, E. Perdomo, M. Pierre, Flavourful Z' portal for vector-like neutrino Dark Matter and $R_{K^{(*)}}$. JHEP **08**, 061 (2018). https://doi.org/10.1007/JHEP08(2018)061
48. M.E. Cabrera, J.A. Casas, A. Delgado, S. Robles, R.R. de Austri, Naturalness of MSSM dark matter. JHEP **08**, 058 (2016). https://doi.org/10.1007/JHEP08(2016)058
49. V. Shtabovenko, R. Mertig, F. Orellana, FeynCalc 9.3: new features and improvements. Comput. Phys. Commun. **256**, 107478 (2020). https://doi.org/10.1016/j.cpc.2020.107478
50. T. Hahn, Generating Feynman diagrams and amplitudes with FeynArts 3. Comput. Phys. Commun. **140**, 418–431 (2001). https://doi.org/10.1016/S0010-4655(01)00290-9
51. Wolfram Research, Inc. Mathematica, Version 13.2. Champaign, IL (2022). https://www.wolfram.com/mathematica. Accessed 15 Jan 2024
52. S. Cebrián, Review on dark matter searches. J. Phys. Conf. Ser. **2502**, 012004 (2022). https://doi.org/10.1088/1742-6596/2502/1/012004
53. J. Kalinowski, W. Kotlarski, K. Mekala, P. Sopicki, A.F. Zarnecki, Dark matter searches with mono-photon signature at future e^+e^- colliders. SciPost Phys. Proc. **8**, 095 (2022a). https://doi.org/10.21468/SciPostPhysProc.8.095
54. J. Kalinowski, W. Kotlarski, K. Mekala, K. Zembaczynski, A.F. Zarnecki, New approach to DM searches with mono-photon signature. in *2022 Snowmass Summer Study* (2022). https://doi.org/10.48550/arXiv.2203.06776
55. E. Tolley, Dark matter searches with Mono-X signatures at the ATLAS experiment. PoS **DIS2016**, 107 (2016). https://doi.org/10.22323/1.265.0107
56. M. Davier, A. Hoecker, B. Malaescu, C.Z. Yuan, Z. Zhang, Reevaluation of the hadronic contribution to the muon magnetic anomaly using new $e+e \to \pi+\pi$-cross section data from babar. Eur. Phys. J. C **66**(1–2), 1–9 (2010). ISSN:1434-6052. https://doi.org/10.1140/epjc/s10052-010-1246-1
57. W. Kilian, T. Ohl, J. Reuter, Whizard-simulating multi-particle processes at LHC and ILC. Eur. Phys. J. C **71**(9) (2011). ISSN:1434-6052. https://doi.org/10.1140/epjc/s10052-011-1742-y
58. J. Blümlein, A. De Freitas, C. Raab, K. Schönwald, The $O(\alpha^2)$ initial state QED corrections to $e^+e^- \to \gamma^*/Z_0^*$. Nucl. Phys. B **956**, 115055 (2020). https://doi.org/10.1016/j.nuclphysb.2020.115055
59. B. McElrath, Invisible quarkonium decays as a sensitive probe of dark matter. Phys. Rev. D **72**(10) (2005). ISSN:1550-2368. https://doi.org/10.1103/physrevd.72.103508
60. J.P. Lees et al., Study of $e^+e^- \to p\bar{p}$ via initial-state radiation at BABAR. Phys. Rev. D **87**(9), 092005 (2013). https://doi.org/10.1103/PhysRevD.87.092005
61. V.P. Druzhinin, S.I. Eidelman, S.I. Serednyakov, E.P. Solodov, Hadron production via e^+e^- collisions with initial state radiation. Rev. Mod. Phys. **83**, 1545 (2011). https://doi.org/10.1103/RevModPhys.83.1545
62. M.N. Achasov et al., Study of the process $e^+e^- \to \eta\pi^0\gamma$ in the energy range $\sqrt{s} = 1.05 - 2.00$ GeV with the SND detector. Eur. Phys. J. C **80**(11), 1008 (2020). https://doi.org/10.1140/epjc/s10052-020-08556-w
63. A. Blondel et al., Standard model theory for the FCC-ee Tera-Z stage, in *Mini Workshop on Precision EW and QCD Calculations for the FCC Studies: Methods and Techniques. CERN Yellow Reports: Monographs*, vol. 3/2019 (CERN, Geneva, 2018). https://doi.org/10.23731/CYRM-2019-003
64. M.-S. Chen, P.M. Zerwas, Equivalent-particle approximations in electron and photon processes of higher order QED. Phys. Rev. D **12**, 187 (1975). https://doi.org/10.1103/PhysRevD.12.187
65. J.-J. Blaising, P. Roloff, A. Sailer, U. Schnoor, Physics performance for Dark Matter searches at $\sqrt{s} = 3$ TeV at CLIC using mono-photons and polarised beams (2021). https://doi.org/10.48550/arXiv.2103.06006
66. V. Khachatryan et al., Performance of photon reconstruction and identification with the CMS detector in proton–proton collisions at sqrt(s) = 8 TeV. JINST **10**(08), P08010 (2015). https://doi.org/10.1088/1748-0221/10/08/P08010
67. J. Kalinowski, W. Kotlarski, P. Sopicki, A.F. Zarnecki, Simulating hard photon production with WHIZARD. Eur. Phys. J. C **80**(7), 634 (2020). https://doi.org/10.1140/epjc/s10052-020-8149-6
68. CMS Collaboration, Search for resonant and nonresonant new phenomena in high-mass dilepton final states at $\sqrt{s} = 13$ TeV. JHEP **07**, 208 (2021). https://doi.org/10.1007/JHEP07(2021)208
69. J. Kalinowski, W. Kotlarski, K. Mekala, P. Sopicki, A.F. Zarnecki, Sensitivity of future linear e^+e^- colliders to processes of dark matter production with light mediator exchange. Eur. Phys. J. C **81**(10) (2021). ISSN:1434-6052. https://doi.org/10.1140/epjc/s10052-021-09758-6
70. A. Tumasyan et al., Search for resonant production of strongly coupled dark matter in proton–proton collisions at 13 TeV. JHEP **06**, 156 (2022). https://doi.org/10.1007/JHEP06(2022)156
71. O. Brunner et al., *The CLIC Project. Accelerator Physics (physics.acc-ph); High Energy Physics—Experiment* (hep-ex) (2022). https://doi.org/10.48550/arXiv.2203.09186
72. H. Dreiner, M. Huck, M. Krämer, D. Schmeier, J. Tattersall, Illuminating dark matter at the ILC. Phys. Rev. D **87**(7), 075015 (2013). https://doi.org/10.1103/PhysRevD.87.075015
73. D. Dannheim, P. Lebrun, L. Linssen, D. Schulte, F. Simon, S. Stapnes, N. Toge, H. Weerts, J. Wells, CLIC e^+e^- linear collider studies (2012). https://doi.org/10.48550/arXiv.1208.1402
74. R.D. Ball et al., Parton distributions from high-precision collider data. Eur. Phys. J. C **77**(10), 663 (2017). https://doi.org/10.1140/epjc/s10052-017-5199-5
75. A. Buckley, J. Ferrando, S. Lloyd, K. Nordström, B. Page, M. Rüfenacht, M. Schönherr, G. Watt, LHAPDF6: parton density access in the LHC precision era. Eur. Phys. J. C **75**, 132 (2015). https://doi.org/10.1140/epjc/s10052-015-3318-8
76. N. Trevisani, Collider searches for dark matter. Universe **4**(11), 131 (2018). https://doi.org/10.3390/universe4110131
77. A.M. Sirunyan et al., Search for disappearing tracks in proton-proton collisions at $\sqrt{s} = 13$ TeV. Phys. Lett. B **806**, 135502 (2020). https://doi.org/10.1016/j.physletb.2020.135502

APPENDIX B – Resonant production of vector DM states characterized by monophoton ISR at high-energy colliders

Resonant production of vector DM states characterized by monophoton ISR at high-energy colliders

G. Gil da Silveira[1,*] and M. S. Mateus Jr.[1,†]

[1] *Group of Analysis and Simulation of Particles (GASP), IF-UFRGS*
Caixa Postal 15051, CEP 91501-970, Porto Alegre, RS, Brazil

Abstract

Dark matter research, aimed at unraveling astrophysical enigmas, faces the challenge of lacking concrete evidence connecting dark matter with the observable universe in both experimental and theoretical particle physics. Our study investigates a simplified extension to the Standard Model (SM) where SM fermions interacts with a hypothetical vector dark matter (DM) particle in high-energy collisions, mediated by a proposed massive spin-1 particle, Z'. We specifically explore vector DM pair production through fermion annihilation in this mediator, focusing on a near-resonance condition ($m_\chi \sim M_{Z'}/2$). This includes examining mono-photon production, a SM signal, as a result of initial state radiation. We also calibrate the coupling constants between DM and SM particles relative to Planck satellite thermal relic density data, particularly near a resonance where traditional models anticipate more relic density suppression. Our findings, consistent with expected relic density at resonance regimes, suggest mass ranges and coupling constants for these DM particles that align with collider and astrophysical limits, to be validated in CLIC and LHC settings.

PACS numbers: 95.35.+d, 13.66.Hk, 25.75.Dw, 12.39.St

* gustavo.silveira@cern.ch
† msmateusjr@gmail.com

I. INTRODUCTION

The Standard Model (SM) of particle physics, while accurately describing numerous phenomena, lacks a viable dark matter (DM) candidate. There is a growing consensus on extending the SM by including new particles and interactions for a more comprehensive understanding of the universe [1–3]. This paper examines such an extension, proposing a simplified model in which interactions between Weakly Interactive Massive Particles (WIMPs) and SM particles are mediated by a new massive boson, Z' [2–9].

If DM particles are heavy and have masses $m_\chi \sim M_{Z'}$, hence the DM pair production will carry much of the mediator mass. Our work aims to accounts for the expected relic density near a resonance, a scenario often overlooked in standard calculations. We compare our predictions for production cross sections with a novel evaluation of the relic density for DM species [10–12], providing new insights into the dark matter sector. In the context of this work, the mediator Z' plays a crucial role in the production of primordial DM until a freeze-out stage is reached. Our model does not presuppose any effective model and instead calculates the total cross section using Feynman rules derived from the simplified model Lagrangian [3, 13–15].

We explore the production of Z' via a monophoton process in both electron-positron annihilation at CLIC and proton-proton collisions at the LHC. These processes are analyzed under the assumption that the DM particles, which are invisible decay products of the Z' mediator, have invariant masses close to the resonance and the photon acts as an observable SM signal. We focus on a Z' mass of 3 TeV considering the current experimental limits [16, 17]. This article continues a previously published work on DM that focused on scalar and fermion final states. Details about the implementation and methodology can be found in Ref. [18].

The paper is structured to initially describe the theoretical modeling of the Z' mediator and its implications for the final state of DM vector in section II. The evaluation of the relic density near a resonance is presented in section III, allowing for effective comparisons with standard calculations. We then discuss the potential observations of this model in high-energy collider environments like CLIC and LHC, focusing on the available mass and coupling constant regions at section IV. Finally, we conclude in section V with the implications of our findings on the understanding of dark matter.

II. SIMPLIFIED MODEL

In particle physics, extensions of the SM are often explored through simplified models, which are powerful in studying new physics, focusing on key parameters such as particle masses and production cross sections [1, 3, 19]. We employ such models, specifically using a new symmetry group, $U_\chi(1)$, as a vector portal to investigate dark matter (DM) interactions with the SM. This approach has been validated in various collider experiments [16, 17, 20, 21]. We examine interactions mediated by a new massive boson, Z', in a framework involving Breit-Wigner resonances. Our focus is on the evaluation of cross sections and analysis of the parameter space for vector DM final states. While our study does not cover the mass acquisition of the Z' boson or the gauge regularization of our Lagrangians, it aligns with methodologies in current literature [22]. For more detailed models on spin-1 mediators and related states, further references are available [1, 2, 9, 15, 17, 20, 21, 23–26].

We introduce a DM candidate as a complex vector field, where two real degrees of freedom of a DM complex field can be combined with the singlet boson state previously defined by the mediator Z'_μ to generate a field tensor and a gauge kinetic term, similar to what is done in gauge theories in $SU(2)$ representations. Following the steps established in Ref. [27], we write an interacting Lagrangian (neglecting quadratic terms) as

$$\begin{aligned}\mathcal{L}_{\text{int}}^{\text{vector}} \supset\ & \bar{\psi}\gamma^\mu \left(g_l P_L + g_r P_R\right) \psi Z'_\mu - i g_\chi \left(\partial^\mu Z'^\nu - \partial^\nu Z'^\mu\right) \chi^\dagger_\mu \chi_\nu, \\ -\ & i g_\chi Z'_\mu \chi^\dagger_\nu \left(\partial^\mu \chi^\nu - \partial^\nu \chi^\mu\right) + i g_\chi Z'^\mu \chi^\nu \left(\partial_\mu \chi^\dagger_\nu - \partial_\nu \chi^\dagger_\mu\right) \end{aligned} \tag{1}$$

where the operators in the last three terms express the couplings of DM to the Z' fields.

Although less common in the literature, vector DM is also a possible candidate to explain the dark matter relic abundance [28–30] and can be of good use in models of self-interacting DM, where it forms gravitational bound states [31], and have significant implications in the primordial universe phenomenology, even more if we are taking into account inflationary models [32]. The DM models featuring stable vector (spin-1) massive particles in the literature we can have models involving millicharged spin-1 particles, where Ref. [33] suggests a minimal, unitary, renormalizable model for massive millicharged vector particles, which are gauge bosons of a spontaneously broken, non-abelian gauge symmetry. This framework potentially provides a vector dark matter candidate and includes an extended Standard Model (SM) gauge group and a dark Higgs boson, which is pivotal for symmetry breaking in the

dark sector [33]. Another interesting concept is the invisible decaying spin-1 dark matter. Ref. [34] discusses a model where DM, interacting through a dark-Higgs Yukawa portal with the SM sector, undergoes slow, loop-suppressed decays to photons and neutrinos, maintaining stability over cosmological timescales. Additionally, there are more generic models, such as those proposed by Ref. [35], focusing on singlet dark sectors based on different spins. These models consider spin-$\frac{1}{2}$ particles under confining spin-1 particles, leading to stable dark matter candidates similar to baryons.

In the context of collider research, there is also a model with a minimal spin-1 isotriplet as the dark sector. Here, Ref. [36] introduces a massive spin-1 matter field, part of the adjoint representation of $SU(2)_L$. They affirm that this model complies with all current experimental constraints, including measurements of dark matter relic density, direct and indirect detection searches, and LHC data, making the neutral component of the triplet a viable dark matter particle. These diverse studies contribute significantly to our understanding of the possibilities for stable vector (spin-1) massive particles as DM candidates, shedding light on the intricate nature of DM in the universe.

Besides, vector DM models often face significant constraints for high-mass final states due to the inverse relationship between the cross section and particle mass. This results in a very narrow scope for thermal DM production that aligns with existing literature limits. In this work, our focus is on TeV-scale masses, a range accessible in high-energy collider experiments. We should stress the fact that simply detecting new particles in experiments does not automatically classify them as DM; in-depth analysis is required to determine their properties and assess if they signify new physics with the potential to answer unresolved questions [15, 17].

For a $2 \to 2$ the total cross section, $\hat{\sigma}_{\rm tot}$, in the center-of-momentum frame is derived using the Mandelstam variable s, such as

$$\hat{\sigma}^{\rm vector} = g_\chi^2 \left(g_l^2 + g_r^2\right) \beta \tag{2}$$

$$\times \frac{\left(-48 M_{Z'}^2 m_\chi^6 - 68 M_{Z'}^2 m_\chi^4 s + 16 M_{Z'}^2 m_\chi^2 s^2 + M_{Z'}^2 s^3 + 192 m_\chi^4 s^2 - 96 m_\chi^2 s^3 + 12 s^4\right)}{192 M_{Z'}^2 m_\chi^4 \sqrt{s}\left[\left(s - M_{Z'}^2\right)^2 + \Gamma^2 M_{Z'}^2\right]}, \tag{3}$$

where $\beta = \sqrt{s - 4m_\chi^2}$. The terms for the Breit-Wigner width, $\Gamma^2 M_{Z'}^2$, in the denominator of the scattering amplitudes correspond to the mediator exchange of a s-channel resonance. As

our investigation is related to processes with a massive spin-1 mediator with an associated decay width, we evaluate the decay of the Z' mediator into DM particles to determine its decay width, $\Gamma^{\rm i}$,

$$\Gamma^{\rm vector} = \frac{g_\chi^2 M_{Z'}^3 \left(1 - 4m_\chi^2/M_{Z'}^2\right)^{\frac{3}{2}}}{192\pi m_\chi^2} + N_f \Gamma_{Z' \to SM}. \tag{4}$$

Within this framework, the parameter N_f is the number of fermions into which the mediator Z' can decay within the SM sector. For example, in e^+e^- collisions where Z' interacts only with leptons, $N_f = 6$. Conversely, when Z' is exclusively coupled with quarks, $N_f = 18$.

The coupling of SM particles and the Z' mediator, in relation to its nature, allows for their classification into distinct types as outlined in Ref. [13]. There are three primary categories. The first, vector coupling, is characterized by the equivalence of left-handed (g_l) and right-handed (g_r) couplings, denoted as ($g_l = g_r$). The second type, axial-vector coupling, is defined by the left-handed coupling being the exact negative of the right-handed coupling, expressed as ($g_l = -g_r$). Lastly, the right (chiral) coupling scenario is identified by the absence of left-handed coupling, succinctly represented as ($g_l = 0$). These categories help in understanding the diverse interaction mechanisms of the Z' boson within the SM. Depending on whether the Z' mediator functions as a vector, axial-vector, or chiral entity, different coupling constants are applied, as detailed in Ref. [13].

For accurate DM production via monophoton processes, radiative corrections to the tree-level DM process are crucial. Previous studies have used soft photon approximations or numerical methods for $3 \to 2$ processes [37–39]. Our approach, inspired by classical methods [40] and applied in various contexts [41–45], involves factoring in hard-photon emission. This method calculates higher-order corrections and precisely evaluates the phase space of the emitted photon, necessary for high-energy scenarios, and differs from simpler models like the Weizsäcker-Williams approximation [13, 46]. We implement this factorization to determine the total cross section for monophoton processes,

$$\sigma'_{\rm tot}(\psi\bar{\psi} \to Z'\gamma \to \gamma\chi\bar{\chi}) = \hat{\sigma}_{\rm tot}(\psi\bar{\psi} \to Z' \to \chi\bar{\chi})(1+\delta), \tag{5}$$

with δ given by Ref. [40].

As discussed in a previously work [18], we set the minimum photon energy fraction $x_\gamma = q_\gamma/E_{beam}$ to 0.04 (equivalent to 60 GeV for a 1.5 TeV beam), based on the photon identification capabilities at CLIC dp [47] and observations from LHC experiments [48].

Despite a slight suppression in the cross section around the minimum photon energy of 0.04, the overall production cross section increases by up to 7% at higher photon energies. This enhancement is independent of the dark sector mass and coupling constants.

According to Ref. [49], DM pair production with a hard photon is feasible with cross sections in the $\mathcal{O}$(fb), making detection viable with sufficient luminosity. Simulations support the observation of monophotons from invisible decays, characterized by high cross section and transverse momentum [50]. The detection strategy involves looking for high p_T photons paired with MET, which typically peaks near the mediator resonance mass.

We verify the regions of relic density in comparison to the partonic cross section for DM particle production (Equation 2) in e^+e^- annihilation at the CLIC collider [51, 52] at a center-of-mass energy of $\sqrt{s} = 3$ TeV. This is followed by an analysis of pp collisions at the LHC with $\sqrt{s} = 14$ TeV, considering the initial-state fermion masses $m_\psi = m_e$ for e^+e^- and $m_\psi = m_q$ for pp collisions. Predictions for CLIC involve straightforward beam-beam annihilation and resonance production. Monophoton production in e^+e^- collisions is calculated by combining the partonic cross section with the ISR photon, as described in Equation 5.

In pp collisions, the production cross section must include photon ISR within the partonic cross section $\hat{\sigma}_{\text{tot}}$, accounting for the post-photon quark momentum loss. Consequently, the production cross section for pp collisions is structured as follows:

$$\sigma'_{\text{tot}}(pp \to Z'\gamma \to \gamma\chi\bar{\chi}) \equiv M^2 \frac{\mathrm{d}\sigma}{\mathrm{d}M^2}\bigg|_{M=M_{Z'}} = \tau \int_\tau^1 f_q(x_1, Q^2) f_{\bar{q}}(\tau/x_1, Q^2) \hat{\sigma}'_{\text{tot}}(\tau s) \frac{\mathrm{d}x_1}{x_1}, \tag{6}$$

$$\hat{\sigma}'_{\text{tot}}(q\bar{q} \to Z'\gamma \to \gamma\chi\bar{\chi}) = \hat{\sigma}_{\text{tot}}(q\bar{q} \to Z' \to \chi\bar{\chi})(1+\delta). \tag{7}$$

III. CALCULATION OF THE DM RELIC DENSITY NEAR A RESONANCE

We examine the parameter space to identify exclusion regions based on relic density, highlighting viable dark sector scenarios. Particle colliders offer an advantage in DM searches due to their multipurpose detectors, capable of measuring numerous observables in expected production processes. The high integrated luminosity at these colliders reduces statistical uncertainties in new physics searches. Despite the high number of background events, they can be effectively managed with selection criteria and controlled for uncertainties and systematic

errors, which are separately simulated and studied [3]. This approach aids in distinguishing genuine signals of new physics from background noise.

In calculating the DM abundance and associated cross sections for its primordial production, standard methods assume equilibrium and ignore resonances. However, for resonant processes such as ours, the usual Boltzmann equation approach with $\langle\sigma v\rangle$ is not sufficient. We address this by modeling $\langle\sigma v\rangle$ as a non-relativistic Breit-Wigner resonance, following the methodology in Ref. [11], suitable for cold DM in the LCDM model[1]:

$$\langle\sigma v\rangle_{\rm res} = \frac{16\pi}{m_\chi^2}\frac{(2J+1)}{(2S+1)^2}x^{3/2}\pi^{1/2}\,\frac{M_{Z'}\Gamma_{Z'}}{m_\chi^2}B_i(1-B_i)\,F(z_R;x), \tag{8}$$

where $x = m_\chi/T$ links the DM particle mass (m_χ) to temperature (T). Here, J and B_i denote the spin and resonance branching fraction of the initial state, with S representing the spin of the DM particle. We focus on the annihilation of DM in SM particles through the mediator Z' in relic density calculations, where the candidates for DM are the initial state in this scenario. The auxiliary variable z_R is defined by using the masses and decay widths of the particles involved as

$$z_R = \frac{M_{Z'}^2 - m_\chi^2}{m_\chi^2} + i\frac{M_{Z'}\Gamma_{Z'}}{m_\chi^2}. \tag{9}$$

The term $F(z_R;x)$ arises from thermally averaging the cross-sectional velocity product, σv, and involves integration over the energy per unit mass ϵ (expressed as $(s-m_\chi^2)/m_\chi^2$).

$$F(z_R;x) = {\rm Re}\frac{i}{\pi}\int_0^\infty \frac{(1+\epsilon)^{1/2}e^{-x\epsilon}}{(1+2\epsilon)(z_R-\epsilon)}{\rm d}\epsilon. \tag{10}$$

The Equation 8 offers a simplified version of the original formula in Ref. [11]. This simplification enables numerical estimation of the dimensionless density parameter, which corresponds to the primordial DM fraction, as outlined in Refs. [11, 22] by

$$\Omega_\chi h^2 \approx 8.76\times10^{-11}\,{\rm GeV}^{-2}\left[\int_{T_0}^{T_f} g_*^{1/2}\langle\sigma v\rangle_{\rm res}\frac{{\rm d}T}{m_\chi}\right]^{-1}, \tag{11}$$

where, T_0 represents the current universe temperature, and T_f is the temperature at the *freeze-out* period. The term g_* denotes the degrees of freedom of particles during the same epoch.

[1] For a broad discussion of the Equation 8, we recommend Ref. [11].

IV. RESULTS AND DISCUSSION

In our study two scenarios for each initial state are analyzed with fixed couplings: $g_{r/l} = 0.01$ and 0.1 for $\ell\ell Z'$ in e^+e^- collisions, and $g_{r/l} = 0.10$ and 0.25 for $q\bar{q}Z'$ in pp collisions, with $g_\chi = 1$ for Z' dark sector coupling [16, 17, 53, 54]. For a pure vector mediator Z', a natural ratio of ~ 0.1 between $g_{Z'\ell\ell}/g_{Z'qq}$ is expected [53]. Larger couplings ($g_{Z'ff} \geq 0.1 \sim 0.3$) are assumed for TeV-scale mediators, potentially evading direct and indirect detection constraints [6, 7].

Here we explore the parameter space by scanning the $g_r \times g_\chi$ couplings for the CLIC and LHC kinematics. While similar exclusion patterns are noted for distinct coupling types, differences emerge in the extent of areas aligning with observed relic density (see Figure 1 and Figure 2), particularly between e^+e^- and pp collisions. In e^+e^- collisions, the overabundance region for $g_r = 0.01$ remains excluded, but becomes accessible with $g_r = 0.1$. However, larger $\ell\ell Z'$ coupling values require analysis under a potential leptophobic mediator behavior, considering more restrictive limits from resonance searches in dileptons [55, 56]. On the other hand, in the LHC regime, regions with $g_r = 0.1$ or $g_r = 0.25$ are further from the relic density overabundance limit and are largely accessible. Notably, the mediator coupling is independent and specific either to leptons or quarks, implying that dilepton resonance search limits are not directly applicable. This analysis highlights the importance of proper evaluation of the relic density near a resonance, which restricts the parameter space, especially for LHC energies, suggesting that LHC data analyses for spin-1 mediators should carefully consider these factors. As a result, the correct calculation of the relic density, using typical SM-DM and DM-DM couplings from the literature ($g_\chi = 1.0$ and $g_{r/l} = 0.25$), extends the parameter space compared to nonresonant calculations [11]. This results in a 3-4 fold improvement in g_χ and about 2 fold in $g_{r/l}$ within LHC kinematics. This differs significantly from results that do not consider resonances [16, 53], underscoring the impact of correct resonance evaluation on $\langle\sigma v\rangle$ and the estimations of the relic density.

In investigating DM production via s-channel resonances, Figure 1 illustrate mass scans for DM production near mediator mass $M_{Z'}$ in both e^+e^- and pp collisions. At CLIC, mass scans are performed with the resonant cross section peaks at 3 TeV, while the LHC explores varying $M_{Z'}$ and m_χ. Photon ISR impacts the cross-section, particularly evident in Figure 1 for CLIC, limiting the upper bound in m_χ. The hatched areas in these figures indicate regions

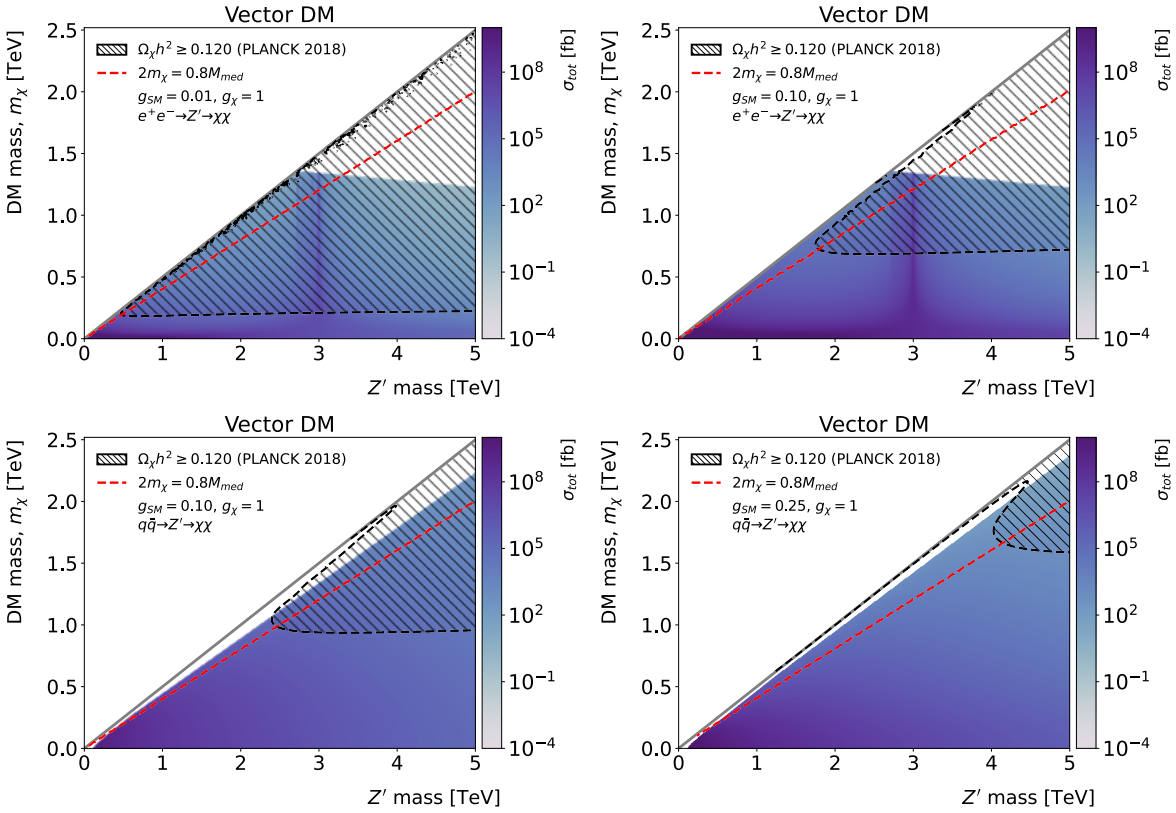

FIG. 1: Scan of the total cross section, including ISR contributions, as a function of dark matter (m_χ) and boson Z' ($M_{Z'}$) masses in e^+e^- (top) and pp (bottom) collision. The red dashed line indicates the threshold for examining the mass range close to the resonance, where the relic density is less suppressed. Plots differ by the use of the g_r coupling to leptons or quarks depending on the scenario.

of relic overabundance, thus excluded. The red dashed line marks the minimum viable m_χ considering the relic density near the Z' resonance. At CLIC, most of the mass regions are excluded due to relic overabundance or kinematic reach, particularly for $g_r = 0.01$. At LHC, with less stringent exclusion criteria, especially for $g_r = 0.25$, shows some accessible m_χ values, although high-mass mediators ($M_{Z'} \geq 4$ TeV) may still fall into overabundance regions.

In particle collider observations, the vector DM exhibits higher cross sections for smaller m_χ and $M_{Z'}$ masses. However, mediators below 2 TeV are mostly excluded, as per Refs. [16, 17], directing attention to higher mass regions. Actual detection rates may be lower than our predictions due to detector efficiencies and background noise. The predicted cross sections for vector DM in both e^+e^- and pp collisions are in the range of 10 to 1000 fb, but will be

reduced after accounting for real-world detector constraints. Nonetheless, these rates are consistent with the current lack of LHC observations. Despite the kinematic constraint near $M_{Z'} = 2m_\chi$, the potential for future observations remains, as this suggests that higher-order processes might not significantly hinder future observational possibilities. In both e^+e^- and pp collisions, the non-excluded regions by relic density are markedly different and occur at varying scales. Vector DM is largely excluded in e^+e^- collisions at CLIC, while pp collisions at the LHC offer less stringent restrictions. The pp collisions can access higher DM masses at the TeV scale, unlike the e^+e^- collisions. Low DM mass regions are inaccessible in e^+e^- collisions, but pp collisions can reach higher DM masses at the TeV scale, depending on the ISR photon energy range.

Figure 2 display the g_r and g_χ coupling distributions for e^+e^- and pp collisions, factoring in photon ISR. With a mediator mass $M_{Z'} = 3$ TeV and DM mass $m_\chi = 1200$ GeV, the figures identify regions conforming to cosmological limits near the resonance. Lower coupling scenarios often lead to overabundance, implying that direct and indirect detection experiments may be more suitable for larger couplings, while collider searches face more restrictions. The coupling type between SM particles and the dark mediator has a minor impact on cross sections, with chiral coupling producing a marginally larger exclusion area due to the characteristics of g_l coupling.

V. CONCLUSION

We proposed a simplified extension of the SM with a new renormalizable symmetry group $U_\chi(1)$ acting as an (axial)vector portal to the dark sector, including a vector DM stable particle. This model, featuring a simplified interaction Lagrangian, evaluates the relic density near the Z' mediator resonance, setting exclusion regions in mass and parameter scans. Consequently, we identify areas with less suppressed relic density, defining proper exclusion limits for DM production mediated by a TeV-scale Z' vector boson. Our model aligns with experimental and cosmological limits, significantly narrowing the range of coupling constants.

In e^+e^- collisions, DM observation is challenging, with limited phase space available for vector DM near the resonance, especially if DM has $\mathcal{O}(0.1)$ coupling to SM leptons. However, in pp collisions, there is a promising detection region for resonances acting as DM

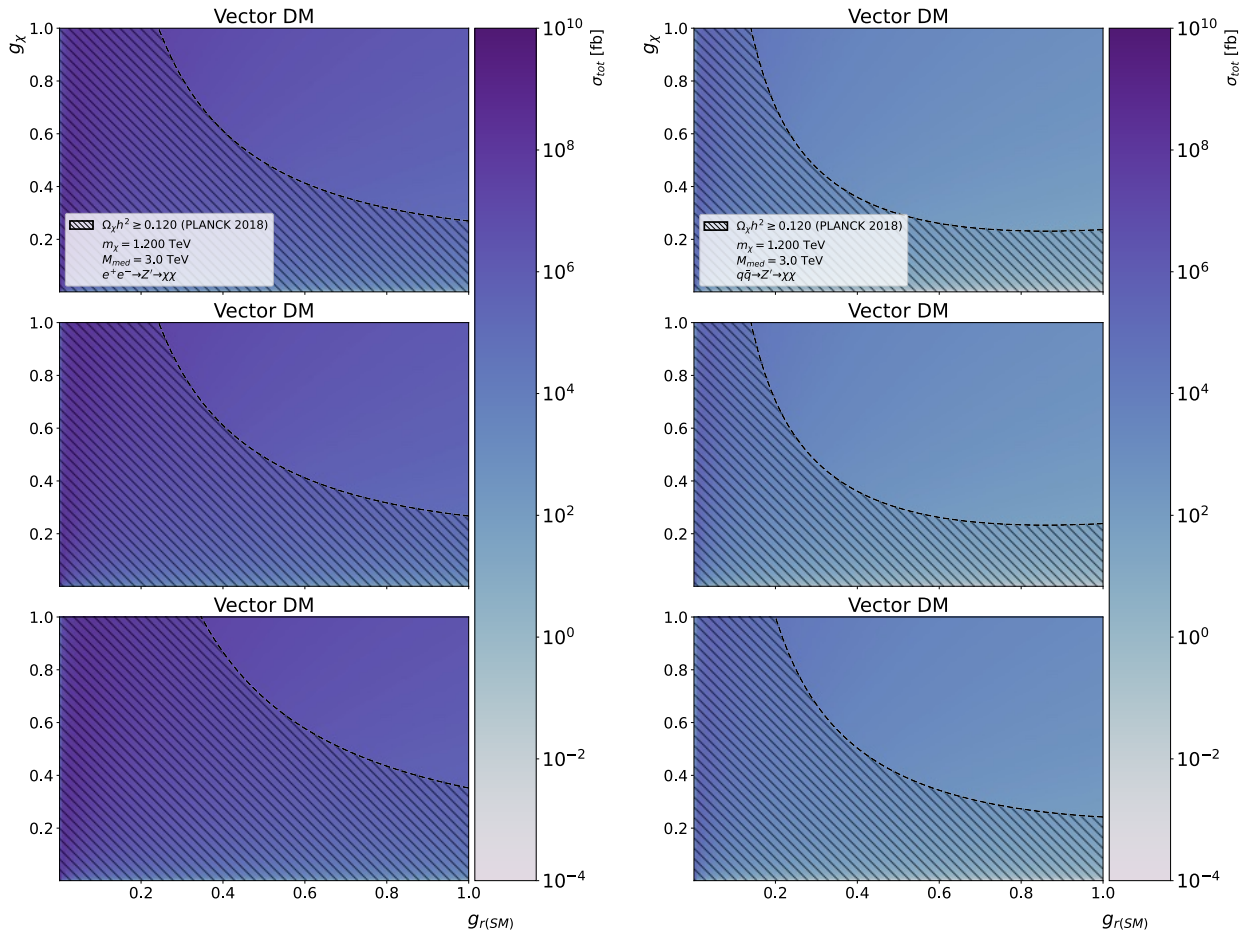

FIG. 2: (Left) This coupling scan displays the total cross section for e^+e^- collisions at $\sqrt{s} = 3$ TeV, categorized by the type of coupling with the Standard Model: vector (top), axial-vector (middle), and chiral (bottom). The horizontal axis shows the dependence of the Z' coupling (g_χ) with the dark sector. For this analysis, the DM particle mass and the mediator mass are set at $m_\chi = 1200$ GeV and $M_{Z'} = 3$ TeV, respectively. (Right) This analysis, similar to first, and focuses on the total cross section in pp collisions at $\sqrt{s} = 14$ TeV.

portals, particularly for larger vector DM couplings in the LHC energy regime. Our calculations show viable regions for resonance production consistent with cosmological and collider constraints. We demonstrate that enhancement to near-resonance $\langle \sigma v \rangle$ reduces exclusion regions in parameter space, expanding accessible couplings by 2-4 times, particularly in the LHC regime. This suggests that experimental limits on the mass of the DM mediator can be refined compared to simpler relic density calculations.

However, it is important to note that DM traces detected in collider experiments might not directly correlate with the DM observed through gravitational effects at cosmological levels. This discrepancy arises from the vastly different time scales involved in traversing detector setups versus the cosmological lifetime of stable primordial DM particles. Additionally, cross-analysis of data from various experiments often relies on specific DM models, complicating independent comparisons [1, 57]. Current DM observation methods at the LHC, like disappearing tracks [58], indicate that searches for mono-photon production with significant missing energy could be a viable way to detect DM particles, potentially revealing the nature of a DM vector mediator produced near its resonance.

ACKNOWLEDGMENTS

This work was partially financed by the Brazilian funding agencies FAPERGS, CAPES and CNPq. This study was financed in part by the Coordenação de Aperfeiçoamento de Pessoal de Nível Superior - Brasil (CAPES) - Finance Code 001. GGS acknowledges funding from the Brazilian agency Conselho Nacional de Desenvolvimento Científico e Tecnológico (CNPq) with grant CNPq/311851/2020-7.

---

[1] R. L. Workman et al. Review of Particle Physics. *PTEP*, 2022:083C01, 2022. doi: 10.1093/ptep/ptac097.

[2] Gianfranco Bertone, Dan Hooper, and Joseph Silk. Particle dark matter: Evidence, candidates and constraints. *Phys. Rept.*, 405:279–390, 2005. doi:10.1016/j.physrep.2004.08.031.

[3] Martin Bauer and Tilman Plehn. *Yet Another Introduction to Dark Matter: The Particle Physics Approach*, volume 959 of *Lecture Notes in Physics*. Springer, 2019. doi:10.1007/978-3-030-16234-4.

[4] Michael Klasen, Karol Kovarik, and Saskia Schmiemann. Direct detection of neutralino dark matter with DM@NLO. *PoS*, EPS-HEP2017:068, 2017. doi:10.22323/1.314.0068.

[5] Michael Duerr, Kai Schmidt-Hoberg, and Sebastian Wild. Self-interacting dark matter with a stable vector mediator. *JCAP*, 09:033, 2018. doi:10.1088/1475-7516/2018/09/033.

[6] Marc Schumann. Direct Detection of WIMP Dark Matter: Concepts and Status. *J. Phys. G*,

46(10):103003, 2019. doi:10.1088/1361-6471/ab2ea5.

[7] Carlos Pérez de los Heros. Status, Challenges and Directions in Indirect Dark Matter Searches. *Symmetry*, 12(10):1648, 2020. doi:10.3390/sym12101648.

[8] Riccardo Catena and Laura Covi. SUSY dark matter(s). *Eur. Phys. J. C*, 74:2703, 2014. doi:10.1140/epjc/s10052-013-2703-4.

[9] Giorgio Arcadi, Abdelhak Djouadi, and Martti Raidal. Dark Matter through the Higgs portal. *Phys. Rept.*, 842:1–180, 2020. doi:10.1016/j.physrep.2019.11.003.

[10] Edward W. Kolb and Michael S. Turner. *The Early Universe*, volume 69. CRC Press., 1990. ISBN 978-0-201-62674-2. doi:10.1201/9780429492860.

[11] Paolo Gondolo and Graciela Gelmini. Cosmic abundances of stable particles: Improved analysis. *Nucl. Phys. B*, 360:145–179, 1991. doi:10.1016/0550-3213(91)90438-4.

[12] Kim Griest and David Seckel. Three exceptions in the calculation of relic abundances. *Physical Review D*, 43(10):3191–3203, May 1991. doi:10.1103/physrevd.43.3191. URL `https://doi.org/10.1103/physrevd.43.3191`.

[13] Daniel Schmeier. Effective Models for Dark Matter at the International Linear Collider, 8 2013. arXiv:1308.4409[hep-ph].

[14] Prateek Agrawal, Zackaria Chacko, Can Kilic, and Rashmish K. Mishra. A Classification of Dark Matter Candidates with Primarily Spin-Dependent Interactions with Matter. *UMD-PP-10-004, RUNHETC-2010-07*, 2010. doi:10.48550/arXiv.1003.1912. arXiv:1003.1912[hep-ph].

[15] Jalal Abdallah et al. Simplified models for dark matter searches at the lhc. *Physics of the Dark Universe*, 9-10:8–23, 2015. ISSN 2212-6864. doi:10.1016/j.dark.2015.08.001.

[16] Georges Aad et al. Search for new phenomena in events with an energetic jet and missing transverse momentum in pp collisions at $\sqrt{s}$ =13 TeV with the ATLAS detector. *Phys. Rev. D*, 103(11):112006, 2021. doi:10.1103/PhysRevD.103.112006.

[17] Armen Tumasyan et al. Search for new particles in events with energetic jets and large missing transverse momentum in proton-proton collisions at $\sqrt{s}$ = 13 TeV. *JHEP*, 11:153, 2021. doi:10.1007/JHEP11(2021)153.

[18] G. Gil da Silveira and M. S. Mateus Jr au2. Investigation of spin-dependent dark matter in mono-photon production at high-energy colliders, 2023.

[19] *The Meaning of anomalous couplings*, volume C960625, 1996. [1063(1996)].

[20] Leszek Roszkowski, Enrico Maria Sessolo, and Sebastian Trojanowski. WIMP dark matter

candidates and searches - current status and future prospects. *Rept. Prog. Phys.*, 81(6):066201, 2018. doi:10.1088/1361-6633/aab913.

[21] Paul Langacker. The Physics of Heavy Z' Gauge Bosons. *Rev. Mod. Phys.*, 81:1199–1228, 2009. doi:10.1103/RevModPhys.81.1199.

[22] Giorgio Arcadi, Maíra Dutra, Pradipta Ghosh, Manfred Lindner, Yann Mambrini, Mathias Pierre, Stefano Profumo, and Farinaldo S. Queiroz. The waning of the WIMP? A review of models, searches, and constraints. *Eur. Phys. J. C*, 78(3):203, 2018. doi:10.1140/epjc/s10052-018-5662-y.

[23] Chia-Feng Chang, Xiao-Gang He, and Jusak Tandean. Two-Higgs-Doublet-Portal Dark-Matter Models in Light of Direct Search and LHC Data. *JHEP*, 04:107, 2017. doi:10.1007/JHEP04(2017)107.

[24] Maximilian Ruhdorfer, Ennio Salvioni, and Andreas Weiler. A Global View of the Off-Shell Higgs Portal. *SciPost Phys.*, 8:027, 2020. doi:10.21468/SciPostPhys.8.2.027.

[25] Jonathan M. Cornell, Stefano Profumo, and William Shepherd. Dark matter in minimal universal extra dimensions with a stable vacuum and the "right" Higgs boson. *Phys. Rev. D*, 89(5):056005, 2014. doi:10.1103/PhysRevD.89.056005.

[26] A. Boyarsky, M. Drewes, T. Lasserre, S. Mertens, and O. Ruchayskiy. Sterile neutrino Dark Matter. *Prog. Part. Nucl. Phys.*, 104:1–45, 2019. doi:10.1016/j.ppnp.2018.07.004.

[27] Herbert Dreiner, Moritz Huck, Michael Krämer, Daniel Schmeier, and Jamie Tattersall. Illuminating Dark Matter at the ILC. *Phys. Rev. D*, 87(7):075015, 2013. doi:10.1103/PhysRevD.87.075015.

[28] Oleg Lebedev, Hyun Min Lee, and Yann Mambrini. Vector Higgs-portal dark matter and the invisible Higgs. *Phys. Lett. B*, 707:570–576, 2012. doi:10.1016/j.physletb.2012.01.029.

[29] Yasaman Farzan and Amin Rezaei Akbarieh. VDM: A model for Vector Dark Matter. *JCAP*, 10:026, 2012. doi:10.1088/1475-7516/2012/10/026.

[30] Thomas Hambye. Hidden vector dark matter. *JHEP*, 01:028, 2009. doi:10.1088/1126-6708/2009/01/028.

[31] Peter Adshead and Kaloian D. Lozanov. Self-gravitating Vector Dark Matter. *Phys. Rev. D*, 103(10):103501, 2021. doi:10.1103/PhysRevD.103.103501.

[32] Borna Salehian, Mohammad Ali Gorji, Hassan Firouzjahi, and Shinji Mukohyama. Vector dark matter production from inflation with symmetry breaking. *Phys. Rev. D*, 103(6):063526,

2021. doi:10.1103/PhysRevD.103.063526.

[33] Emidio Gabrielli, Luca Marzola, Martti Raidal, and Hardi Veermäe. Dark matter and spin-1 milli-charged particles. *Journal of High Energy Physics*, 2015(8), August 2015. ISSN 1029-8479. doi:10.1007/jhep08(2015)150. URL http://dx.doi.org/10.1007/JHEP08(2015)150.

[34] Cédric Delaunay, Teng Ma, and Yotam Soreq. Stealth decaying spin-1 dark matter. *Journal of High Energy Physics*, 2021(2), February 2021. ISSN 1029-8479. doi:10.1007/jhep02(2021)010. URL http://dx.doi.org/10.1007/JHEP02(2021)010.

[35] Mark P. Hertzberg and McCullen Sandora. Dark matter and naturalness. *Journal of High Energy Physics*, 2019(12), December 2019. ISSN 1029-8479. doi:10.1007/jhep12(2019)037. URL http://dx.doi.org/10.1007/JHEP12(2019)037.

[36] Alexander Belyaev, Giacomo Cacciapaglia, James McKay, Dixon Marin, and Alfonso R. Zerwekh. Minimal spin-one isotriplet dark matter. *Physical Review D*, 99(11), June 2019. ISSN 2470-0029. doi:10.1103/physrevd.99.115003. URL http://dx.doi.org/10.1103/PhysRevD.99.115003.

[37] M. Davier, A. Hoecker, B. Malaescu, C. Z. Yuan, and Z. Zhang. Reevaluation of the hadronic contribution to the muon magnetic anomaly using new $e + e \to \pi + \pi$ - cross section data from babar. *The European Physical Journal C*, 66(1–2):1–9, February 2010. ISSN 1434-6052. doi:10.1140/epjc/s10052-010-1246-1. URL http://dx.doi.org/10.1140/epjc/s10052-010-1246-1.

[38] Wolfgang Kilian, Thorsten Ohl, and Jürgen Reuter. Whizard—simulating multi-particle processes at lhc and ilc. *The European Physical Journal C*, 71(9), September 2011. ISSN 1434-6052. doi:10.1140/epjc/s10052-011-1742-y. URL http://dx.doi.org/10.1140/epjc/s10052-011-1742-y.

[39] J. Blümlein, A. De Freitas, C. Raab, and K. Schönwald. The $O(\alpha^2)$ initial state QED corrections to $e^+e^- \to \gamma^*/Z_0^*$. *Nucl. Phys. B*, 956:115055, 2020. doi:10.1016/j.nuclphysb.2020.115055.

[40] G. Bonneau and F. Martin. Hard photon emission in e^+e^- reactions. *Nucl. Phys. B*, 27: 381–397, 1971. doi:10.1016/0550-3213(71)90102-7.

[41] Bob McElrath. Invisible quarkonium decays as a sensitive probe of dark matter. *Physical Review D*, 72(10), November 2005. ISSN 1550-2368. doi:10.1103/physrevd.72.103508. URL http://dx.doi.org/10.1103/PhysRevD.72.103508.

[42] J. P. Lees et al. Study of $e^+e^- \to p\bar{p}$ via initial-state radiation at BABAR. *Phys. Rev. D*, 87 (9):092005, 2013. doi:10.1103/PhysRevD.87.092005.

[43] V. P. Druzhinin, S. I. Eidelman, S. I. Serednyakov, and E. P. Solodov. Hadron Production via e^+e^- Collisions with Initial State Radiation. *Rev. Mod. Phys.*, 83:1545, 2011. doi: 10.1103/RevModPhys.83.1545.

[44] M. N. Achasov et al. Study of the process $e^+e^- \to \eta\pi^0\gamma$ in the energy range $\sqrt{s} = 1.05$-2.00 GeV with the SND detector. *Eur. Phys. J. C*, 80(11):1008, 2020. doi:10.1140/epjc/s10052-020-08556-w.

[45] A. Blondel et al. Standard model theory for the FCC-ee Tera-Z stage. In *Mini Workshop on Precision EW and QCD Calculations for the FCC Studies : Methods and Techniques*, volume 3/2019 of *CERN Yellow Reports: Monographs*, Geneva, 9 2018. CERN. doi:10.23731/CYRM-2019-003.

[46] Min-Shih Chen and Peter M. Zerwas. Equivalent-Particle Approximations in electron and Photon Processes of Higher Order QED. *Phys. Rev. D*, 12:187, 1975. doi: 10.1103/PhysRevD.12.187.

[47] J-J. Blaising, P. Roloff, A. Sailer, and U. Schnoor. Physics performance for Dark Matter searches at $\sqrt{s} = 3$ TeV at CLIC using mono-photons and polarised beams. ., 3 2021.

[48] Vardan Khachatryan et al. Performance of Photon Reconstruction and Identification with the CMS Detector in Proton-Proton Collisions at sqrt(s) = 8 TeV. *JINST*, 10(08):P08010, 2015. doi:10.1088/1748-0221/10/08/P08010.

[49] J. Kalinowski, W. Kotlarski, P. Sopicki, and A. F. Zarnecki. Simulating hard photon production with WHIZARD. *Eur. Phys. J. C*, 80(7):634, 2020. doi:10.1140/epjc/s10052-020-8149-6.

[50] Jan Kalinowski, Wojciech Kotlarski, Krzysztof Mekala, Kamil Zembaczynski, and Aleksander Filip Zarnecki. New approach to DM searches with mono-photon signature. In *2022 Snowmass Summer Study*, 3 2022.

[51] Dominik Dannheim, Philippe Lebrun, Lucie Linssen, Daniel Schulte, Frank Simon, Steinar Stapnes, Nobukazu Toge, Harry Weerts, and James Wells. CLIC e^+e^- Linear Collider Studies, 8 2012. .

[52] O. Brunner et al. The CLIC project. *Accelerator Physics (physics.acc-ph); High Energy Physics - Experiment (hep-ex)*, 3 2022.

[53] Andreas Albert et al. Recommendations of the LHC Dark Matter Working Group: Com-

paring LHC searches for dark matter mediators in visible and invisible decay channels and calculations of the thermal relic density. *Phys. Dark Univ.*, 26:100377, 2019. doi: 10.1016/j.dark.2019.100377.

[54] Daniel Abercrombie, Nural Akchurin, and Ece Akilli et. al. Dark matter benchmark models for early lhc run-2 searches: Report of the atlas/cms dark matter forum. *Physics of the Dark Universe*, 27:100371, 2020. ISSN 2212-6864. doi:https://doi.org/10.1016/j.dark.2019.100371. URL `https://www.sciencedirect.com/science/article/pii/S2212686419301712`.

[55] CMS Collaboration. Search for resonant and nonresonant new phenomena in high-mass dilepton final states at $\sqrt{s} = 13$ tev. *JHEP 07 (2021) 208*, 2021. doi:10.1007/JHEP07(2021)208.

[56] Jan Kalinowski, Wojciech Kotlarski, Krzysztof Mekala, Pawel Sopicki, and Aleksander Filip Zarnecki. Sensitivity of future linear e^+e^- colliders to processes of dark matter production with light mediator exchange. *The European Physical Journal C*, 81(10), October 2021. ISSN 1434-6052. doi:10.1140/epjc/s10052-021-09758-6. URL `http://dx.doi.org/10.1140/epjc/s10052-021-09758-6`.

[57] Nicolò Trevisani. Collider Searches for Dark Matter. *Universe*, 4(11):131, 2018. doi: 10.3390/universe4110131.

[58] Albert M Sirunyan et al. Search for disappearing tracks in proton-proton collisions at $\sqrt{s} =$ 13 TeV. *Phys. Lett. B*, 806:135502, 2020. doi:10.1016/j.physletb.2020.135502.

APPENDIX C – Investigation of the nature of a massive vector mediator for dark matter through e^+e^- collisions

Received: 20 October 2020 | Revised: 27 October 2020 | Accepted: 11 October 2020

DOI: 10.1002/asna.202113943

Astronomische Nachrichten

ORIGINAL ARTICLE

Investigation of the nature of a massive vector mediator for dark matter through e^+e^- collisions

Marcio Mateus Jr[1] | **Gustavo Gil da Silveira**[1,2]

[1]Instituto de Física, Universidade Federal do Rio Grande do Sul (UFRGS), Porto Alegre, Brazil

[2]Instituto de Física, Universidade do Estado do Rio de Janeiro (UERJ), Rio de Janeiro, Brazil

Correspondence
Marcio Mateus Jr. and Gustavo Gil da Silveira, Instituto de Física, Universidade Federal do Rio Grande do Sul (UFRGS), Porto Alegre, Brazil.
Email: msmateusjr@gmail.com (M. M. J.) and gustavo.silveira@cern.ch (G. G. S.)

Abstract

Our work aims to investigate the interaction between fermions and dark matter (DM) particles in electron-positron collisions through interaction of a new massive vector mediator, Z'. The production of scalar, fermionic, and vector DM pairs via electron-positron annihilation into the new boson is investigated, evaluating the total cross section in the center-of-mass frame. As a result, the possible values of the coupling constants between the DM and the Standard Model of the Elementary Particles particles are mapped according to the exclusion limits obtained by the CMS and ATLAS experiments and the Planck satellite. We show that there are several possibilities for mass ranges of this new massive mediator and for the DM particles, which are not excluded by collider and astrophysical limits.

KEYWORDS

cosmology, dark matter, electron-positron collisions, particle physics

1 | INTRODUCTION

Several studies have been proposed to investigate the dark matter (DM), trying to decipher its origin and nature. Distinct approaches aim to understand how DM interacts and what are the possible mechanisms for detecting it. Theories beyond the Standard Model of the Elementary Particles (SM) investigate the possible couplings of DM with conventional matter in order to observe its interaction in the laboratory.

This work focuses on investigating the interaction between fermions and DM particles by interaction through vector bosons, which would be the mediators of some kind of manifestation of DM. Thus, our goal is to establish new exclusion limits for the differential and total cross sections for the coupling of this vector boson to conventional matter, employing three possible candidates, that is, fermion, scalar, and vector, for relic DM.

2 | THEORETICAL MODELING AND RESULTS

2.1 | Diagrams and interaction Lagrangians

This work explores a framework to probe the limits and analyze parameters for the thermal production of DM through a process that involves an interaction of the SM with the dark sector mediated by a new massive boson mediator (Z') described with a Breit-Wigner (BW) resonance peak. Accordingly, we investigate three possible spin-dependent DM fields. Making use of the Feynman rules, we compute the total cross sections for the following diagrams and their respective Lagrangians[1] (Dreiner et al. 2013):

[1]We have used $\hbar = c = k_B = 1$.

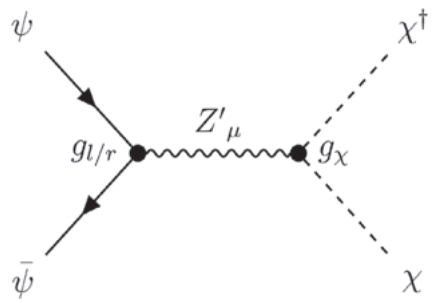

FIGURE 1 A simplified Feynman diagram for the interaction of Standard Model of the Elementary Particles fermion with a scalar dark matter field through a Z' boson

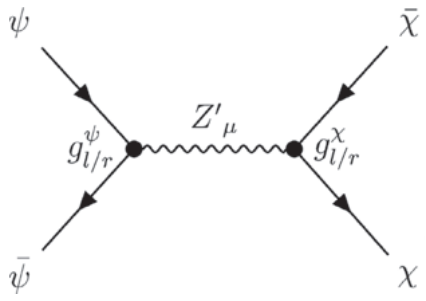

FIGURE 2 A simplified Feynman diagram for the interaction of Standard Model of the Elementary Particles fermion with a fermionic dark matter field through a Z' boson

2.1.1 | Scalar DM

Let ψ be any SM fermionic spinor and Z'_μ a real vector field corresponding to an on-shell massive vector boson, we can write a Feynman diagram representing the interaction of this mediator with a DM candidate, χ, as indicated in Figure 1, where $g_{l/r}$ and g_χ are couplings of this vector boson with the SM and DM fields, respectively. Hence, the interaction Lagrangian of this process is written as

$$\begin{aligned}\mathcal{L}_{\text{int}}^{scalar} = &-\frac{1}{4}F^{\mu\nu}F_{\mu\nu} + \frac{1}{2}M_{med}^2 Z'^{\mu}Z'_{\mu} \\ &+ \overline{\psi}\gamma^{\mu}\left(g_l P_L + g_r P_R\right)\psi Z'_{\mu} \\ &+ g_\chi\left(\chi^\dagger\partial_\mu\chi - \chi\partial_\mu\chi^\dagger\right)Z'^{\mu},\end{aligned} \tag{1}$$

where we used M_{med} to indicate the mediator mass and γ^μ are the usual Dirac matrices. Besides that, Z'_μ indicates a real vector field with field tensor given by $F_{\mu\nu} \equiv \partial_\mu Z'_\nu - \partial_\nu Z'_\mu$ which, along with the mass element defined by the term $\frac{1}{2}M_\Omega^2 Z'^{\mu}Z'_{\mu}$, compose the kinetic term of the Z' boson. The P_L and P_R operators refer to left and right-handed operators, defined by $P_L \equiv (1-\gamma^5)$ and $P_R \equiv (1+\gamma^5)$ with g_l and g_r representing chiral coupling magnitudes.

2.1.2 | Fermion DM

For a DM particle characterized as a Majorana fermion, we have a Feynman diagram describing the exchange of a Z' boson in the s-channel as shown in the Figure 2. Hence, the interaction Lagrangian of this interaction can be written as

$$\begin{aligned}\mathcal{L}_{\text{int}}^{fermion} = &-\frac{1}{4}F^{\mu\nu}F_{\mu\nu} + \frac{1}{2}M_{med}^2 Z'^{\mu}Z'_{\mu} \\ &+ \left[\overline{\psi}\gamma^{\mu}\left(g_l P_L + g_r P_R\right)\psi\right. \\ &+ \left.\overline{\chi}\gamma^{\mu}\left(g_l P_L + g_r P_R\right)\chi\right]Z'_{\mu}\end{aligned} \tag{2}$$

where we will adopt $g^\psi_{l/r} \neq g^\chi_{l/r}$ in the following results. Moreover, we see that the interaction of the Z' boson with the DM field is given by the operators in the last term of Equation (2) which also contains the adjoint spinor for the DM particle $\overline{\chi}$ and once again the chiral operators and couplings.

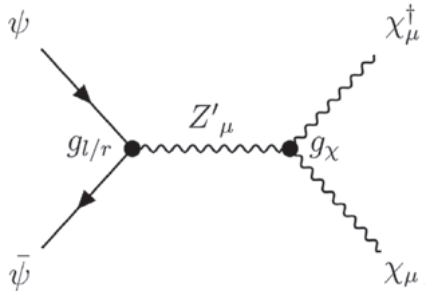

FIGURE 3 A simplified Feynman diagram for the interaction of Standard Model of the Elementary Particles fermion with a complex vector dark matter field through a Z' boson

2.1.3 | Vector DM

Lastly, for a DM candidate in the form of a complex vector field, we express a Feynman diagram for the interaction of this field with the SM as indicated in Figure 3. Two real degrees of freedom of a DM complex field can be combined with the singlet vector boson state previously defined by the mediator Z'_μ to generate a field tensor and a gauge kinetic term in a similar way as done in gauge theories in $SU(2)$ representations. Following the steps established in Dreiner et al. (2013), we write an interacting Lagrangian neglecting quadratic terms as

$$\begin{aligned}\mathcal{L}_{\text{int}}^{vector} = &-\frac{1}{4}F^{\mu\nu}F_{\mu\nu} + \frac{1}{2}M_{med}^2 Z'^{\mu}Z'_{\mu} \\ &+ \overline{\psi}\gamma^{\mu}\left(g_l P_L + g_r P_R\right)\psi Z'_{\mu} \\ &- ig_\chi Z'_\mu\chi_\nu^\dagger\left(\partial^\mu\chi^\nu - \partial^\nu\chi^\mu\right) \\ &+ ig_\chi Z'^{\mu}\chi^\nu\left(\partial_\mu\chi_\nu^\dagger - \partial_\nu\chi_\mu^\dagger\right) \\ &- ig_\chi\left(\partial^\mu Z'^{\nu} - \partial^\nu Z'^{\mu}\right)\chi_\mu^\dagger\chi_\nu,\end{aligned} \tag{3}$$

TABLE 1 Some of the used parameters (PDG Collaboration et al. 2018; PLANCK Collaboration et al. 2020)

Parameter	Value
SM fermion mass (GeV)	$m_e = 511 \times 10^{-6}$
SM coupling (left)	$g_l = 0{,}25$
SM coupling (right)	$g_r = 0{,}25$
Scalar and Fermion DM coupling	$g_\chi = 1$
Vector DM coupling	$g_\chi = 10^{-7}$
Dimensionless Hubble parameter	$h^2 = 0{,}459$
Present day CMB temperature (GeV)	$T_0 \approx 2{,}396 \times 10^{-13}$
Critical density (GeV cm^{-3})	$\rho_{\text{crit}} = 1{,}05 \times 10^{-5}\ h^2$
Cold DM relic density	$\Omega_\chi = 0{,}120\ h^2$

Abbreviations: CMB, Cosmic Microwave Background; DM, dark matter; SM, Standard Model of the Elementary Particles.

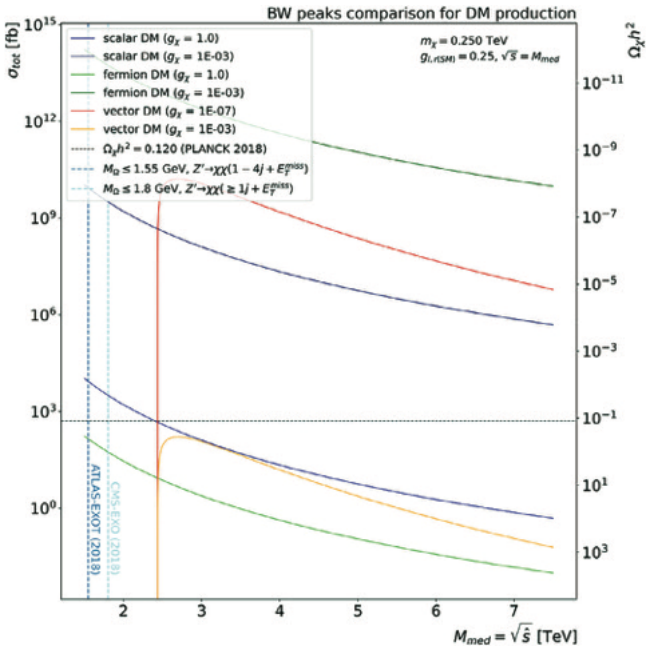

FIGURE 4 Variation of the resonance peaks for $Z^{'}$ boson production with mass ranged from 0.3 TeV to 6.0 TeV, with the same center-of-mass energy of the processes. The dark matter (DM) particle mass in this case was fixed in $m_\chi = 200$ GeV. Limits both on the vector mediator mass and relic density DM thermal production were drawn for comparison purposes

where the operators in the last three terms express the couplings of DM and Z' fields.

In addition, we integrated analytically the differential cross sections for the computation of the total cross sections (σ_{tot}) adding the respective scattering amplitudes of those processes where s and t are the Mandelstam variables and m_e is the SM fermion (electron) mass.

3 | DISCUSSION AND CONCLUSIONS

Once the analytical results are evaluated, we compute the total cross section in DM (m_χ) and mediator (M_{med}) mass ranges as employed in the literature. Using data from CMS Collaboration et al. (2018) and PLANCK Collaboration et al. (2020) we are able to estimate exclusion limits for the proposed models. For estimated DM abundance, we assume a scenario with m_χ composing the whole mass of the DM cold relic density. For these evaluations, we used the recommendations shown in Bauer & Plehn (2017), Griest & Seckel (1991), Kolb (1994) and Profumo (2013) and adopted the parameters described in the Table 1.

In Figure 4, there is a comparison between the maximum values for the production cross section, that is, the value at the top of a BW peak, for a range of M_{med} masses. We varied the mediator mass from 0.3 to 6 TeV for fixed DM mass of $m_\chi = 200$ GeV, and observed that the peaks decrease with an increasing in $\sqrt{s}$. We also note that the vector DM shows a cutoff value where the process is kinetically forbidden when $M_\Omega \lesssim 2,75$ TeV. As we can see in the Figure 4, the sensitivity of the vector DM is very high with the parameter g_χ, since its cross section increases by many orders of magnitude when we change the coupling from $g_\chi = 10^{-3}$ to $g_\chi = 10^{-7}$. The other DM candidates also vary within this parameter, but by a less amount.

Besides that, for all plots we inserted some exclusion limits, where the black dotted line indicates the minimum cross section so that those processes reproduce the cold dark matter (CDM) abundance observed by PLANCK Collaboration et al. (2020) and the blue dotted lines and regions in Figure 4 and subsequent figures bound the region where the mediator mass is less than 1.8 TeV (CMS Collaboration 2018; Collaboration 2018). To analyze in more detail the three cases, we evaluate how the cross section in the production peak of the Z' behaves when we vary the DM mass candidate m_χ and the mass M_{med} of the mediator itself. Therefore, we presented in the Figure 5 this estimation where m_χ ranges from 0.001 to 2 TeV, while the mediator mass ranges from 1 to 4.5 TeV.

We note a significant increasing in the magnitude of the cross section in the region where $M_{med} \approx 2\ m_\chi$, in both scalar and fermionic cases. In the vector case, this increasing occurs next to the kinematic forbidden region for that case. However, in our analyses, we find no significant difference between the different coupling regimes, that is, chiral, vector, and axial-vector, of Z' boson with the

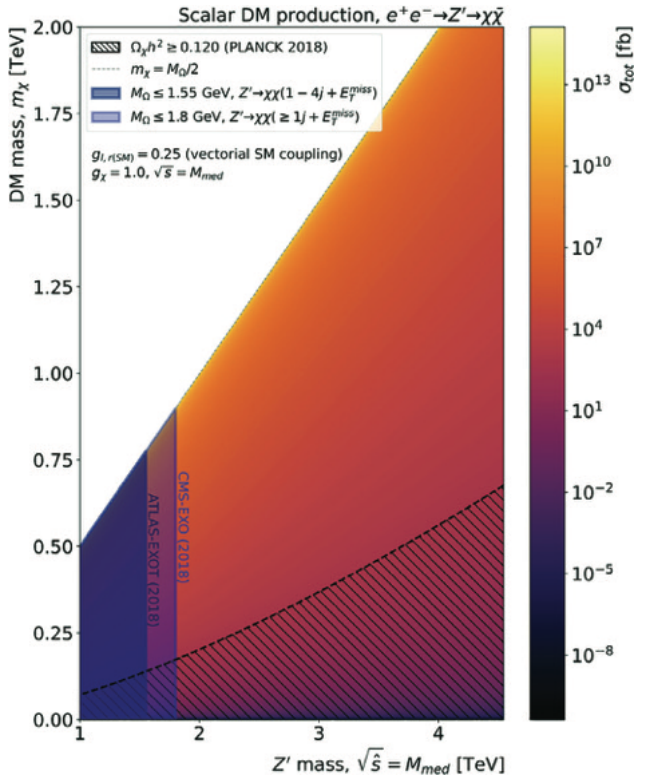

FIGURE 5 Total cross section heat map in terms of the dark matter (DM) particle mass (m_χ) and the Z' boson (M_{med}) for the scalar DM particle. The shaded regions indicate exclusion limits on the mass of massive vectors mediators discussed in ATLAS Collaboration (2018) and Collaboration (2018) and the region with cross section less than the necessary for relic density abundance thermal production of cold dark matter, observed by PLANCK Collaboration et al. (2020), are hashed in black

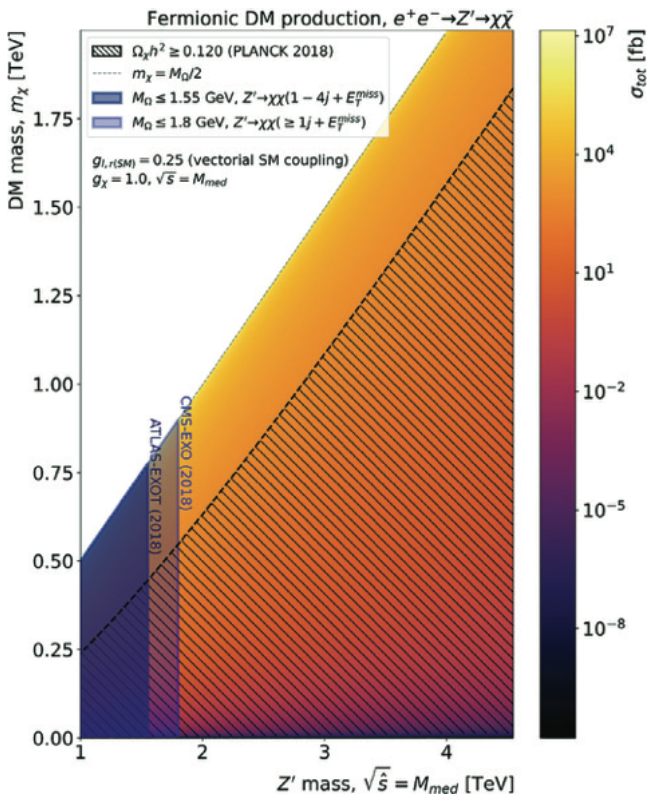

FIGURE 6 Same plot as Figure 5, but for the fermionc dark matter (DM) case

SM field, hence, all the results are from a vector coupling ($g_r = g_l$) with the SM (Figures 6 and 7).

4 | CONCLUSION

To characterize this model, we presented a SM extension with a new renormalizable symmetry group U(1) acting as a vector portal for DM, which is distinguished by the composition of its field, that is, scalar, fermionic, and complex vector, by three respective possible interaction Lagrangians.

Therefore, these results show that our models are within the parameter space probed in the experimental and cosmological limits. Note that, to reproduce similar cross sections with the other models, the vector DM needs a much smaller coupling constant ($g_\chi = 10^{-7}$) and has a reduced mass range. This work aims to further narrow our parameter space, especially the mass range of the mediator mass, with both existing data and new experiments such

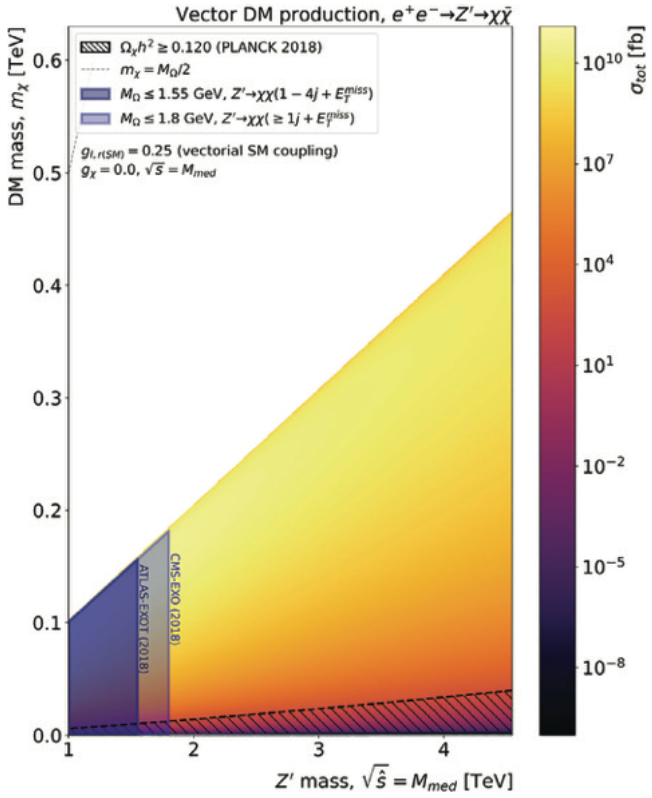

FIGURE 7 Same plot as Figure 5, but for the vector dark matter (DM) case

as the Future Circular Collider and the Compact Linear Collider.

Furthermore, the experimental viability of observation of these processes are focused in the use of disappearing tracks, as already done by the Large Hadron Collider (LHC) experiments (CMS Collaboration et al. 2020). Nevertheless, this study will be extended with initial- and/or final-state radiation, where some species of DM could decay into more detectable SM particles.

REFERENCES

ATLAS Collaboration 2018, *JHEP*, *1*, 126.

Bauer, M., & Plehn, T. 2017, Yet another introduction to dark matter, https://arxiv.org/abs/1705.01987

CMS Collaboration 2018, *JHEP*, *8*, 130.

CMS Collaboration, Sirunyan, A. M., Tumasyan, A., et al. 2018, *Phys. Rev. D*, *97*, 092005.

CMS Collaboration, Sirunyan, A., Tumasyan, A., et al. 2020, *Phys. Lett. B*, *806*, 135502.

Collaboration, C 2018, *Phys. Rev. D*, *97*, 092005.

Dreiner, H. K., Huck, M., Krämer, M., Schmeier, D., & Tattersall, J. 2013, *Phys. Rev. D*, *87*, 075015.

Griest, K., & Seckel, D. 1991, *Phys. Rev. D*, *43*, 3191.

Kolb, E. 1994, *The Early Universe*, Westview Press (New York).

PDG Collaboration, Tanabashi, M., Hagiwara, K., et al. 2018, *Phys. Rev. D*, *98*, 030001.

PLANCK Collaboration, Aghanim, N., Akrami, Y., et al. 2020, *A&A*, *641*, A6.

Profumo, S. 2013, TASI 2012 Lectures on Astrophysical Probes of Dark Matter, https://arxiv.org/abs/1301.0952

AUTHOR BIOGRAPHY

Marcio Mateus is a Ph.D student at the Physics Institute of the Federal University of Rio Grande do Sul. He works under the supervision of Dr. Gustavo Gil da Silveira, who also works on the CMS experiment collaboration at CERN. For his master thesis he studied a spin dependent dark matter (DM) model that couples with ordinary matter through a new massive gauge boson mediator in electron-positron colliders. In his Ph.D. research he now studies how to expand this model to hadron colliders and other general purpose DM detectors and study the implications of these DM models in different cosmological and experimental scenarios.

How to cite this article: Mateus Jr M, Gil da Silveira G. Investigation of the nature of a massive vector mediator for dark matter through e^+e^- collisions. *Astron. Nachr*. 2021;1–5. https://doi.org/10.1002/asna.202113943